DISS. ETH NO 28467

TOP-DOWN INFLUENCES ON CORTICAL SOMATOTOPIC MAPS

A thesis submitted to attain the degree of
DOCTOR OF SCIENCES
(DR. sc. ETH Zurich)

presented by

FINN-LENNART RABE

M.A. in Cognition and Communication, University of Copenhagen

born on 13.04.1990

accepted on the recommendation of
Prof. Dr. Nicole Wenderoth
Prof. Dr. Christian Ruff
Dr. Sanne Kikkert

2022

Acknowledgments

I want say thank you to everyone who accompanied and supported me on this journey for the last four years.

I also want to thank the members of the Neural Control of Movements Lab. Especially, Weronika, Ernest and Dan for sacrificing their time to reading parts of my thesis.

My special gratitude goes to the to my two supervisors Nici and Sanne. I could always annoy you with questions and you were able to reschedule when I was stuck with something.

And.. I want to thank the academy (joke intended for Luis).

Finally, I want to say thanks to my family. They kept my spirits up over that period and sent me texts of encouragement as well as small sweets.

Zusammenfassung

In dem Moment wo wir mit unseren Fingern einen Gegenstand berühren oder diese benutzen, um die Eigenschaften des Gegenstandes ausfindig zu machen, werden Neuronen an (teilweise) ganz bestimmten Orten in unserem Gehirn aktiviert. Diese Entdeckung lässt vermuten, dass neuronale Repräsentationen bestimmter Eigenschaften eines Gegenstandes in unserer Umgebung durch die Topographie sensorischer Hirnregionen strukturiert werden. Die topographische Karte in unserem Somatosensorischen Cortex wird auch als somatotope Karte bezeichnet. Dabei wird die Grösse einer Repräsentation, z.B. von einem Körperteil, nicht durch die eigentliche Grösse, sondern durch die Anzahl oder Dichte der in der Haut liegenden Rezeptoren bestimmt. Das Stimulieren oder Bewegen zum Beispiel von Fingern, in denen sich vergleichsweise viele Rezeptoren befinden, führt zu klar unterscheidbaren Repräsentationen im Primär Somatosensorischen Cortex (S1). Das heisst, die Somatotopie bildet die anatomischen Gegebenheiten, durch die wir somatosensorische Reize lokalisieren bzw. verarbeiten können und die Selbstwahrnehmung unseres Körpers entsteht.

Bezeichnend ist, dass latente Veränderungen in den somatotopen Aktivierungen nicht nur durch periphere sensorische Erfahrungen hervorgerufen werden, sondern auch einen kortikalen Ursprung haben können. Letzteres ist bisher noch nicht völlig nachvollziehbar. In den folgenden Studien nahmen unsere Teilnehmer an unterschiedlichen Experimenten teil, bei denen die neuronalen Repräsentationen von Fingern aktiviert wurden. Besonderer Fokus lag dabei auf Perioden oder Bedingungen, in denen periphere sensorische Reize abwesend waren. Sollten wir dennoch fingerspezifische Veränderungen in der Hirnaktivität finden, dann könnten wir diese einem puren kortikalen Ursprung zusprechen.

In unserer ersten Studie untersuchten wir ob die kognitiven Anforderungen einer vibrotaktilen Frequenzunterscheidungsaufgabe die somatotopen Fingerrepäsentationen in S1 beeinflussen. Als erstes untersuchten wir die Aktivitätsunterschiede im Repräsentationsbereich der Hand in S1, um frühere wissenschaftliche Ergebnisse zu bestätigen. Besonderes Merkmal legten wir auf die Frage, ob die dem Stimulusort äquivalente Repräsentation stärker ausgeprägt war, wenn unsere Studienteilnehmer Eigenschaften des somatosensorischen Reizes erinnern mussten. Unsere Ergebnisse zeigen, dass die altbekannten Repräsentationsausprägungen während taktiler Stimulationen auch unter bestimmten Umständen in deren Abwesenheit weiterhin bestehen.

Basierend auf den Ergebnissen der ersten Studie, war das Ziel der zweiten Studie, Hirnregionen zu identifizieren, die während vibrotaktiler Frequenzunterscheidung mit somtotopen Arealen in S1 interagieren. Wir konnten zeigen, dass subkortikale Regionen, denen bisher eine «Top-Down»-Kontrollrolle zugeschrieben wurde, mit den fingerspezifischen somatotopen Arealen interagierten. Dass die dynamischen Veränderungen dieser funktionalen Verknüpfungen den Erfolg bei der Frequenzunterscheidung vorhersagen können, bestätigt dessen Relevanz für somatotope Informationsverarbeitung.

In der dritten Studie untersuchten wir, ob selbst Menschen mit beinahe oder komplettem Verlust sensomotorischer Funktionen durch ein Rückenmarkstrauma, weiterhin in der Lage waren die fingerspezifischen Repräsentationen im ipsilateralen S1 zu aktivieren während sie lediglich versuchen ihre Finger zu bewegen. Unsere Ergebnisse zeigen, dass es diesen Menschen nicht nur möglich war Fingerrepräsentationen zu aktivieren, sondern dass die Struktur dieser Repräsentationen denen von Menschen ohne Rückenmarkstrauma glich. Da wir diese Ergebnisse auch bei Menschen mit einem kompletten Verlust der Funktionen fanden, liegt es nahe, dass interhemisphärische Verbindungen diese somatotopen Aktivierungen im ipislateralen S1 hervorrufen.

Zusammengefasst zeigt diese Arbeit, dass Fingerrepräsentationen innerhalb von somatotopen Hirnarealen nicht nur durch taktile Stimulation oder erkennbare Bewegungen, sondern auch durch Prozesse aktiviert werden können, wobei periphere sensorische Reize abwesend sind. Im weiteren Sinne bestätigen unsere Ergebnisse die Hypothese, dass somatotope Karten dem Gehirn das notwenige neurophysiologische Gerüst verleihen. Wir können zu dem zeigen, dass das auch der Fall ist, wenn es mittel- bis langfristig keine peripheren Reize gibt. Damit zeigt die Arbeit ihre Relevanz für die Forschung über kognitive Kontrolle und ihr potenzieller Nutzen dieser Prozesse für Neuroprothesen bei Menschen mit einem Rückenmarkstrauma.

Abstract

Whenever we touch an object with our fingers or move these fingers to explore the object, firing of neurons resides in (partially) spatially distinct locations in our brain. This gave rise to the idea that representations, e.g. specific features of the object, of the world around us are embedded in topographically-organized sensory brain regions. The topographic map in the somatosensory cortex is known as the somatotopic map. Here, the representational size of a body part does not correspond to its actual size but to the density of tactile receptors in the skin of that specific body part. For instance, stimulating or moving specific fingers results in more spatial distinguishable representations in the primary somatosensory cortex (S1) than stimulations to or movements of the different parts of the trunk. Thus, these somatotopic maps establish an anatomical foundation through which we can localize and process somatosensory inputs and create awareness of our own body.

More strikingly, latent changes to somatotopic activations can not only be provoked through peripheral sensory experiences, but can have a purely cortical origin. However, the full scope of these cortical influences on somatotopic representations are not yet fully understood. In the following studies, we exposed participants to different tasks that required them to activate finger representations in S1. We specifically investigated periods or conditions, i.e. (partial) loss of sensorimotor function, where peripheral sensory input was absent to ensure that if we still observe finger-specific activity changes, we potentially can attribute them to corticocortical processing.

In the first study, we investigated whether task demands during a vibrotactile frequency discrimination task modulated finger representations in S1. To reaffirm previous findings, we analyzed neural activity changes in an area of S1 that represents the hand. Furthermore, we also investigated whether cortical finger representations corresponding to the applied stimulus location were more pronounced when participants had to retain somatosensory information, i.e. in the absence of tactile inputs. Our results indicate that the well-known modulated somatotopic activity changes during tactile stimulations might also persist through periods of absence of tactile input.

Building on the results from the first study, during the second study we aimed to identify brain regions that functionally interacted with finger-specific areas within the somatotopic map of S1 during vibrotactile frequency discrimination. We showed that subcortical regions,

previously implicated in top-down control, was functionally coupled to these somatotopic areas during vibrotactile stimulation to meet task demands. Crucially, dynamical changes of this functional coupling predicted task performance.

In the third study, we examined whether finger representations in ipsilateral S1 can be activated during (attempted) unimanual movements even after a partial or complete loss of sensorimotor function in the hands following a cervical Spinal Cord Injury (SCI). Strikingly, we observed that SCI patients were not only able to activate finger representations in S1, but also their representational geometry seemed not to differ from healthy controls. Since we also found this in patients with the most severe cases of hand paralysis, we suggest that interhemispheric connections are generating these somatotopic activations in ipsilateral S1.

Together, our work demonstrates that finger representations, residing within somatotopic maps, can not only be activated via tactile stimulation or overt movements, but also by mechanism that do not require any peripheral sensory inputs. More broadly, our findings are consistent with the hypothesis that somatotopic maps provide the neurophysiological framework for somatosensory information processing. Our work shows that this is true for instances of no peripheral experiences. Therefore, it also highlights its relevance for research of cognitive control and its potential exploitation using neuroprotheses after a SCI.

Contents

List of figures

List of tables

List of appendices

1 General Introduction

1.1 Motivation

As humans, we are able to perceive environmental stimuli through our senses and react to them via thoughts, emotions, decisions and actions. In neuroscience, one of the key questions is how the processes that occur in our brain relate to these external stimuli. As neuroscientists, we want to know whether a specific pattern of neural activity in the brain actually represents a specific stimulus in the environment (Shea, 2018). If so, then neurophysiological mechanisms must give rise to mentally represented information about the environment, which itself has a meaning and a purpose (Kriegeskorte & Diedrichsen, 2019). Here, meaning would convey a specific feature of a percept, e.g. object orientation information, while purpose reflects its influence on cognitive processes and the resulting behavior. The storage and manipulation of these internal representations would be crucial for perception, memory, decision making, motor control and subjective experience.

Interestingly, lower-level processing of these representations seems to occur within modality-specific brain regions, e.g. features of visual stimuli are represented within visual cortex while features of tactile stimuli are represented in somatosensory cortex. More specifically, receptor surfaces in the skin seem to map onto an equivalent spatially-ordered and modality-specific population of neurons in sensory regions of the brain (Kaas, 1997). This topographic mapping was observed across all sensory regions of the brain, e.g. stimulation to different body parts is represented in spatially (distinct) areas of the somatosensory cortex, known as somatotopy, and is well described in monkeys (Shoham & Grinvald, 2001; Tommerdahl et al., 1993) and humans (Francis et al., 2000a; Sanchez-Panchuelo et al., 2010; Schweizer et al., 2008). These somatotopic maps establish an anatomical foundation through which we can localize somatosensory inputs and create awareness of one's own body. Common approaches to probe cortical representations within these somatotopic maps to investigate underlying neurophysiological processes are tactile stimulations and movement tasks. Less is known about how finger representations within somatotopic maps are modulated when tactile inputs are at least partially or fully absent. Here modulation could occur through corticocortical connections in the brain.

The overall aim of the thesis is to resolve these issues. We investigated finger representations within somatotopic maps of S1 in two specific cases. First, a vibrotactile frequency discrimination task requires agents to encode vibrotactile information and retain this information in the absence of any tactile input for subsequent decision making. Whether

somatotopic maps mediate these processes and how changes of cortical representations meet task demands is unknown. Second, in the case of an abrupt loss of sensory function caused by a disruption to sensory processing between the periphery and the brain, it is unknow whether (attempted) unimanual movements still evoke the usual finger representations within ipsilateral S1.

In the following sections, we provide a more detailed description of somatotopy and introduce a potential process mediating the modulation of somatotopic maps in the absence of sensory input. We will also provide an overview of different cases where sensory input is absent and its potential neurophysiological consequences on somatotopic maps. Finally, we will provide an overview of appropriate tools to identify potential representational changes within somatotopic maps, and the mechanisms that might drive these changes.

1.2 Somatotopy of the somatosensory cortex

As described above, somatotopy refers to a positional relationship of body parts and their distinct location in the cerebral cortex. Penfield and Boldrey (1937) demonstrated for the first time that distinct body part sensations could be evoked through electrically stimulating the cortical surface of the somatosensory cortex in awake epilepsy patients. Further investigations in non-human primates revealed that S1 consists of distorted somatotopic map, where body parts are proportionally represented based receptor surfaces instead of the size of the body part, giving rise to the concept of the homunculus (Penfield, 1947). Parcellations of S1 can be referred to as Brodmann area (BA) 3a, 3b, 1 and 2 and all of these seem to possess a reasonably complete representation of the body (Sanchez-Panchuelo et al., 2010, 2014; Willoughby et al., 2021).

1.3 Receptors that activate the somatosensory network

Nonetheless, each parcellation is connected to different receptors. BA 3a receives proprioceptive input from muscle spindles, while BA 3b gathers substantial inputs from cutaneous mechanoreceptors. There are four major types of mechanoreceptors that send tactile information to the central nervous system, namely, Meissner's corpuscles, Pacinian corpuscles, Merkle's disks and Ruffini corpuscles. Specifically, Meissner's corpuscles provide information to area 3b and 1 in contralateral S1 (Mountcastle et al., 1969). In contrast, Pacinian corpuscles project in a more dispersed manner to area 3a and 2 in contralateral S1 and bilaterally to S2.

1.4 Non-invasive techniques to study somatotopy

Even though cortical electrical stimulation was fruitful for the discovery of somatotopic maps in humans, it proved impractical for extensive research due to its invasiveness. Emerging non-invasive imaging techniques provided the necessary spatial resolution to further investigate somatotopic maps. Similar to electrophysiological findings, neuroimaging studies using different approaches, i.e., Magnetoencephalography MEG; Baumgartner et al., 1991), positron emission tomography (PET; Fox et al., 1987) and functional magnetic resonance imaging (fMRI; Sanchez Panchuelo et al., 2018; Sanchez-Panchuelo et al., 2010, 2014; Willoughby et al., 2021) demonstrated that tactile stimulation of body parts resulted in observable distinct representations in the somatosensory cortex. More strikingly, neuroimaging studies discovered finger-specific maps in S1 and their spatial organization corresponded to the anatomy of the stimulated hand, with fingers specifically represented along the inferior lateral direction (**Figure 1.1**; Besle et al., 2013; Francis et al., 2000b; Gelnar et al., 1998; Stippich et al., 1999).

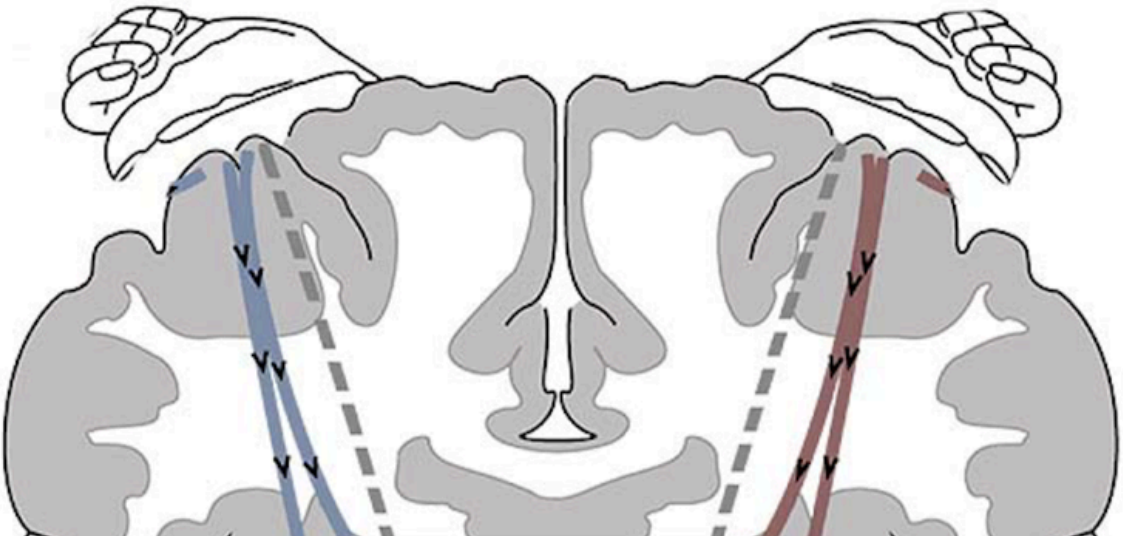

Figure 1. 1 Visualization of hand somatotopy in S1

Simplified visualization of hand somatotopy in somatosensory cortex in both hemispheres. Coronal plane slice view at the level of the somatosensory cortex. Electrophysiological and fMRI findings suggest a 'thumbs-down' neural representation of fingers along the inferior lateral direction.

1.5 Non-peripheral sensory processes modulating somatotopic maps

Interestingly, finger-specific somatotopic maps are not exclusively activated by tactile or proprioceptive stimulation, but they can also be modulated through other mechanisms like (i) *attempted movement*s which do not produce overt motor output or the associated tactile or proprioceptive feedback (P. Ariani et al., 2021; Guan et al., 2021; Kikkert et al., 2021) (ii) *observed* (Kuehn et al., 2018) or *actively imagined* touch (Schmidt & Blankenburg, 2019), (iii) or directing *attention* to a specific finger (Puckett et al., 2017). These results suggest that changes in activity patterns reflecting cortical finger representations might be influenced by higher-level brain areas instead of low-level primary sensory brain areas.

In the following sections we will describe the definitions for *high-lever* and *lower-level* brain area, introduce the concept of *top-down control* (**section 1.3**), will elaborate on *vibrotactile frequency discrimination* (**section 1.4**), and *attempted movements* (**section 1.5**), both of which reflect cases where peripheral sensory inputs are temporally, partially or fully absent.

1.6 Top-down control mechanisms

In the previous section, we presented multiple cases where changes of cortical representations within the somatotopic map supposedly neither had a tactile nor proprioceptive origin. Interestingly, neural processing of sensory information can be modulated from higher level areas (i.e. top) to lower level (i.e. bottom) primary sensory areas, known as top-down control (Mesulam, 1998; Miller & Cohen, 2001). This modulation can lead to gating task-relevant sensory information and allowing for dynamic sensorimotor and more abstract processing of sensory stimuli (Alexander et al., 1986; del Cul et al., 2007; Manita et al., 2015). Thus, top-down control has the ability to regulate perception and cortical processing in the absence of sensory input and has been associated to cognitive processes, such as attention and memory (Corbetta & Shulman, 2002; Tomita et al., 1999; Zanto et al., 2011). It therefore has the potential to influence cortical representations within somatotopic maps and we will elaborate on two specific cases where this potentially could occur in the following sections.

1.7 Neural mechanism underlying vibrotactile frequency discrimination

A common approach to investigate neural finger representations is by applying mechanical vibrations to the skin in the range of 5 – 50 Hz, which elicits a flutter sensation (Mountcastle et al., 1967; Romo & Salinas, 2003). A flutter sensation on a specific body part activates neurons in corresponding cortical representations in S1. The neural firing is thought to oscillate at the stimulus frequency and is activated by Meissner's corpuscles (Mountcastle et al., 1969; Talbot et al., 1968). Thus, fast adapting cutaneous mechanoreceptors enable a dynamic representation of the flutter sensation (Romo et al., 1998).

The approach can also be extended to investigate tactile working memory (WM) when adding a subsequent second stimulation and a stimulation-absent delay period between both stimulations (**Figure 1.2**). WM is a physiological construct and describes mental representations of sensory information in the absence of any sensory input (for review, Baddeley, 2003). Since WM enables the storage and manipulation of information, as well as guiding executive processes, it is thought to be crucial for a multitude of cognitive processes (for review, see Baddeley, 2012) .

The vibrotactile frequency discrimination task requires the agent to encode stimulus features (e.g. the frequency) from the first stimulation (f1), store these in WM, encode the second stimulus (f2) and compare both stimuli in order to formulate a decision.

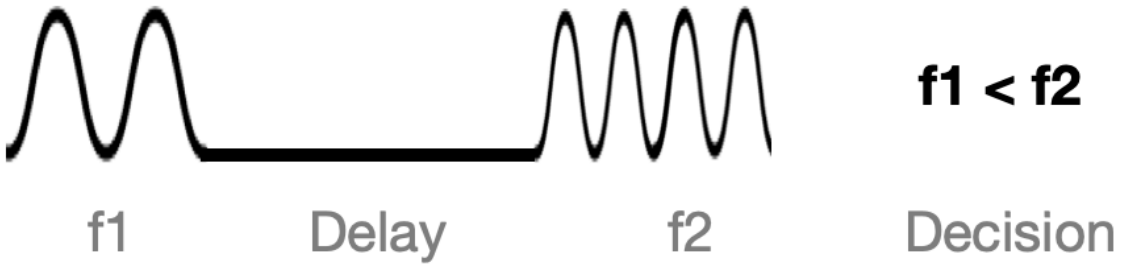

Figure 1. 2 Conventional vibrotactile frequency discrimination paradigm.

*The agent receives two subsequent vibrotactile stimulations (*f1 *and* f2*) with varying frequencies within the flutter range, which are separated by a delay period. To successfully perform the task, the agent has to mentally represent both frequencies, compare them and indicate the appropriate decision.*

Using vibrotactile frequency discrimination to investigate tactile WM exploits modality-specific processing, which suggests that these sensory regions also store the stimulus information in a topographic manner.

Neurophysiological studies on WM in primates have previously exhibited sustained firing of neurons in sensory regions during the period of information storage (Romo et al., 1999; Schmidt et al., 2014; Zhou & Fuster, 1996). These neurons have been also labelled as "memory cells". In particular, the existence of such "memory cells" in primary sensory cortices suggest that lower-level regions are not only involved in the stimulus perception, but also could serve as a memory buffer for sensory information (D'Esposito & Postle, 2015). It is very likely that the observed activity during the delay period in primary sensory regions reflects the neural representation of stimulus information in order to guide an appropriate behavioral response (Wang et al., 2013). This idea has been conceptualized in sensory recruitment models of WM (D'Esposito & Postle, 2015; Harrison & Tong, 2009; Pasternak & Greenlee, 2005). These models postulate that sensory information is retained in modality-specific sensory brain regions, thus suggesting storage in a topographic format. Indeed, event-related potential (ERP) studies of tactile WM revealed that the sustained rehearsal of tactile information resided within somatotopically organized brain areas (Katus et al., 2014, 2015). However, it is important to note that the involvement of S1 in tactile WM in monkey (for review, see Romo & Salinas, 2003) and humans (Harris et al., 2001, 2002; A. L. Kaas et al., 2013; Preuschhof et al., 2006; Schmidt et al., 2017, 2021; Schmidt & Blankenburg, 2018; Wang et al., 2013; Wu et al., 2018) is still debated.

While the role of sensory brain regions in storing WM features is not fully resolved, there is consensus on the involvement of PFC in modulating cortical representations of WM contents via top-down control in order to guide behavior (for review, see Gazzaley & Nobre, 2012). Tactile WM tasks revealed that applying single pulse transcranial magnetic stimulation (TMS) to dorsal lateral PFC during stimulus presentation lowered attention-related modulation of event-related potentials (ERPs) in somatosensory cortex (Bolton & Staines, 2011; Gogulski et al., 2015), presumably via frontal-striatal loops.

Attention has been suggested as an integral part of performing WM tasks (Cowan et al., 2013; Logie & Cowan, 2015; Schmidt & Blankenburg, 2018, 2019) as it filters information by sensory modality or body location (Gomez-Ramirez et al., 2011), and therefore regulates what will and will not be cortically represented (Desimone & Duncan, 1995). According to the attention-based rehearsal account, shifting attention to the memorized stimulus location during a tactile task increases memory accuracy (Awh et al., 2006; Awh & Jonides, 2001, but

see also: Theeuwes et al., 2009). Taken together, frontal-striatal loops have the potential to influence the somatotopic map via top-down control and will be the subject in **chapter 3**.

1.8 Cortical (re)organization after Spinal Cord Injury

The brain is not only limited to the representation of sensory information but is also required to direct movement execution in order to interact with the environment. The channel which transmits motor and sensory information between the body and the brain is the spinal cord. It consists of spinal neuronal cell bodies which are embedded in vertically oriented myelinated spinal tracts (for review, Bican et al., 2013). These cell bodies can either contain sensory or motor neurons, transmitting afferent information from the body to the brain or efferent information from the brain to the body. While axons from spinal sensory neurons access the spinal cord, motor neurons exit it via segmental nerves or roots. These roots can be categorized into five vertebrae corresponding to different sections of the body, namely cervical, thoracic, lumbar, sacrum and coccyx. The sections follow a cranial to caudal mapping, e.g. cervical vertebrae receive sensory information from skin areas and send motor outputs to muscles in the upper limbs (for review, Bican et al., 2013).

SCI induces a sudden disruption to neuronal tissue within the spinal tract. After injury individuals experience a complete or incomplete loss of sensation and muscle function below the level of injury, which can manifest as loss of power, sensation, respiration, temperature, bladder control and sexual function (Jensen et al., 2007). It is important to note that each individual might experience very different symptoms since each injury is unique.

Following a cervical SCI resulting in tetraplegia, individuals' limbs and torso are generally (partly) affected (Curt et al., 1998; Kalsi-Ryan et al., 2014; Petersen et al., 2012). S1 therefore receives dampened or no afferent input and is exposed to changes in motor behavior (Ozdemir & Perez, 2018). Seminal non-human primate studies have shown that this results in extensive reorganization in S1 where deprived body part representations (e.g., of the hand) become responsive to cortically neighboring and intact body parts (e.g., of the lips; Halder et al., 2018; Jain et al., 2008; Kambi et al., 2014). Furthermore, they found that finger representations became less distinct in S1 and additionally, S1 decreased its response to tactile stimulations (Cramer et al., 2005; Freund, Rothwell, et al., 2011; Hotz-Boendermaker et al., 2008). Nevertheless, recently it was revealed that tetraplegic patients who suffer from a complete SCI and therefore have little to no connections between the periphery and brain, showed preserved representations of individual fingers of the paralyzed hand that can be activated through attempted hand movements, but these representations deteriorate over

time (Flesher et al., 2016; Guan et al., 2021; Kikkert et al., 2021). Therefore, potential permanent changes in the somatotopic map after SCI is an ongoing debate. Based on new insights, rehabilitation strategies could be adjusted accordingly.

1.9 Tools that capture neural representations

1.9.1 Functional Magnetic Resonance Imaging

As described above, fMRI is a prominent tool to investigate neural representations. In general, MRI relies on the magnetic properties of hydrogen atoms in order to image a certain part of the body. The hydrogen nucleus consists of a single positively charged proton and no neutrons (Logothetis, 2002). After the excitation of these protons, they return to a state of equilibrium. The process of return is called relaxation and it's time can be measured in two directions, i.e T1 and T2 (Logothetis, 2002).

Since certain molecules like hemoglobin can influence the dephasing of nuclei, a contrast signal can display the increased neuronal activity in the brain. Within fMRI studies the most common contrast signal is the blood oxygenation level dependent signal (BOLD, Ogawa et al., 1990). The BOLD signal is measurable due to two distinct phenomena. First, the magnetic properties of hemoglobin change slightly if the molecule loses its oxygen molecule and becomes deoxyhemoglobin. Secondly, with increased activation in a brain area, the blood flow overcompensates the metabolic oxygen rate resulting in reduced delivery of oxygen that exits the metabolized cell. This is followed by a decrease in oxygen extraction rate (OEF). Taken together, the BOLD signal occurs due to a decreasing OEF, while neural activity increases. Therefore, fMRI is able to measure the effects of neurovascular coupling that indirectly relates to neuronal activity.

Since the MRI scanner measures the BOLD signal across all three dimension of the brain millimeter by millimeter, a whole brain image, also called volume, consists of three-dimensional pixels, so-called voxels. The BOLD signal across time within a voxel is usually referred to as the voxel time-series. Before any statistical inferences can be computed, BOLD measurements are usually preprocessed, mainly to remove artefacts and to align sequentially acquired images.

1.9.2 Mass-univariate analysis to inspect fMRI data

To reveal brain activations, voxel time-series of these preprocessed images are used in a general linear model (GLM) in order to infer experimental condition-dependent neural

activations. Here, voxel-wise parameter estimates, also called beta estimates, are obtained by minimizing the quadratic error between the predicted and the measured time-series (Friston et al., 1994). Since the estimation is done for each voxel separately, such approaches can be referred to as mass-univariate analysis. This analysis also allows to statistically compare between different beta estimates corresponding to different events of the experiment by using contrast vectors.

1.9.3 Multi-voxel pattern analysis to inspect fMRI data

Multivariate approaches have gained major ground in neuroscientific research over the last decade. In contrast to classical univariate approaches for fMRI analysis, multivariate approaches have great potential to study neural representations (Kriegeskorte, 2008). In fMRI studies, it is often referred to as multi-voxel-pattern analyses (MVPA), and it allows for a joint analysis of multiple voxels (information driven). This is in contrast to a common mass-univariate analysis where statistical inferences are made at each voxel individually (activation driven). For the latter, multivariate-like extensions exist when measurements are pooled within predefined regions of interest (ROI) or by increasing spatial smoothing across voxels (Hebart & Baker, 2018). Nonetheless, these extensions neglect the individual voxel's contribution to discriminating between stimuli and they do not take the covariance between all voxels into account. MVPA on the other hand accounts for this. Moreover, the covariance between voxels can contain additional information which can be decoded by MVPA.
While univariate approaches are usually implemented via a GLM, MVPA can rely on supervised and unsupervised machine learning algorithms. Neural representations can conventionally be captured by supervised algorithms, specifically linear classifiers (Haynes & Rees, 2006; Norman et al., 2006; Pereira et al., 2009).

The MVPA procedure consists of two steps, i.e. training the classifier on parts of the data and testing the classifier on the rest of the data. During the first step, a linear classifier, e.g. a support vector machine (SVM), aims to find the 'decision boundary' (hyperplane in multi-voxel space) that best distinguishes two experimental conditions in the multivariate response (multi-voxel) space of the training data (as depicted in **Figure 1.3**). For instance, SVM identifies the points (support vectors) from both conditions that are closest to the line and tries to maximize the distance between the decision boundary and the points. During the second step, the algorithm classifies unseen and 'blinded' test data points as one of the two experimental conditions depending on their geometric position relative to the decision boundary. When comparing predicted to actual data point affiliation, their (dis-)accordance

can be formulated into classification accuracies, reflecting the probability of an ROI to distinguish between condition information.

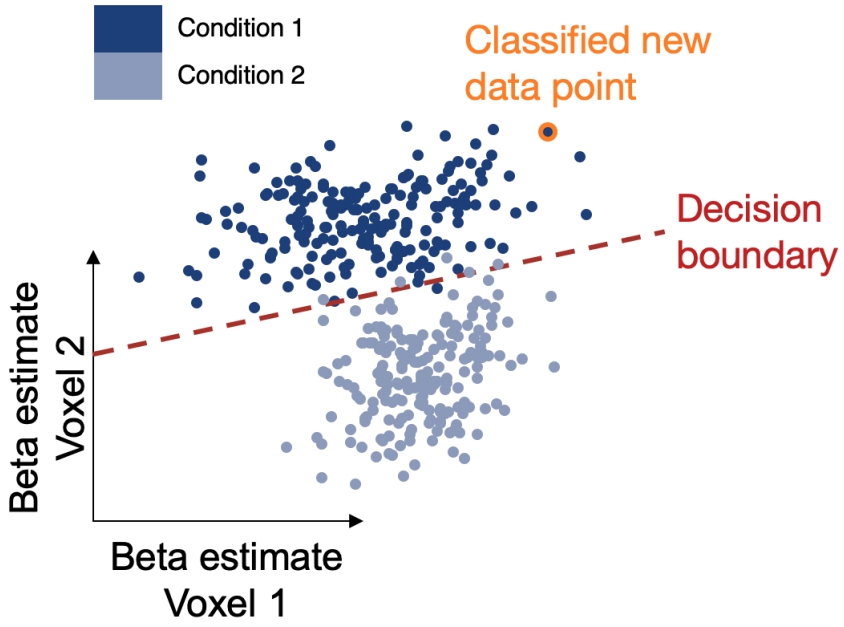

Figure 1. 3 Simplified 2-D visualization of linear classification

*Each data point represents a trial-based beta estimate in multi-voxel space. The distribution of data points for each condition (*dark blue *or* light blue*) reflects the population response in a region of interest (ROI). The MVPA algorithm aims to find the line (*red*) that best separates the condition-dependent population responses, also called the decision boundary. To obtain classification accuracies, the algorithm compares newly classified data points (*orange*) to their true condition affiliation.*

To reduce the possibility of overfitting the training data, which means that the decision boundary does not generalize well to unseen data, it is advised to alternate the chunking into train and test data sets, so-called cross-validation. Here data can be split in an arbitrary number of chunks, all containing different train and test data sets. A final classification accuracy is obtained by averaging over all chunks' classification results.

1.9.4 Representational similarity analysis to inspect fMRI data

Linear classifiers utilize different strategies to best discriminate between experimental conditions. While SVM defines the criterion to search for the decision boundary that is maximally distant to any data point, the linear discriminant aims to find the transformation that maximizes the between-condition variance and minimizes within-condition variance. A generalization of the linear discriminant approach is the representational similarity analysis

(RSA, Kriegeskorte, 2008). RSA has the advantage to provide us with a complete picture of the information-based structure in the multivariate response space, also referred to as geometric representation of information. Such geometry is driven by the distances in multi-voxel response space that delineates the representation of at least two or more conditions or stimuli. It reveals the representation of individual conditions, instead of just the categories of conditions. This potentially incorporates all possible stimulus features, whereas an SVM classifier only distinguishes between a subset of features (Diedrichsen & Kriegeskorte, 2017).

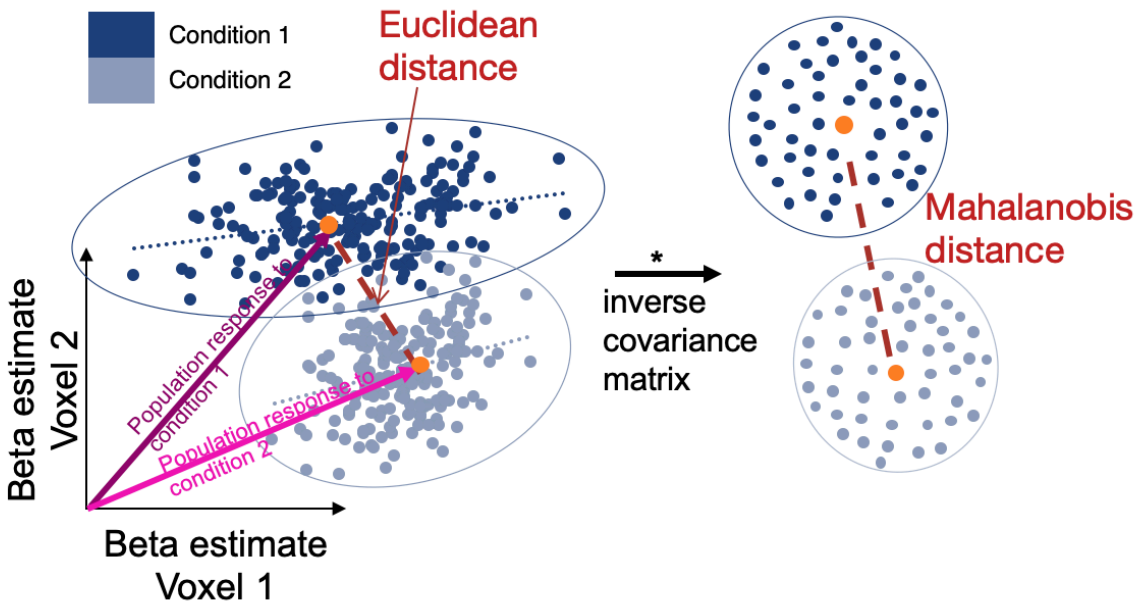

Figure 1. 4 Simplified 2-D visualization of RSA

RSA uses a distance measure to characterize the representational space in a ROI. Using Pythagorean theorem, one can calculate the distance (Euclidean distance, red*) between the mean vectors of both population responses (*orange*). However, to account for the multivariate noise of the data, the RSA algorithm multiplies the population response with the inverse covariance matrix of the multivariate noise. This result is the noise-normalized Euclidean distance, also called Mahalanobis distance. The line around the data points corresponds to the error ellipsoid and is only displayed for visualization purposes.*

Suppose we have the same brain responses for two conditions as in the previous section, then RSA tries to find the distance between the mean vector of each population response (**Figure 1.4**). Since the Euclidean distance does not account for the multivariate noise in each condition, we multiply the mean vector with the inverse of the covariance matrix of the noise to obtain the Mahalanobis distance. This transformation is therefore the multivariate equivalent to z-scoring in univariate analysis and can be thought of as the Euclidean distance in the transformed space. Nevertheless, spatial correlations due to voxel-by-voxel correlation

can still lead to dissimilar response patterns which results in distance estimates greater than zero (Walther et al., 2016). Therefore, it is necessary to cross-validate the distance estimates, resulting in the so-called Crossnobis distance, which renders the noise between conditions as independent (Kriegeskorte & Bandettini, 2007; Nili et al., 2014).

The resulting representational geometries can be characterized by representational dissimilarity matrices (RDMs). These RDMs abstract from individual responses in neurons and provide a sufficient statistic that are stable even when we compare idiosyncratic brains. Thus, we can correlate representations among different regions, groups of participants or species (Kriegeskorte, 2008).

1.9.5 Multivariate analyses that capture neural tuning

How much information a response pattern contains, depends on the shape of the tuning curve (Kriegeskorte & Wei, 2021). Thus, a set of tuning curves dictate the population response, from which we can obtain our representational distance measure (Kriegeskorte & Wei, 2021). Neural tuning is a descriptive tool, referring to a property of neurons by which they preferentially encode a specific type of information, e.g. thumb-movement-dependent firing in S1 neurons. A tuning curve reflects the change of mean neural activity of a neuron selective to a stimulus feature, e.g. higher activity during thumb movements than compared to little finger movements. Thus, the curve reflects how changes of the neuron's neural activity reflect a specific stimulus feature. Any tuning would suggest some kind of involvement of that neuron in information processing of that specific feature.

The tuning of these curves can also be modulated by spatial context (Maffei & Fiorentini, 1976), temporal context (Movshon & Lennie, 1979), internal states of animals such as attention (Treue & Trujillo, 1999), and learning (Schoups et al., 2001). For example, 'sharpening' of these curves would decrease their width and increase stimulus selectivity and thus could improve task performance (Schoups et al., 2001). RSA enables us to detect this stimulus selectivity by estimating the representational distance between stimuli. Higher stimulus selectivity should result in greater distances.

1.9.6 Functional connectivity analysis to inspect fMRI data

In the sections above, we focused on activation-based and information-based analysis approaches and how they enable us to capture cortical representations. Another major strength of fMRI is that it allows us to identify neural activity in networks of brain regions simultaneously (O'Reilly et al., 2012). More importantly, certain analysis approaches exploit the data to investigate functional interactions or even the information flow and how it changes

within a network of brain regions over time (Smith et al., 2012) or under different conditions (Cacioppo & Decety, 2011). Such approaches are usually referred to as functional or effective connectivity analysis (Friston, 2011; Stephan, 2004). A prominent technique to investigate functional connectivity is psychophysiological interactions (PPI) analysis. It is a measure of condition-dependent correlational changes between neural activity in various brain regions (Friston et al., 1997). PPI analysis requires identification of a seed region of interest under a specific experimental task. It does not allow one to infer the directionality of the information flow, but its whole-brain approach enables us to identify all other voxels across the brain that interact with the seed region of interest. In summary, PPI detects brain regions whose neural activity interacts with the physiological component (seed time series) under a psychological component (experimental condition). PPI analysis can be implemented as a GLM, whereby our univariate analysis is extended by two regressors: the seed time series and an interaction term (main effect of condition x seed time series). From a significant PPI effect (condition-dependent interaction increase) we can infer functional coupling between other voxels and the seed region of interest during a specific experimental condition manipulation.

PPI analysis has the potential to provide us with a more holistic view on somatotopic changes in the brain, by not only observing somatotopic changes but also taking networks of brain regions into account that might drive these changes. In chapter 3, will address how functional coupling between subcortical regions and S1 might contribute to changes in finger representations.

1.10 Aims of the thesis

The aim of this PhD thesis was to investigate cortical representational changes within somatotopic maps, in the absence of somatosensory input and propose top-down mechanisms that might mediate these changes. In two separate experiments we instructed i) healthy participants to perform a vibrotactile discrimination task ii) healthy participants and tetraplegic patients to perform (attempted) unimanual movements. In both experiments, we collected fMRI data.

The main open questions addressed in this thesis are:

(i) Do vibrotactile stimulus processing and stimulus feature storage, i.e. in the absence of tactile input, engage somatotopic maps in S1 during a vibrotactile frequency discrimination task?

(ii) During the same task, are somatotopic maps in S1 functionally coupled to a network of other brain regions during vibrotactile stimulation and is this coupling related task performance?

(iii) Can ipsilateral finger representations in S1 still be activated via bi-hemispheric connections after a partial or complete loss of peripheral sensory input?

1.11 Chapter 2 overview

In chapter 2, we address the debated role of S1 in tactile WM. We built on previous findings on somatotopic maps' involvement in somatosensory processing and investigate whether WM content also resides within these maps during the delay period of the task, i.e. in the absence of tactile input. Even though the task goal was to discriminate between two subsequent frequencies, separated by a delay period, we hypothesized that task-relevant features processing would reside within the somatotopic map of S1. Since the low spatial resolution during our neuroimaging did not allow us to capture small groups of frequency-tuned neurons, we used the well-capturable finger representations of S1 as a hallmark for somatosensory information processing and retention. Our results indicate that finger representations, captured via different multivariate analysis approaches, are modulated through task demands and provide new room for speculations on what role somatotopic maps in S1 play during tactile WM.

1.12 Chapter 3 overview

In chapter 3, we further explored the previously collected neuroimaging data (*chapter 2*). We focused on brain networks that influence somatotopic maps in S1 during somatosensory processing in a vibrotactile frequency discrimination task. We used PPI analysis to identify brain regions that were functionally coupled to finger-specific areas in S1. We found that dorsal striatum seemed to be functionally coupled to these areas during the first stimulation. Crucially, this functionally coupling appeared to predict task performance. This indicates that functional connectivity in this network could mediate task-relevant information processing, presumably via top-down control mechanisms.

1.13 Chapter 4 overview

In chapter 4, we investigated the effects on finger representations when an abrupt partial or full disconnection between periphery and the brain occurs. Such a disruption can occur following tetraplegia. In addition, tetraplegic patients also allow us to explore what mechanisms drive ipsilateral finger representations during unimanual movements, which is not fully resolved yet. Our results suggest that tetraplegic patients were still able to activate ipsilateral finger representations, captured by RSA analysis, during unimanual movements. This is very likely driven by bi-hemispheric connections since we also found such representations in a patient that showed a complete loss of sensory function in both hands.

1.14 Chapter 5 overview

In chapter 5, the main findings from chapter 2-4 are summarized, followed by a discussion of the individual findings. We also discuss limitations of our studies and present future considerations in the research of WM, tetraplegia, movement control and somatotopy.

2 Solving a working memory task modulates finger representations in primary somatosensory cortex

Finn Rabe, Sanne Kikkert, Nicole Wenderoth (2022). Solving a working memory task modulates finger representations in primary somatosensory cortex. *bioRxiv.*

2.1 Abstract

It is well-established that several cortical areas represent vibrotactile stimuli in somatotopic maps. However, less is known about whether somatotopic representations are modulated in the absence of tactile input. Here, we used a vibrotactile frequency discrimination task as a tool to investigate this in further detail. Participants were required to actively perceive and process tactile stimuli in comparison to a no-task control condition where the identical stimuli were passively perceived (no memory condition). Importantly, both vibrotactile stimuli were either applied to the right index or little finger, allowing us to investigate whether working memory (WM) task demands affect the geometry of these finger representations in S1. Using multi-voxel pattern analysis (MVPA) and representational similarity analysis (RSA), we found that S1 finger representations were more dissimilar during the memory than the no memory condition. Interestingly, this effect was not only observed while tactile stimuli were presented, but also during the delay period of the WM condition. These results suggest that when a task demands participants to attentively process tactile stimuli, then this modulates finger representation in S1.

2.2 Introduction

Topographic representations such as the somatotopic map in the somatosensory cortex have been shown to be ubiquitous in the cerebral cortex of mammals. They consist of orderly representations of receptor surfaces on different body parts (J. Kaas, 1997; J. H. Kaas, 1993; Penfield & Boldrey, 1937; Silver & Kastner, 2009). These somatotopic maps are incredibly specific to the point where the sensation of each finger can be assigned to its own cortical region, so called finger representations (Besle et al., 2013; Martuzzi et al., 2014; Sanchez Panchuelo et al., 2018; Sanders et al., 2019). Importantly, finger-specific somatosensory representations can be activated by tactile or proprioceptive stimulation, but additionally they are also modulated through other mechanisms like (i) *attempted movement*s which do not produce overt motor output or the associated tactile or proprioceptive feedback (P. Ariani et al., 2021; Guan et al., 2021; Kikkert et al., 2021) (ii) *observed* (Kuehn et al., 2018) or *actively imagined* touch (Schmidt & Blankenburg, 2019), (iii) or directing *attention* to a specific finger (Puckett et al., 2017).

Here we ask whether somatotopic representations in S1 are modulated by changing task demands during a vibrotactile frequency discrimination task, i.e. when somatosensory stimuli are (i) encoded, (ii) kept in WM and (iii) compared to a second stimulus for subsequent decision making (Christophel et al., 2017). This makes it an ideal paradigm to investigate whether task-demands modify the representational geometry in S1. Previous research suggests that S1 is not only involved in vibrotactile stimulus perception, but also in keeping information about the stimulus in working memory (WM) during the delay period of a vibrotactile frequency discrimination task, i.e. in the absence of tactile stimulation (Harris et al., 2001, 2002). Indeed, a non-human primate study recorded single-unit activity from the S1 hand area while subjects had to match an object with a specific surface to a previously presented surface stimulus (Y. D. Zhou & Fuster, 1996; Y. D. Zhou & Fuster, 2000). The authors observed cells that were not only active while the tactile stimulus was present, but also sustained their firing during the WM delay period. This suggests that primary sensory cortices could serve as a memory buffer for stimulus information (D'Esposito & Postle, 2015), an idea that has been conceptualized as the 'sensory recruitment' model of WM (Katus et al., 2015; Pasternak & Greenlee, 2005). According to this model, WM is maintained in those brain regions that are involved in encoding sensory stimuli.

Human neuroimaging studies on vibrotactile WM only partly support that S1 is involved in maintaining sensory information during the delay period. Several studies have shown that the average activity level of S1 (as detected by a "mass-univariate" statistical

approach) is not significantly larger during the WM delay period than during a control condition (for reviews see Christophel et al., 2017). Other studies, in contrast, used a more sensitive multi-voxel pattern analysis (MVPA) approach and were able to decode spatial features of Braille stimuli from S1 during the delay period (Schmidt & Blankenburg, 2018). MVPA can detect stimulus information in spatially distributed patterns of activation in a region of interest (ROI) by accounting for the covariance between all voxels, which mass-univariate analysis usually does not (Weaverdyck et al., 2020). Interestingly, similar to the aforementioned observations in non-human primates, during the delay period spatial layouts could be decoded from an area that usually represents the hand (Schmidt & Blankenburg, 2018). This area has been characterized by its fine-grained finger representations (Besle et al., 2013; Martuzzi et al., 2014; Sanchez Panchuelo et al., 2018; Sanders et al., 2019)

Here we used a tactile WM task to investigate whether somatotopic finger representations are modulated by task demands. To answer this question, participants were asked to perform a vibrotactile frequency discrimination task on the index or little finger while we collected fMRI data that were analyzed with multivariate analysis techniques. If we find above chance level classification accuracies and high representational dissimilarities between finger-related activity patterns in S1 during a specific task period, then this would indicate neural processing during this task period occurs in a somatotopic fashion. Lower classification accuracies and dissimilarities between fingers during a specific task period, by contrast, indicate that the S1 activity is not finger specific. While it is highly likely that task demands modulate somatosensory representations during the tactile stimulation periods, we aimed to see whether S1 processing occurs in a somatotopic fashion during the delay period, i.e. in the absence of tactile stimuli.

2.3 Materials and Methods

2.3.1 Participants

Thirty young healthy volunteers (19 females; mean age= 24.48, SEM= 0.44) participated in our study. Our sample size was comparable to those in previous reports on fMRI decoding of WM content using discrimination tasks (Ester et al., 2009; Schmidt et al., 2017). All participants were neurologically intact and reported to be right-handed. All of them gave written informed consent and the study protocol was approved by the local ethics committee (BASEC-Nr. 2018-01078). Three participants had to be excluded due to excessive head motion based on our criterion (see 'Preprocessing of fMRI data' section for more detail).

2.3.2 Experimental Procedure and Tasks

2.3.2.1 Tactile Stimuli

Vibrotactile stimuli (duration = 2s, sampling rate = 1kHz) were applied to the right index or right little finger using a MR-compatible piezoelectric device (PTS-T1, Dancer Design, UK). We selected these fingers as they have the largest inter-finger somatotopic distance (Besle et al., 2013; Ejaz et al., 2015; Kolasinski et al., 2016a; Sanders et al., 2019), allowing us to robustly detect the modulation of somatotopic representations by the WM task. The one bin piezoelectric wafers were mounted to the fingertips using custom 3D-printed retainers that were fixed with a Velcro strap. Participants were asked to report any tingling sensation in case the retainer was mounted too tightly. The stimulation consisted of mechanical sinusoids that were transmitted from the testing computer to the piezoelectric device using a C Series Voltage Output Module (National Instruments) and the in-house NI-DAQmx driver.

2.3.2.2 Sensory detection threshold estimation

To ensure similar task difficulty across runs of the main experiment (Harris et al., 2006), we determined the sensory detection threshold (SDT) for both fingers prior to starting the main experiment. SDT was defined as the stimulation intensity at which the participants detected the stimulus 50% of the time. We stimulated each finger only once per trial at base frequency (20 Hz) and participants were asked to press a button upon detection of a stimulation. To reliably estimate SDT, we applied a conventional Bayesian-based Quest procedure (QuestHandler in PsychoPy). After each detected or undetected stimulus the algorithm searched for the most probable psychometric function via maximum likelihood estimation over the course of 25 trials starting with a stimulation amplitude of 0.1 Volts (Watson & Pelli,

1983). The Weibull psychometric function was calculated using the following formula:

$$(1)\quad \Psi(x)=\delta\gamma+(1-\delta)[1-(1-\gamma)\exp(-10beta(x-T+\epsilon))]$$

where x is the stimulus intensity in Volts and T is the estimated sensory detection threshold. This procedure was performed prior to the first run. If the percentage of correctly discriminated memory trials in a run was below 60% or above 90%, then we redetermined the SDT using a shortened version of the Quest procedure. In such a case we started the Quest procedure with the previously determined stimulation intensity to reduce the number of iterations (new iterations = 7 trials). This procedure was applied to keep task difficulty at comparable levels throughout the experiment.

We analyzed changes in behavioral performance occurred across runs, potentially due to perceptual learning, cooling of the fingertips, or fatiguing effects using a repeated measures two-way ANOVA (2 fingers x 4 runs).

2.3.2.3 Main experimental task

The main experimental task was generated using PsychoPy (Peirce et al., 2019). The experimental task consisted of memory and no memory trials. During a memory trial, participants performed a two-alternative forced choice (2AFC) discrimination task. Two vibrotactile stimuli were consecutively applied to the same finger (i.e., the index or the little finger), separated by a jittered 6-8s delay. We targeted cutaneous mechanoreceptors that respond to stimulations in the flutter range (Mountcastle et al., 1967). One of two stimuli vibrated at 20 Hz (2s duration at SDT intensity) while the vibration frequency of the other stimulus varied between 22, 24 or 26 Hz (same duration and intensity). Participants had to indicate by means of a button press whether the first or the second stimulation was higher in frequency (half of the participants) or whether the first or the second stimulation was lower in frequency (the other half of the participants), following previously published procedures (Pleger et al., 2006, 2008, 2009). Responses were recorded via index and middle finger button presses of the other (left) hand using a MR-compatible fiber optic device. We randomized the order of how the response options (f1 and f2) appeared on the screen on a trial-by-trail basis to prevent somatotopy-specific anticipatory motor activity. After a 3s response period participants received visual feedback (1s) indicating whether their response was correct (highlighted by green color) or incorrect (red; **Figure 2.1**). Participants were instructed to focus their gaze on the fixation cross in the middle of the screen during the complete trial.

Vibrotactile stimuli trials targeted either the index or the little finger and which finger would be stimulated per trial was counterbalanced across each run.

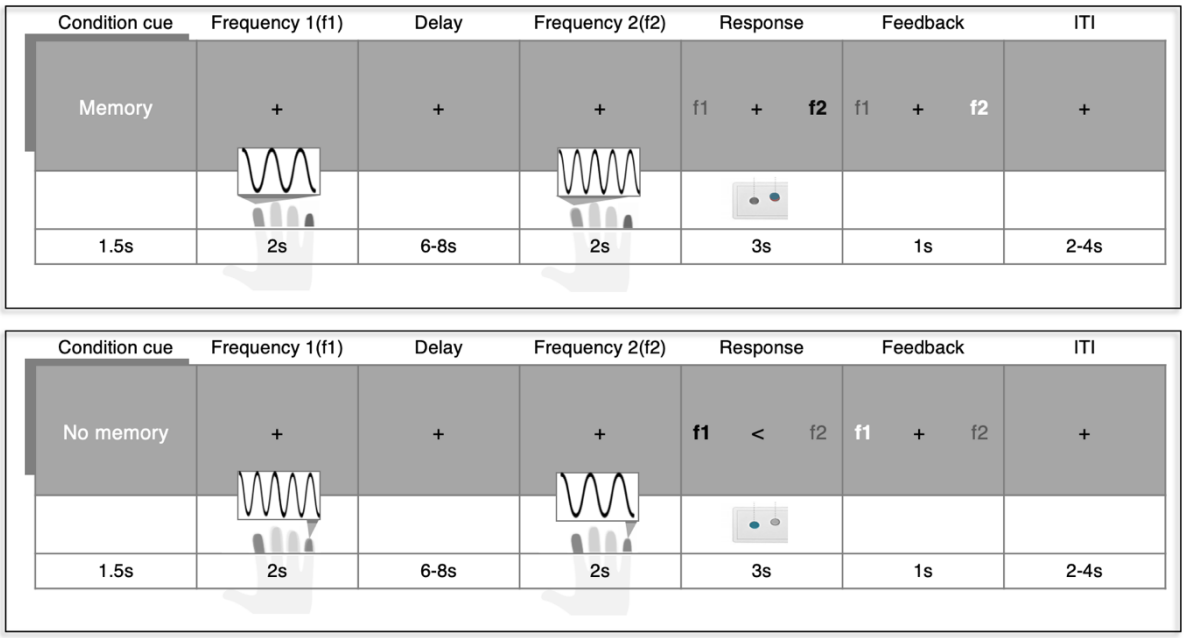

Figure 2. 1 Vibrotactile frequency discrimination task

During memory trials (top) two vibrotactile stimuli that differed in frequency were consecutively applied to the same finger (in this example the index finger). Both stimulations were separated by a jittered delay period, during which participants had to keep the first stimulation frequency (f1) in memory in order to compare it to the frequency of the second stimulus (f2). During the 3s response period participants had to indicate which of the two stimulation frequencies (f1 and f2) was higher by means of a left hand button press. The mapping between the discrimination response and which button to press was indicated on the screen and randomized across trials. Subjects received feedback whether their response was correct or incorrect. The target finger (index or little finger) were intermixed within a run and the inter trial interval (ITI) was jittered between 2-4s. During no memory trials (bottom), vibrotactile stimulations and visual information remained the same. However, participants were instructed not to focus on the stimulation and also not to compare the vibrotactile frequencies. They simply had to press the button indicated by the arrow in the middle of the screen.

To disentangle WM processes from general responses to the stimuli, we also included no memory trials. During a no memory trial participants received the exact same vibratory stimulations as during memory trials, but they were instructed not to focus on the stimuli or on their vibration frequencies. During the response period subjects were informed by a visual cue (pointing arrow) which button to press. To ensure participants did not switch cognitive strategies, the indicated response was always contrary to the response that would be expected when correctly discriminating both frequencies. Memory and no memory trials conditions were separated in mini blocks of 4 trials. Participants were informed whether they

had to perform the memory or no memory task by means of a visual cue (1.5s) at the beginning of each trial. Prior to the experiment, participants were familiarized with the memory and no memory tasks by completing 12 trials.

The order of stimulus sites (stimulated finger) was counterbalanced both within and across mini blocks. Stimulation frequencies were counterbalanced across the experiment. Each stimulus frequency was presented equally often in both memory and no memory condition. Jittered timings for Inter-stimulus-interval (ISI, 6-8s) and Inter-trial-interval (ITI, 2-4s) were randomly drawn from a uniform distribution. All participants completed 4 runs consisting of 48 trials each. Each run consisted of 6 memory and 6 no memory mini blocks in a counterbalanced order.

2.3.3 Behavioral analysis

We defined the discrimination accuracy per participant as the percentage of correctly discriminated trials separately for each condition. We expected that greater frequency differences would facilitate discrimination between both tactile vibrations while the stimulus site should have no effect. We therefore investigated whether behavioral performances differed across frequency differences and across fingers using a two-way repeated-measures ANOVA.

2.3.4 MRI data acquisition

Functional as well as structural MRI images were acquired on a Philips Ingenia 3 Tesla MRI (Best, The Netherlands) using a 32-element head coil. fMRI data was collected using an echo-planar-imaging (EPI) sequence acquiring 36 transversal slices centred at the bicommissural line and with whole brain coverage, though excluding most of cerebellum (repetition time (TR): 2s, echo time (TE): 30ms, spatial resolution: $3mm^3$, FOV = $222 \times 222mm^2$, 85° flip angle, slice orientation: transversal, SENSE factor (AP): 2, 472 functional volumes per run). Anatomical images were acquired during SDT estimation using a MPRAGE T1-weighted sequence (TR = 7.7ms, TE = 3.6ms, FOV = $240 \times 240mm^2$, flip angle: 8°, resolution: $1mm^3$, number of slices: 160, slice thickness: 2.2mm, slice orientation: sagittal).

2.3.5 Preprocessing of fMRI data

Conventional pre-processing steps for fMRI data were applied to each individual run in native three-dimensional space, using FSL's Expert Analysis Tool FEAT (v6.00; fsl.fmrib.ox.ac.uk/fsl/fslwiki). The following steps were included: Motion correction using MCFLIRT (Jenkinson, 2002), brain extraction using automated brain extraction tool BET

(Smith, 2002), high-pass filtering (100Hz), slice-time correction, and spatial smoothing using a 3mm FWHM (full width at half maximum) Gaussian kernel using FEAT. Functional data was aligned to structural images initially using FLIRT (Jenkinson & Smith, 2001), and optimised using boundary-based registration (Greve & Fischl, 2009a). BOLD EPI data was assessed for excessive motion using motion parameter estimates from MCFLIRT. If the functional data from a participant showed greater than 1.5mm (half the voxel size) of absolute mean displacement, this participant was excluded from all further analysis.

To reduce physiological noise artifacts, these CSF and white matter were used to extract scan-wise time series which were then added to the model as nuisance regressors in addition to the standard motion parameters.

Structural images were transformed to Montreal Neurological Institute (MNI) standard space using nonlinear registration (FNIRT), and the resulting warp fields were applied to the functional statistical images.

2.3.6 Definition of regions of interest

We used each individual participant T1-weighted image to create a cortical surface reconstruction by means of Freesurfer (Fischl et al., 1999). We identified regions of interest (ROIs), specifically SI, anatomically for each subject based on the probabilistic Brodmann area parcellation provided by Freesurfer (Fischl, 2012). More specifically, an S1 hand ROI was defined by combining Brodmann areas (BA) 1, 2, 3a, and 3b. We then converted this S1 ROI to volumetric space. Any holes were filled and non-zero voxels were mean dilated. Next, the axial slices spanning 2cm medial/lateral to the hand area (T. A. Yousry et al., 1997) were identified on the 2mm MNI standard brain (min-max MNI z-coordinates=40-62). This mask was non-linearly transformed to each participant's native structural space. Finally, we used this mask to restrict the S1 ROI and extracted an S1 hand area ROI. Similar ROI definition has been previously used (Diedrichsen, Wiestler, & Ejaz, 2013; Ejaz et al., 2015; Wiestler & Diedrichsen, 2013). The S1 hand area ROI was used to both extract time-binned estimates as well as to decode information about the stimulus site during the delay period. Additionally, we defined two ROIs (supramarginal lobule and inferior frontal gyrus) that were previously observed by MVPA studies to play role in WM. These ROIs were based on a functional contrast (memory vs. no memory) obtained from BOLD responses during the delay period. Each ROI was binarized and multiplied by its corresponding anatomical mask using both Harvard-Oxford and Juelich Histological Atlas.

2.3.7 Univariate analysis

First-level parameter estimates were computed per run using a voxel-based general linear model (GLM) based on the gamma hemodynamic response function (similar to Preuschhof et al., 2006). Time series statistical analysis was carried out using FILM (FMRIB's Improved Linear Model) with local autocorrelation correction.

To find neural correlates of WM we contrasted beta estimates from the delay period during memory trials to those in no memory trials. We then used a fixed effects higher-level analysis to average activity across runs for each individual participant. Finally, to make inferences on the population level, we computed a mixed effects analysis (Flame 1). From this we obtained statistical group maps (Z-statistic images) for each contrast of interest, e.g. contrasting memory delay activity to no memory delay activity. Z-statistic images were thresholded using clusters determined by $Z > 3.1$ and statistical significance was determined at the cluster level ($p < .05$ family-wise-error-corrected (FWE)).

To further explore whether finger specific activity levels were maintained in a somatotopic fashion, we first computed somatotopic ROIs by contrasting finger-specific activity during the first stimulation. We did this by contrasting activity associated with right index stimulations to right little finger stimulations, which elicited a finger specific map (finger cluster) in the lateral part of S1 while the reverse contrast revealed more medially located activity (**Figure 2.3A,** *middle*). These S1 activity maps were in line with previous findings on finger somatotopy.

We then compared z-scored beta estimates between trials where either the index or the little finger was stimulated within each finger ROI. Again, we computed a fixed-effects analysis as mentioned before. We extracted the beta estimates separately for each participant within each pre-defined finger cluster.

Information retention in WM is not always reflected by constant delay activity, especially when the duration of the delay period can be somewhat anticipated (Rose et al., 2016). WM delay activity has been shown to decrease until shortly before memory retrieval when the remembered stimulus information is reactivated as suggested by an increase of neural oscillations in the theta band (Rose et al., 2016). We therefore hypothesized that the BOLD activity level would vary in a U-shaped fashion over the delay period. To test this hypothesis, we conducted a parametric modulation analysis. Our parametric modulation regressor was modelled to predict activity in three consecutive time-bins of the delay period in a U-shaped manner (**Figure 2.4**). The length of each time-bin equaled one TR (i.e., 2s). Since we jittered the delay period between 6 and 8 s, we only modelled the first three time-

bins of the delay period (2-6s). The remaining time of the delay was modelled as a separate regressor of no interest. By contrasting memory and no memory trials, we obtained Z-statistic images. These images were thresholded using clusters determined by $Z > 3.1$ and a familywise error–corrected cluster significance threshold of $p < 0.05$ was applied to the suprathreshold clusters.

To further visualize the results of the parametric modulation, we extracted activity estimates per time-bin. To do so, we modelled each time-bin of the delay period separately in a voxel-based general linear model (GLM) based on the gamma hemodynamic response function. The remaining time of the delay was modelled as a separate regressor of no interest. We then extracted the z-scored estimates per time-bin within the previously defined S1 Hand area ROI. All statistical maps were overlaid onto a MNI152 standard-space T1-weighted average structural template image and projected onto a cortical surface using Connectome's Workbench (Marcus et al., 2011).

2.3.8 Variance inflation factor (VIF)

To test whether multicollinearity between the parameter estimates in our GLM was sufficiently low, we calculated the variance inflation factor (VIF). This represents how much the variance of an individual regressor can be explained due to correlation to other regressors in our model (Zuur et al., 2010). For each variable, VIF was computed by the following formula:

$$VIF = \frac{Var(E)}{Var(X)}$$

where *Var(E)* reflects the mean estimation variance of all regression weights (stimulation and information storage regressors for each finger) while *Var(X)* reflects the mean estimation variance in case all regressors would be estimated individually. A VIF of 1 indicates total absence of collinearity between the regressor of interest and all other regressors in our GLM while a large VIF signals a serious collinearity problem. There is no clear threshold for acceptable multicollinearity. Previous literature however recommends that the VIF is ideally smaller than 2.5 (Johnston et al., 2018). In our case, the VIF was 1.45, averaging across regressors reflecting the first stimulation, the delay and the second stimulation.

2.3.9 Multivariate Pattern analysis

2.3.9.1 Multi-voxel pattern analysis

We used multi-voxel pattern analysis (MVPA) to decode which finger was stimulated based on activity during both stimulus presentations (f1 and f2) and during the absence of tactile stimuli (delay period). This analysis was conducted for voxels within the S1 hand area mask that have been shown to possess fine-grained finger representations. First-level parameter estimates were computed for all events of each trial and each participant using a voxel-based general linear model (GLM) in SPM (v12) based on the gamma hemodynamic response function. This resulted in 192 beta estimates (48 trials x 4 runs) during each period per participant across both conditions. 96 beta estimates for each memory and no memory condition.

We trained a linear classifier (support vector machine, SVM) to predict which finger was stimulated in a specific trail based on the respective period activity using the nilearn toolbox (Abraham et al., 2014). We calculated classification accuracies using a leave-one-run-out cross-validation approach. The accuracies were averaged across folds, resulting in one accuracy per condition and per participant.

2.3.9.2 Representational similarity analysis (RSA)

RSA has the ability to identify the invariant representational structure of fingers independent of amplitude, shape and exact location of activated brain regions during the WM task (Ejaz et al., 2015). It allowed us to obtain a measure of how distinguishable somatotopic representations between working-memory and no working-memory trials are. We computed representational distances between activity patterns related to different fingers (index vs.little finger) for both working-memory and no working-memory conditions. The distances were obtained using a prewhitened crossvalidated Mahalanobis distances (Crossnobis distances, (Diedrichsen, Wiestler, & Ejaz, 2013; Walther et al., 2016). We obtained voxel-wise parameter estimates (betas) for each finger * memory condition * timepoint versus rest (using univariate analysis) and residuals of our GLM within the hand area of S1. These betas were prewhitened using the residuals. Based on the prewhitened betas, we computed squared Mahalanobis distances between all possible finger*condition*timepoint combinations for each fold (i.e. run) and averaged them across folds. A distance greater than 0 reflects dissociable cortical representations while 0 shows no dissociation. The distance measures between all possible representations were assembled in a representational dissimilarity matrix (RDM). For

visualization, we only extracted distances between the finger representations during memory vs. no memory for each time point (f1, delay and f2) of the task.

2.3.10 Statistical data analysis

To detect outliers, we used the robustbase toolbox (Finger, 2010). $\mathbf{S_n}$ identifies an outlier (x_j) if the median distance of x_i from all other points, was greater than the outlier criterion (λ=3) times the median absolute distance of every point from every other point:

$$(2)\quad \frac{med_{j\neq i}\,|\,x_i - x_j\,|}{S_n} > \lambda \; where \; S_n = \; c_n \underset{i=1:n}{med}\left\{\underset{j\neq 1}{med}|\,x_i - x_j\right\},$$

where c_n is a bias correction factor for finite sample sizes (Rousseeuw & Croux, 1993). We detected no outliers for behavioral data that had to be excluded from any further analysis.

Before conducting any repeated measures ANOVA testing, we validated the assumptions for normaility and spherecity using a Shapiro-Wilk and Mauchy test. Effect sizes of different variables were measured using eta squared. ANOVA analysis was done using the pingouin toolbox (Vallat, 2018). P-values were Greenhouse-Geisser corrected if sphericity could not be assumed. T-statistics were corrected for multiple comparisons using one-step Bonferroni correction.

Bayesian analysis was carried out using pingouin toolbox for the main comparisons to investigate support for the null hypothesis. Following the conventional cut-offs, a BF smaller than 1/3 is considered substantial evidence in favor of the null hypothesis. A BF greater than 3 is considered substantial evidence, and a BF greater than 10 is considered strong evidence in favor of the alternative hypothesis. A BF between 1/3 and 3 is considered weak or anecdotal evidence (Dienes, 2014; Kass & Raftery, 1995).

2.4 Results

2.4.1 Behavioral performance improved better with greater frequency differences

A two-way ANOVA showed that behavioral performances differed significantly depending on the frequency differences between the first and second vibrotactile stimulus ($F(2, 156) = 5.06$, $p < .001$, $\eta^2 = 0.06$); **Figure 2.2A**), but not between stimulated fingers ($F(1, 156) = .44$, $p = .51$, $\eta^2 < 0.01$). There was no interaction effect; $F(1, 156) = .88$, $p = .42$, $\eta^2 = 0.01$). A

post hoc test (Tuckey's HSD) on pairwise comparisons on frequency differences pairs revealed that discrimination accuracy was significantly different between 2 and 6 Hz differences (q = 4.48, p < .01) and showed no significant difference for the rest of the pairs (4 Hz vs 6 Hz: q = 2.67, p = .15 and 2 Hz vs 4 Hz q = 1.81, p = .41). We further analyzed whether behavioral performance changed across runs despite our efforts to re-adjust the detection threshold (**Figure 2.2B)** and found only insignificant differences across runs (F(3, 2496) = 2.0, p = .11, η^2 < 0.01) and across fingers (F(1, 2496) = .48, p =.49, η^2 < 0.01), and no significant interaction effect (F(3, 2496) = .47, p = .47, η^2 < 0.01).

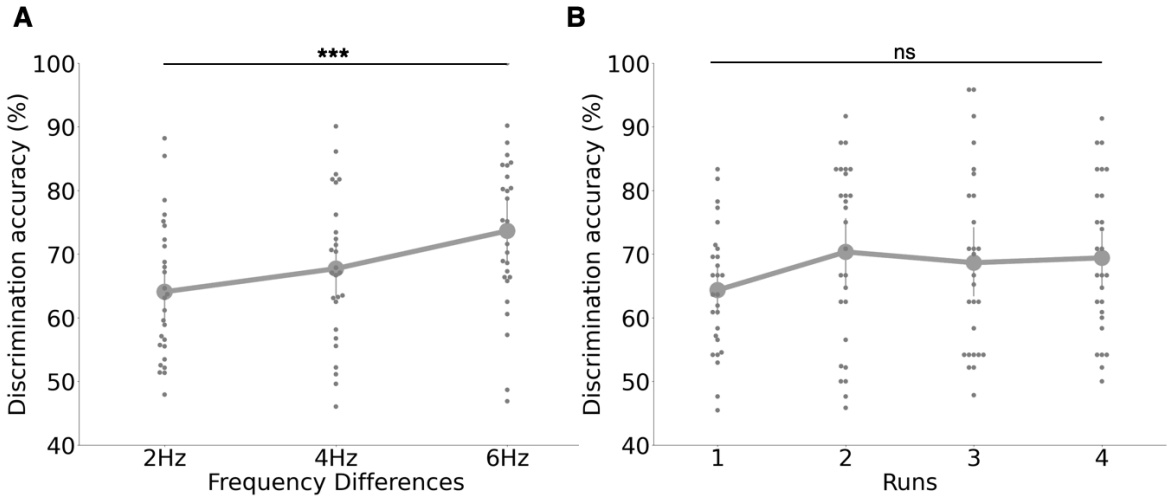

Figure 2. 2 Frequency discrimination results

(A) *Discrimination accuracy (% of correct answers) improved when frequency differences were larger. The blue dots reflect the group mean and the blue error bars indicate the standard deviation of the discrimination accuracy per frequency difference across the whole experiment.* ***B.*** *Behavioral performance was not significantly different across runs. The blue dots reflect the group mean and the blue error bars indicate the standard deviation of discrimination accuracies across each run. This demonstrates that our SDT criterion assured stable discrimination accuracies across runs. Grey dots represent individual participants' results. *** = p < .001; ns = non-significant.*

2.4.2 Mass-univariate analysis revealed no activations in S1 during somatosensory stimulus storage

We first contrasted activity levels during vibrotactile stimulation between fingers (i.e., index>little and little>index finger), and, as expected, observed separated finger representations in contralateral S1 (**Figure. 2.3A** *middle*) with the little finger being represented more medially than the index finger, which parallels previous findings (Besle et al., 2013; Kikkert et al., 2021; Kolasinski et al., 2016; Martuzzi et al., 2014; Sanchez Panchuelo

et al., 2018; Sanders et al., 2019). We then assessed whether finger-specific activity (measured through t-scored beta estimates) was modulated within the corresponding finger-specific cluster during memory compared to no memory trials at different timepoints of the task (f1, delay period, and f2). Our repeated measures ANOVA revealed that t-scored index finger beta estimates in the index finger cluster defined above significantly differed between time points (timepoints main effect: $F(1, 52) = 52.15$, $p_{corr} < .001$, $\eta^2 = .49$), but not between memory conditions (conditions main effect: $F(2, 26) = .14$, $p_{corr} = .5$, $\eta^2 < .05$) and. There was no significant interaction effect ($F(2, 52) = 2.04$, $p_{corr} = .14$, $\eta^2 < .05$; **Figure 2.3A,** *left*). Extracted t-scored little finger beta estimates from the little finger cluster also revealed a time point main effect ($F(1, 52) = 38.63$, $p_{corr} < .001$, $\eta^2 = .45$), no interaction effect ($F(2, 52) = .54$, $p_{corr} = .58$, $\eta^2 < 0.05$; **Figure 2. 3A,** *right*), and additionally a condition main effect $F(1, 26) = 8.75$, $p_{corr} < .01$, $\eta^2 < .05$).

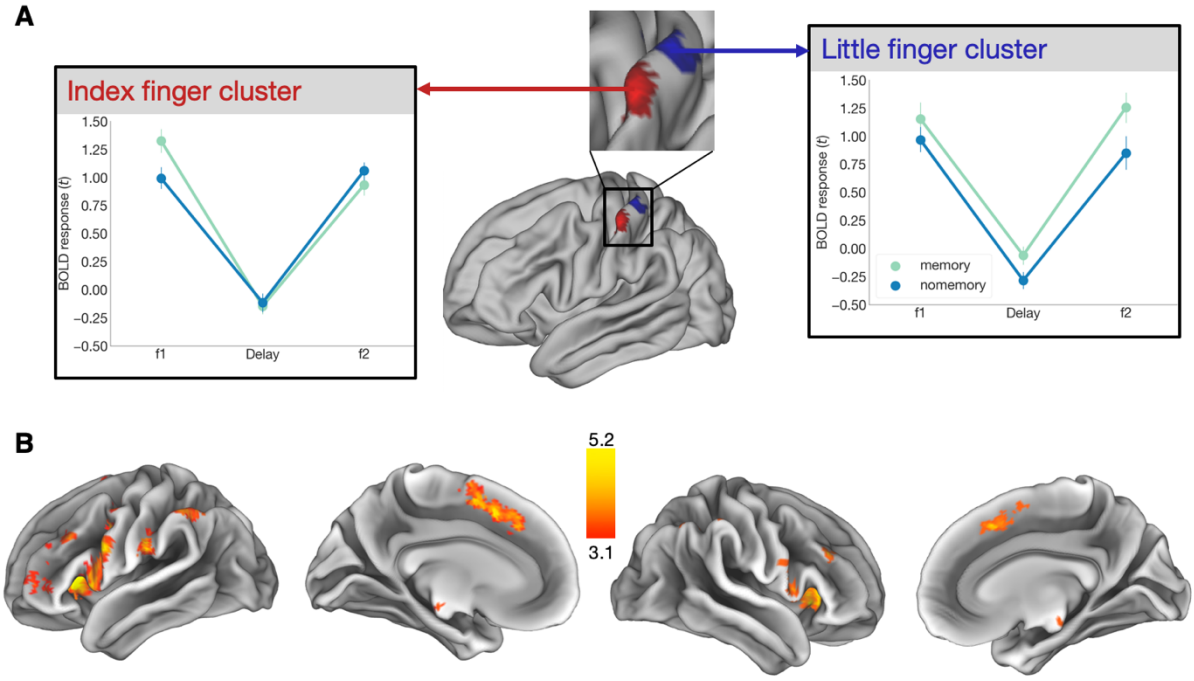

Figure 2. 3 Univariate group results during presence and absence of tactile stimulation

A*. We determined brain regions that were more active during the delay period of the memory compared to the no memory condition. A statistical map (Z > 3.1) was obtained by contrasting delay period activity in memory trials to no memory trials. The map was projected onto a cortical surface contralateral (*top*) and ipsilateral (*bottom*) to the stimulus site. Maintaining tactile information during the delay period recruited a network of brain regions (for more details, see* ***Table 1****).* ***B.*** *S1 areas activated during index (red) and little (blue) finger stimulation (*middle*). Clusters activated during index and little finger stimulation Z-statistic images were*

thresholded using clusters determined by Z > 3.1, p < .05 family-wise-error-corrected (FWE) cluster significance and were projected onto a cortical surface. Finger maps were located in contralateral S1. We then extracted the t-scored beta estimates within these finger-specific S1 areas during memory and no memory trials at different timepoints (f1, delay and f2) by contrasting cluster-specific finger activities (e.g. index finger cluster: index finger memory trials > little finger memory trials; bottom). Point plots are centered at the mean and error bars reflect the standard error.

Finally, we determined brain areas that were more active during the delay period in the memory compared to the no memory condition. We found that maintaining tactile information during the delay period involved a distributed brain network: i.e., bilateral frontal lobe, bilateral (medial/inferior) frontal gyrus (MFG, IFG), bilateral pre-motor cortex and supplementary motor area (PMC, SMA), contralateral secondary somatosensory cortex (S2), bilateral inferior parietal lobule (IPL), bilateral superior parietal lobule (SPL), bilateral supramarginal gyrus (SMG), bilateral caudate, bilateral thalamus, bilateral nucleus accumbens, and bilateral insula (**Figure 2.3B**, **Table 2.1** and **Appendix 2.1**). As in previous human WM fMRI studies, this univariate analysis did not reveal significant S1 activity.

Anatomical region	**Peak MNI Coordinates**			**Mean Fisher Z**	**U-shaped activity**
	X	Y	Z		
Left Frontal Pole	-42	52	2	4.33	3.29
Right Frontal Pole	40	46	32	3.86	3.16
Left IFG	-52	16	2	5.14	6.44
Right IFG	58	10	18	4.59	5.47
Left MFG	-44	30	34	4.45	-
Left PMC (+SMA)	-4	8	50	5.49	5.81
Right PMC (+SMA)	8	20	46	5.78	5.66
Left S2	-56	-23	20	3.25	5.75
Right S2	54	-14	16	-	5.14
Left S1	-54	-22	46	-	5.63
Right S1	56	-16	40	-	5.75
Left IPS	-42	-52	48	5.14	-
Left IPL	-56	-20	28	4.78	5.52

Right IPL	46	-48	52	4.86	5.67
Left SMG	-42	-46	40	4.77	-
Right SMG	51	-32	46	4.16	-
Left SPL	-50	-48	58	4.64	4.97
Left Insular cortex	-30	24	6	5.61	5.41
Right Insular cortex	36	22	-2	5.41	5.32
Left Accumbens	-12	14	-6	5.27	-
Right Accumbens	10	12	-4	4.16	-
Left Putamen	-18	6	-10	4.96	4.42
Right Putamen	20	10	-8	4.34	3.71
Left Caudate	-12	18	0	4.80	5.45
Right Caudate	14	18	4	4.97	4.32
Left Thalamus	-8	-24	-16	3.86	3.81
Right Thalamus	2	-20	-12	3.91	3.99

Table 2. 1 Clusters of activation during delay period

Identified brain regions in which the local activity during the delay period reflected tactile WM processing as shown in Figure 2.3B. In a next step we parametrically modulated the delay activity, assuming a U-shaped activity during the delay period. For visualization purposes overlap of brain areas was just added the additional z stats for the parametric modulation results. All z-statistic images were thresholded using clusters determined by $Z > 3.1$ and $p < .05$ family-wise-error-corrected (FWE) cluster significance. Mean Fischer Z indicates peak z-values. Areas were labeled according to the Juelich Histological Atlas and Havard-Oxford (Sub-)cortcial Structural Atlas (Eickhoff et al., 2005). MFG= medial frontal gyrus, IFG = inferior frontal gyrus, PMC = pre-motor cortex, SMA = supplementary motor area, IPL = inferior parietal lobule, SPL = superior parietal lobule, SMG = supramarginal gyrus.

2.4.3 Temporal modulation of delay period activity in contralateral S1

We hypothesized the reason why we did not find significant S1 activations during delay period could be due to the temporal unfolding of the S1 BOLD signal during that period. Thus, we were interested to examine whether brain activity temporally changed during the delay period. We parametrically modulated the delay period regressors by an hypothesized U-shaped activity changes and computed the associated statistical maps. A U-shaped activity modulation was found in a similar network of brain regions as displayed in **Figure 2.4** and **Appendix. 2.2**. In addition, we also found significant changes in BOLD signal in bilateral S1 and S2. S1 activity overlapped with the area that usually represents the hand. For

visualization purposes only, we extracted the activity at each time bin (i.e., from a separate GLM not involving a parametric modulation regressor) within the contralateral S1 hand area to demonstrate U-shaped activity across time bins (**Appendix. 2.3**) Detailed cluster information is displayed in **Table 2.1**.

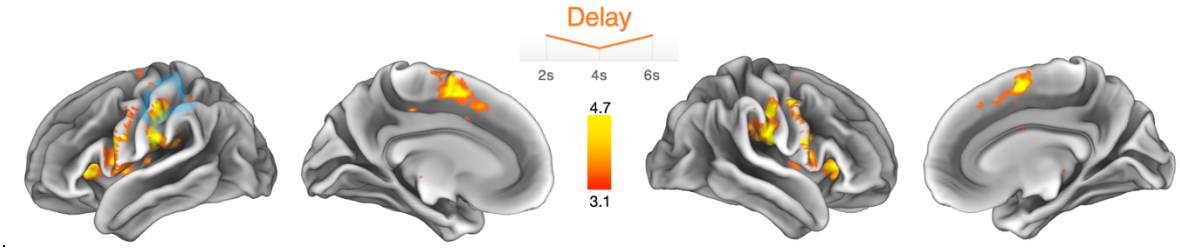

Figure 2. 4 U-shaped parametric modulation of WM-related activity

Brain regions exhibiting u-shaped modulated delay activity patterns (see insert at the top reflecting the parametric modulator entered into the GLM) during the delay period (2-6s). The contrast shows the difference between the memory and no memory condition in the contralateral (left) and ipsilateral hemisphere (right). The area highlighted in blue represents the S1 hand area.

2.4.4 Finger-specific representational changes during vibrotactile frequency discrimination

We hypothesized that executing a WM task would modulate finger specific representations in S1. To test this hypothesis, we used MVPA to decode the stimulated finger (i. e., index versus little finger) during the first stimulation (f1), during the delay period, and the second stimulation (f2) separately for memory and no memory trials (**Figure 2.5A**). We did this in the contralateral S1 hand ROI, which has shown to possess fine-grained finger representations (Besle et al., 2013; Martuzzi et al., 2014; Sanchez Panchuelo et al., 2018; Sanders et al., 2019), and a control white matter ROI.

First, we investigated whether our MVPA results were greater than chance level. Permutation tests allowed us to obtain approximated chance levels. Indeed, classification accuracies were significantly greater than this chance level for f1 and f2, irrespective of whether it was a memory or no memory trial ($t(25,25) >= 13.24$, $p < .001$). During the delay period, however, classification exceeded the chance level only for memory trials ($t(26) = 4.55$, $p < .001$) but not for no memory trials ($t(26) = 1.5$, $p = .15$).

Second, classification accuracies obtained from contralateral S1 hand area differed significantly between time points (f1, delay, and f2; time point main effect: $F(2, 52) = 156.52$, $p_{corr} < .001$, $\eta^2 = .77$) and between memory conditions (condition main effect: F(1,

26) = 48.42, p_{corr} < .001, η^2 < .05). There was no interaction effect (i.e., F(2, 52) = .5, p_{corr} = .59, η^2 < 0.001).

We then investigated the representational geometry of memorized tactile stimuli (**Figure 2.5B**). We hypothesized that executing a WM task would modulate the finger representational geometry in S1. Our repeated measures ANOVA revealed that the cross-validated Mahalanobis (Crossnobis) distances between fingers obtained from the contralateral S1 hand area differed significantly between time points (f1, delay, and f2; time point main effect: F(2, 52) = 151.21, p_{corr} < .001, η^2 = .73) and between memory and no memory trials (condition main effect: F(1, 26) = 39.81, p_{corr} < .001, η^2 = .06). We also found an interaction effect (i.e., F(2, 52) = 28.65, p_{corr} < .001, η^2 < 0.05). We could show that geometrical differences of finger representations between memory versus no memory trials reached significance when independently tested for each of the three time points and, interestingly, for the delay period (i.e. in the absence of any tactile stimulation). This was confirmed by pairwise comparisons (f1 memory vs. f1 no memory: t(26) = 4.09, p_{corr} < .01; BF_{10} = 81.73 , Delay memory vs. delay no memory: t(26) = 2.9, p_{corr} < .05; BF_{10} = 5.96, f2 memory vs. f2 no memory: t(26) = 7.4, p_{corr} < .001; BF_{10} > 100, with the Bayes factor (BF) showing substantial evidence in favor of the null hypothesis.

We also explored ROIs of the superior parietal lobe (SPL; **Figure 2.5C**) and inferior frontal gyrus (IFG; **Figure 2.5D**) that have been implicated to be involved in vibrotactile WM (Schmidt et al., 2017, 2021; Schmidt & Blankenburg, 2018). ROIs were based on clusters obtained in the univariate analysis described in *Methods section (Defining regions of interest*). We found no significant differences in classification accuracies based on activity patterns within the contralateral IFG (time point main effect, F(2, 52) = 0.93, p_{corr} = 0.4, η^2 < .05; condition main effect, F(1, 26) = 0.38, p_{corr} = 0.55, η^2 < .05; and time point x condition interaction effect F(2, 52) = 1.28, p_{corr} = .28, η^2 < .05) or within the contralateral SPL (time point main effect, F(2, 52) = .75, p_{corr} = .46, η^2 < .05; condition main effect, F(1, 26) = .85, p_{corr} = .37, η^2 < .05; and time point x condition interaction effect F(2, 52) = .68, p_{corr} = .51, η^2 < .05).

Together, these results suggest that during a vibrotactile WM task activit is modulated in a finger-specific fashion in S1, even in the absence of any tactile stimulation, but not in other areas of the WM network.

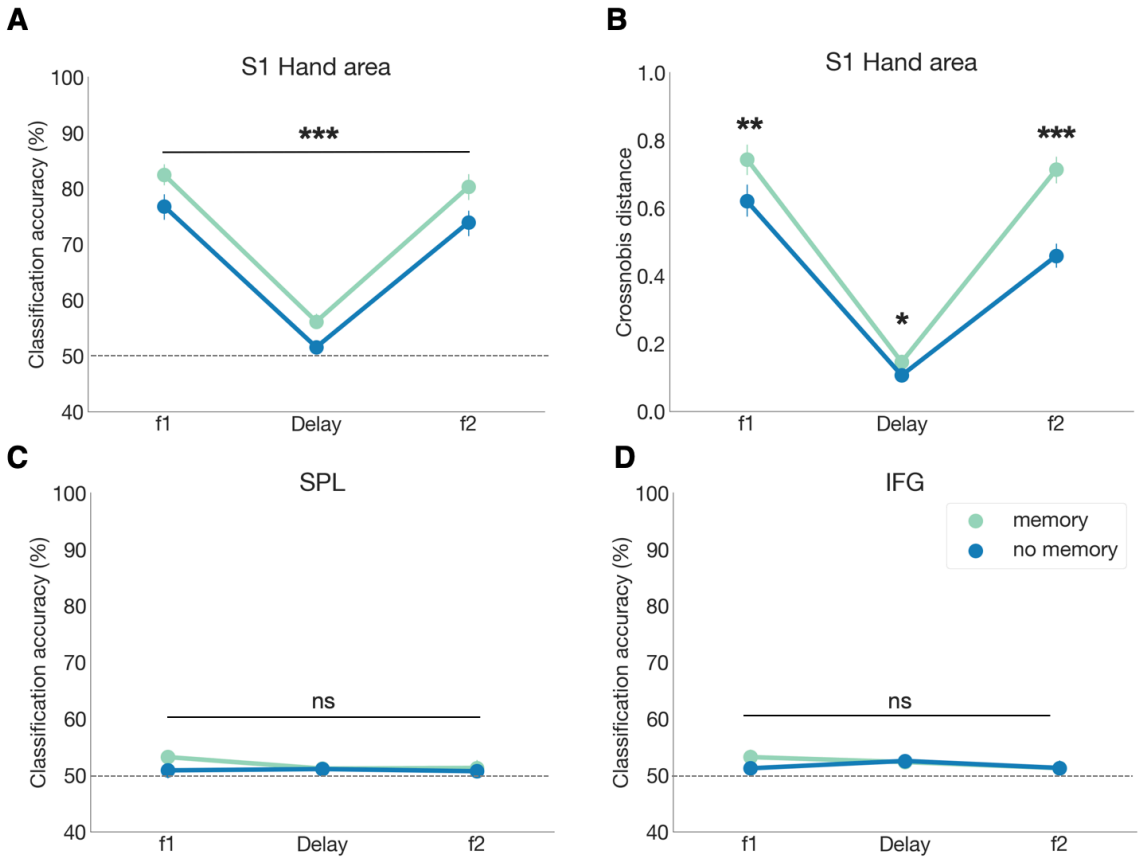

Figure 2. 5 Multivariate results on somatotopic modulations during WM task

We investigated whether activity patterns within a ROI with fine-grained finger somatotopy became more distinct at different timepoints (f1, delay and f2) during memory trials compared to no memory trials. ***A****. Classification accuracies (index vs. little finger) based on activity patterns in hand area within contralateral S1.* ***B****. Cross-validated Mahalanobis (Crossnobis) distances between fingers x condition in the same ROI.* ***C,D****. Further explorative analysis of ROIs that previously were indicated to be involved in vibrotactile WM, but where no fine-grained somatotopy is assumed. The point plots are centered at the mean and error bars reflect the standard error. Grey dotted lines reflect the theoretical chance level. If interaction effects were significant, pairwise comparison results for comparing memory vs. no memory conditions separately for each time point are indicated by * p < .05, ** p < .01 *** p < .001. S1 = primary somatosensory cortex, IFG = inferior frontal gyrus, SPL = superior parietal lobule.*

2.5 Discussion

In the present study, we demonstrated that finger-specific, somatosensory information in S1 is modulated by cognitive processes underlying a tactile WM task. This was the case during the tactile stimulation periods but also during the delay period (i.e. in the absence of any tactile stimulation). We propose that performing a WM task significantly modulated finger representations in S1, probably due to top-down control mechanisms that are associated with attentional control and sharpening tuning curves of neurons in S1.

2.5.1 Modulation of finger representations during stimulus perception

When exposed to a stimulus, stimulus-selective neurons are activated that can be quantified using tuning curves. Previously, specific neurons have shown 'tuned' responses to different features of the stimulus, e.g. stimulus location or stimulus orientation (Campbell et al., 1968; Henry et al., 1974; Scobey & Gabor, 1989). For instance, responses of neuronal populations in primary visual cortex (V1) can be modulated by changes in stimulus orientation (Hubel & Wiesel, 1968). The product of multiple tuning curves can be defined as the neural population code (Ben-Yishai et al., 1995; Georgopoulos et al., 1986). A linear decoder has the ability to capture the information kept in the neural population code (Kriegeskorte & Wei, 2021). Similarly, neural tuning also determines the representational geometry in the multivariate response space and these changes in geometry can be detected by RSA (Kriegeskorte & Wei, 2021). Our data indicates that neural tuning was modulated by the task demands of the WM task. Interestingly, this effect was not only present during stimulus presentation but, to an extent, also during the delay period.

It is uncertain which specific cognitive mechanism might have driven the observed S1 modulation. A discrimination task usually requires the enhancement of neural activity related to relevant stimuli and suppressing of activity related to irrelevant stimuli. Such amplification of relevant information has been conceptualized as generalized models of attention (for a review see, Burton & Sinclair, 2000). Attention has been suggested as an integral part of performing WM tasks (Cowan et al., 2013; Logie & Cowan, 2015; Schmidt & Blankenburg, 2018, 2019) as it filters information by sensory modality or by body location (Gomez-Ramirez et al., 2011) and, thereby, attention regulates what will be cortically represented and what will not (Desimone & Duncan, 1995). Furthermore, it has been shown that volitionally directing attention towards a spot on the body surface which was tacitly stimulated increases BOLD responses in S1 (Nelson et al., 2004a; Puckett et al., 2017; Sterr et al., 2007). Even the expectation over being stimulated on a specific finger was sufficient to modulate neural

activity in S1 in a somatotopic manner (Roland, 1981, Drevet et al. 1995). Our multivariate results support this notion. During both time points of stimulation (f1 and f2) we obtained higher classification accuracies and crossnobis distances for the memory than the no memory condition from activity patterns in the S1 hand area.

There is accumulating evidence that attention modulates tuning curves in the specific sensory modality (Bisley, 2011; McAdams & Maunsell, 1999; Reynolds et al., 2000). In our case, shifting attention to either index or little finger would relocate the spotlight of the attentional field accordingly in order to modulate responses in those voxels that somatotopically represent the attended finger. This extends recent univariate findings on attentional modulations of finger representations in S1 using ultra high field fMRI (Puckett et al., 2017). In that study, participants had to shift their attention to one (indicated by a cue) of the four simultaneously stimulated finger tips at a time. Compared to a control condition they found distinct finger representations in S1, suggesting a somatotopic change due to task demand.

2.5.2 Modulation of finger representations during the WM delay period

Interestingly this effect was not only present during stimulus presentation but, to a smaller extent, also during the delay period. Our analysis of the delay period revealed that finger representations in S1 were modulated by the WM task, even in the absence of tactile stimuli. The general involvement of S1 is in line with neuroimaging studies in humans using MVPA revealing that tactospatial information is retained during the delay period by a neural population code in S1, SPL, PMC and posterior parietal cortex (PPC) while preserved frequency information is reflected by activity patterns in dorsal PMC, SMA and IFG (Schmidt et al., 2017; Schmidt & Blankenburg, 2018).

However, our result needs to be interpreted with caution since the memory delay period in our experiment was relatively short (6-8s) compared to other fMRI studies investigating vibrotactile WM that often employ delays of 12s or more to avoid any carry-over effects of the tactile stimulus (Schmidt & Blankenburg, 2018; Wu et al., 2018). The low VIF of the regressors suggested that activity related to stimulus perception and WM storage could be disentangled by our model. However, based on our study design alone, it is difficult to reliably disentangle whether the effects during the delay period truly represent WM processes or rather residue brain activity from the stimulation period which might differ due to task demands.

Therefore, this result could also be interpreted along the lines of spatial attention. Models of attention-based rehearsal assume that spatial attention contributes to spatial

contents of WM (Awh et al., 2006; Awh & Jonides, 2001; Theeuwes et al., 2009). This could occur through focusing attention to memorized locations during the delay period of the WM tasks (Awh et al., 2000; Jha, 2002). In addition, these shifts have been shown to reflect dynamic strategies to enhance memory accuracy (Awh et al., 2006; Awh & Jonides, 2001; Katus et al., 2014).

Note that the decoded stimulus locations were task-irrelevant features in our case, therefore unlikely to relate to discrimination performance. Nevertheless, spatial attentional shifts between memory and no memory trials could have at least led to transient storage of stimulus location information. It is likely that when stimulus location information becomes task-relevant, then it could also influence task performance. A human psychophysical study demonstrated that when two subsequent vibrotactile stimuli are applied to the same finger or to the corresponding finger of the other hand, discrimination performance was better compared to trials where stimuli were sequentially delivered to different fingers (Harris et al., 2001).

The hypothesis that attentional mechanism might be an important mediator of the observed modulation of finger representations during the delay period receives indirect support from the temporal modulation of brain activity during that period. In line with previous research (Pasternak & Greenlee, 2005; Preuschhof et al., 2006), we identified a widespread parieto-fronto-insular network which is typically involved in tactile WM. We could show that fronto-partial areas, insular cortices, subcortical regions (i.e. caudate and thalamus), S1 and S2 demonstrated a U-shaped activity profile across the delay period, which might provide a glimpse into the temporal modulation of WM related brain activity (Cohen et al. 1997). Task-relevant modulation could occur through prefrontal cortex (PFC) by modulating cortical representations of WM contents via top-down control in order to guide behavior (for review, see Gazzaley & Nobre, 2012).

Indeed, the frontal-striatal-thalamic loops could play a key role in boosting relevant stimulus information while reducing irrelevant ones (Staines et al., 2002, McNab et al. 2008). It is likely that the final increase in delay activity might be driven by anticipation of increasing attentional demands, although we jittered the length of the delay period to prevent for anticipatory activity (Rose et al., 2016). Therefore, it is very likely that attentional mechanisms which are closely intertwined with WM (LaBar et al., 1999; Naghavi & Nyberg, 2005) are driving our results.

In summary, our findings are in line with the idea that greater representational dissimilarities during WM might reflect attentional top-down control which optimally tunes somatotopic finger representation for performing the WM task.

2.6 Conclusions

Our results extend previous findings on somatotopic representations of S1 by confirming that changing task demands during a vibrotactile frequency discrimination task modulate finger representations. Higher classification accuracies and larger dissimilarities between finger representations suggest that neural tuning was sharpened, most likely due to top-down attentional mechanisms that are inherent to WM tasks.

2.7 Appendices

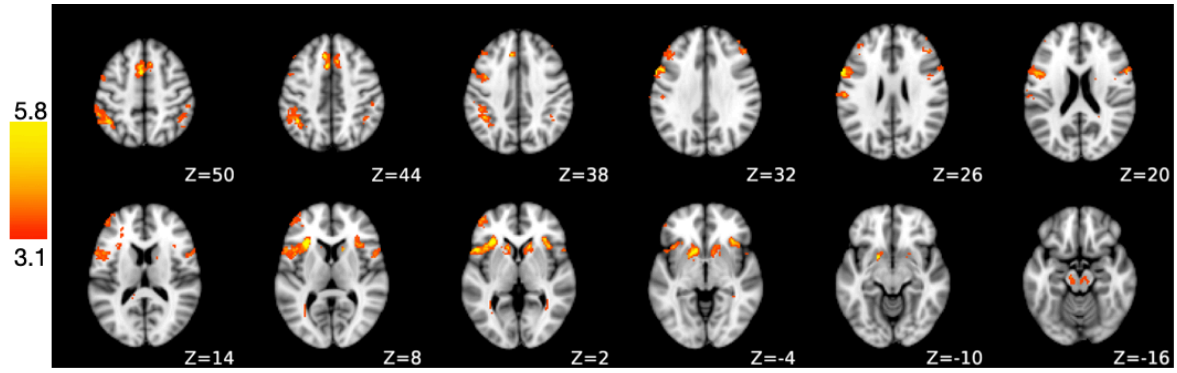

Appendix 2. 1 Slice view of univariate group results.

We identified brain regions that were more activate during the delay period of the memory compared to the no memory condition. A statistical map (Z > 3.1) was obtained by contrasting modulated delay period activity in memory trials to no memory trials.

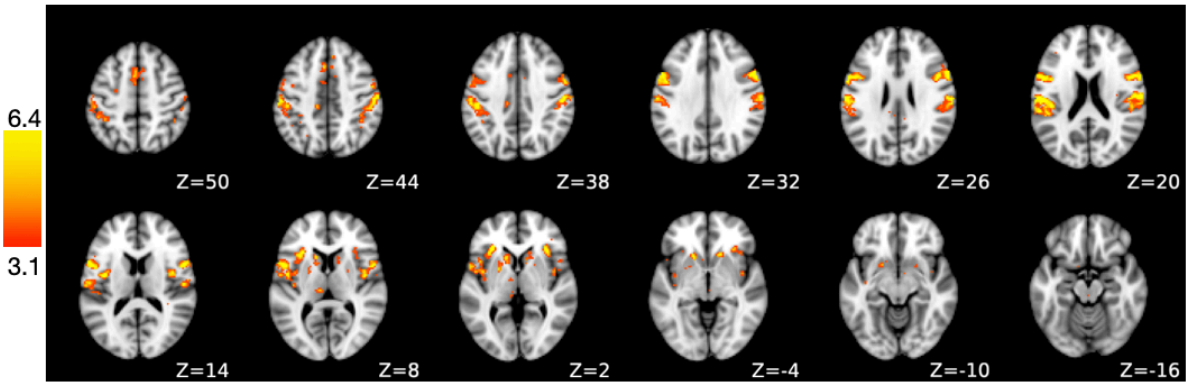

Appendix 2. 2 Slice view of parametric modulation results during delay period

We identified brain regions exhibiting u-shaped modulated delay activity patterns during the delay period (2-6s). A statistical map (Z > 3.1) was obtained by contrasting delay period activity in memory trials to no memory trials.

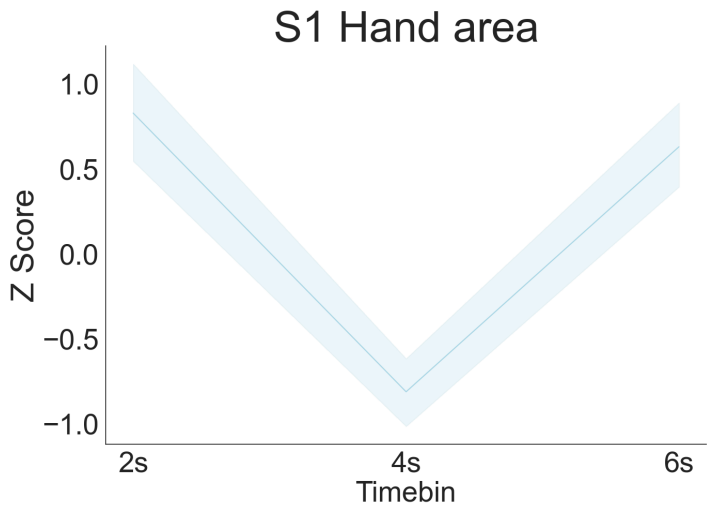

Appendix 2. 3 Time-binned S1 hand area activity during delay period

For visualization purposes only, each time point between 2 and 6s of the delay period (each time bin corresponding to one TR) was modeled as a separate regressor in a univariate GLM. Z scores of the beta estimates were extracted from the S1 hand area for each time bin of the delay period and averaged across participants. Blue shading reflects the 95% confidence interval.

3 Performing a vibrotactile frequency discrimination task modulates coupling between S1 and dorsal striatum

Finn Rabe, Sanne Kikkert, Nicole Wenderoth (2022). Performing a vibrotactile frequency discrimination task modulates coupling between S1 and dorsal striatum

3.1 Abstract

Tactile stimulations of different body parts result in distinct activity patterns in primary somatosensory cortex, known as somatotopy. Recently, we could show that when tactile stimuli are either passively perceived or actively processed during a vibrotactile frequency discrimination task, somatotopic maps in S1 were modulated by task demands. Specifically, the attempt to meet task demands (successful frequency discrimination) resulted in more dissociable finger representations in the hand area of S1 (Rabe et al., 2022), presumably because task-relevant information was enhanced in somatotopic coordinates. These changes in S1 activity were accompanied by brain-wide activity changes in neural networks known to be involved in working memory (WM) and attentional control. However, little is known about whether performing a tactile WM task changes the functional connectivity between S1 and these neural networks. In the current study, we used a psychophysiological interaction (PPI) analysis to identify brain regions that change their functional coupled to S1 during vibrotactile stimulations when a WM-task is performed. We found that left S1 increased functional connectivity with right putamen and caudate, subareas of the dorsal striatum, during the first stimulus presentation in the WM task and that connectivity changes between these areas predicted task performance but was unrelated to modulating somatotopic representations in S1.

3.2 Introduction

Tactile stimulations of different body parts result in distinct cortical representations across monkeys and humans, known as somatotopy (Romo & Salinas, 2003; Stippich et al., 1999). However, S1 activity is not solely driven by afferent somatosensory input. For example, shifting attention to tactile stimuli or even anticipating the stimulus (Drevets et al., 1995; Meyer et al., 1991; Roland, 1981, 1982) can increase neural activity in S1 beyond levels typically observed during passive perception. We have recently demonstrated that during a vibrotactile frequency discrimination task, the cortical representational geometry in S1 changed depending on task demands (Rabe et al., 2022). Thus, processes inherent to the working memory (WM) task modulated the cortical representations of the stimulus location resulting in more dissociable finger representations in S1, presumably to enhance task-relevant processing within finger-specific maps S1. However, which brain area or network is involved in modulating neural activity in S1 and, particularly, its somatotopic maps during a tactile WM task is currently unknown.

The function of elevating activity towards relevant information while suppressing neural activity to irrelevant stimulus information has been conceptualized as attention (Desimone & Duncan, 1995; Burton & Sinclair, 2000). In fact, it is generally accepted that attention is an important mechanism inherent to WM tasks (for review, see Oberauer, 2019). For example, tactile attention influences such processing in the primary somatosensory cortex (S1) via elevation of neural activity to task-relevant features of the stimulus, e.g. frequency or duration (Burton & Sinclair, 2000; Sinclair et al., 2000). It is also known from work in monkeys (Shoham & Grinvald, 2001; Tommerdahl et al., 1993) and humans (Francis et al., 2000a; Sanchez-Panchuelo et al., 2010; Schweizer et al., 2008) that selective information processing based on the stimulus location, modulates the cortical representation of which body part was stimulated during tactile stimulation. However, how performing a vibrotactile working memory tasks with different fingers modulates cortical representations in comparison to passively perceiving vibrotactile stimuli remains not fully unexplored. Previous neuroimaging studies in humans have demonstrated that specific task demands (e.g. voluntarily shifting attention to tactile stimuli on different parts of the body) can increase the BOLD signal in somatosensory cortices (Goltz et al., 2013; Nelson et al., 2004a; Puckett et al., 2017; Sterr et al., 2007), insular cortex, and subcortical regions (Rabe et al., 2022; Sörös et al., 2007). Additionally, neural activity increases could be observed in S2 and inferior parietal cortex (Fujiwara et al., 2002; Ledberg et al., 1995; Mima et al., 1998; Nelson et al., 2004b).

However, little is known about how WM task demands modulate the connectivity between these areas and S1 in order to optimize behavioral performance and, particularly, whether areas upstream from S1 might modulate somatotopic maps. One approach to investigate functional dependencies between brain regions is correlation analysis. To implement this, individual activations in a certain brain region of interest (ROI) can be extracted and then be correlated with other ROIs. Using such an approach recently revealed a linear relationship of attention-related neural activity between intrahemispheric somatosensory cortices during vibrotactile stimulation (Goltz et al., 2013).

Here we aimed to examine which brain regions contribute to top-down modulation of (low level) somatotopic activity in S1 during a vibrotactile discrimination task. We used an assumption-free approach to identify brain regions showing correlated activity with finger specific activations in S1 depending on whether tactile stimuli are processed in the context of a vibrotactile discrimination task or not.

For this, we employed a whole-brain data driven psychophysiological interaction (PPI) analysis on previously collected neuroimaging data (Rabe et al., 2022). By using PPI, we aimed to detect brain regions whose neural activity interact with finger-specific ROIs under varying WM task demands. We investigated this functional integration during two different task conditions: a condition that required the participant to attend to tactile stimuli since the information had to be kept in WM for performing a vibrotactile discrimination task (memory condition) and a condition in which the participant was asked not to attend to the stimulus (i.e., no memory condition). We further investigated whether such functional coupling between finger-specific activity in S1 and other brain regions can be correlated to behavioral performance and to the modulation of finger representations in S1, which we previously observed (Rabe et al., 2022). We hypothesized that S1 and regions responsible for top-down control are coupled in a task-dependent manner during somatosensory processing. We expected that solving the tactile WM task which includes directing attention towards the stimulus location (i.e. to one of the two stimulated fingers) modulates functional coupling of S1 with other brain areas which, in turn, is related to the participant's behavioral discrimination performance, or to the finger-specific information content which can be decoded from S1 somatotopy.

3.3 Materials and Methods

The data used in this manuscript have been published previously in bioRxiv (Rabe et al., 2022). We previously used this dataset to investigate finger representational changes during vibrotactile frequency discrimination in S1. Here we focused on the condition-dependent functional connectivity during stimulus presentation of the task. The experimental task, fMRI data acquisition, and fMRI data preprocessing were performed identically as in (Rabe et al. 2021). We briefly restate them here for the reader's convenience.

3.3.1 Participants

Thirty young healthy volunteers (19 females; mean age= 24.48, SEM= 0.44) participated in our study. Our sample size was comparable to those in previous reports on fMRI decoding of WM content using discrimination tasks (Ester et al., 2009; Schmidt et al., 2017). All participants were neurologically intact and reported to be right-handed. All of them gave written informed consent and the study protocol was approved by the local ethics committee (BASEC-Nr. 2018-01078). Three participants had to be excluded due to excessive head motion based on our criterion (see 'Preprocessing of fMRI data' section for more detail). One additional participant was excluded because we could not find any statistically significant finger clusters in S1 during vibrotactile stimulation.

3.3.2 Experimental Procedure and Tasks

3.3.2.1 Tactile Stimuli

Vibrotactile stimuli (duration = 2s, sampling rate = 1kHz) were applied to the right index or right little finger using a MR-compatible piezoelectric device (PTS-T1, Dancer Design, UK). We selected these fingers as they have the largest inter-finger somatotopic distance (Besle et al., 2013; Ejaz et al., 2015; Kolasinski et al., 2016a; Sanders et al., 2019), allowing us to robustly detect the modulation of somatotopic representations by the WM task. The one bin piezoelectric wafers were mounted to the fingertips using custom 3D-printed retainers that were fixed with a Velcro strap. Participants were asked to report any tingling sensation in case the retainer was mounted too tightly. The stimulation consisted of mechanical sinusoids that were transmitted from the testing computer to the piezoelectric device using a C Series Voltage Output Module (National Instruments) and the in-house NI-DAQmx driver.

3.3.2.2 Sensory detection threshold estimation

To ensure similar task difficulty across runs of the main experiment (Harris et al., 2006), we determined the sensory detection threshold (SDT) for both fingers prior to starting the main experiment. SDT was defined as the stimulation intensity at which the participants detected the stimulus 50% of the time. We stimulated each finger only once per trial at base frequency (20 Hz) and participants were asked to press a button upon detection of a stimulation. To reliably estimate SDT, we applied a conventional Bayesian-based Quest procedure (QuestHandler in PsychoPy). After each detected or undetected stimulus the algorithm searched for the most probable psychometric function via maximum likelihood estimation over the course of 25 trials starting with a stimulation amplitude of 0.1 Volts (Watson & Pelli, 1983). The Weibull psychometric function was calculated using the following formula:

$$\Psi(x)=\delta\gamma+(1-\delta)[1-(1-\gamma)\exp(-10beta(x-T+\epsilon))] \quad (3)$$

where x is the stimulus intensity in Volts and T is the estimated sensory detection threshold. This procedure was performed prior to the first run. If the percentage of correctly discriminated memory trials in a run was below 60% or above 90%, then we redetermined the SDT using a shortened version of the Quest procedure. In such a case we started the Quest procedure with the previously determined stimulation intensity to reduce the number of iterations (new iterations = 7 trials). This procedure was applied to keep task difficulty at comparable levels throughout the experiment.

3.3.2.3 Main experimental task

The main experimental task was generated using PsychoPy (Peirce et al., 2019). The experimental task consisted of memory and no memory trials. During a memory trial, participants performed a two-alternative forced choice (2AFC) discrimination task. Two vibrotactile stimuli were consecutively applied to the same finger (i.e., the index or the little finger), separated by a jittered 6-8s delay. We targeted cutaneous mechanoreceptors that respond to stimulations in the flutter range (Mountcastle et al., 1967). One of two stimuli vibrated at 20 Hz (2s duration at SDT intensity) while the vibration frequency of the other stimulus varied between 22, 24 or 26 Hz (same duration and intensity). Participants had to indicate by means of a button press whether the first or the second stimulation was higher in frequency (half of the participants) or whether the first or the second stimulation was lower in frequency (the other half of the participants), following previously published procedures (Pleger et al., 2006, 2008, 2009). Responses were recorded via index and middle finger button

presses of the other (left) hand using a MR-compatible fiber optic device. We randomized the order of how the response options (f1 and f2) appeared on the screen on a trial-by-trail basis to prevent somatotopy-specific anticipatory motor activity. After a 3s response period participants received visual feedback (1s) indicating whether their response was correct (highlighted by green color) or incorrect (red; **Figure 3.1**). Participants were instructed to focus their gaze on the fixation cross in the middle of the screen during the complete trial. Vibrotactile stimuli trials targeted either the index or the little finger and which finger would be stimulated per trial was counterbalanced across each run.

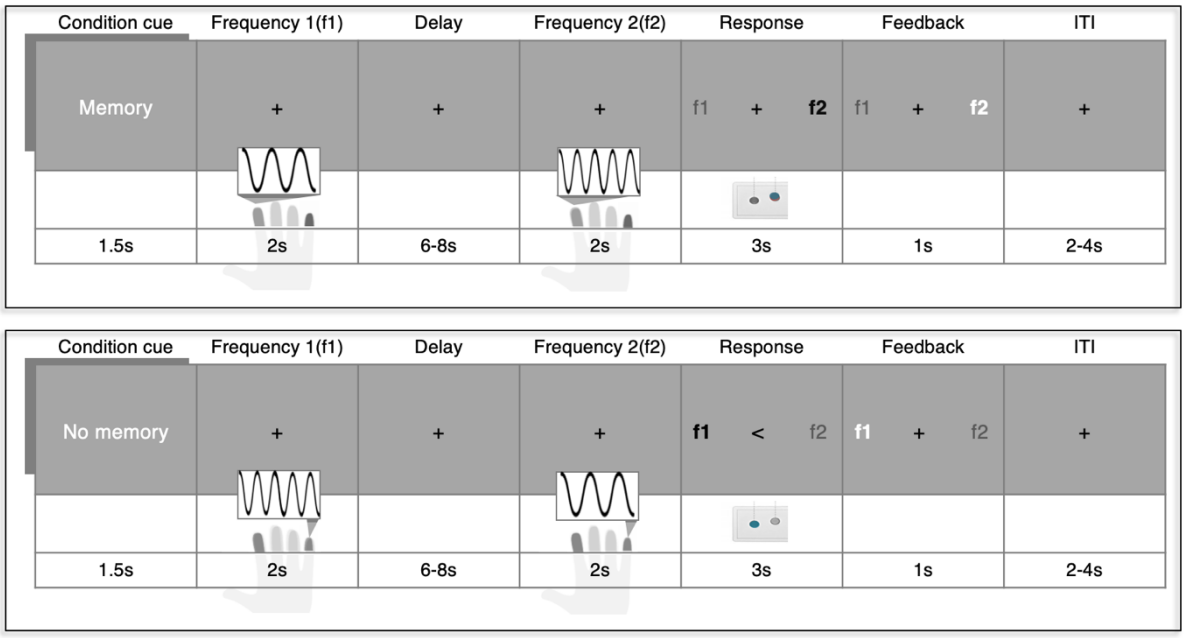

Figure 3. 1 Vibrotactile frequency discrimination task

During memory trials (top) two vibrotactile stimuli that differed in frequency were consecutively applied to the same finger (in this example the index finger). Both stimulations were separated by a jittered delay period, during which participants had to keep the first stimulation frequency (f1) in memory in order to compare it to the frequency of the second stimulus (f2). During the 3s response period participants had to indicate which of the two stimulation frequencies (f1 and f2) was higher by means of a left hand button press. The mapping between the discrimination response and which button to press was indicated on the screen and randomized across trials. Subjects received feedback whether their response was correct or incorrect. The target finger (index or little finger) were intermixed within a run and the inter trial interval (ITI) was jittered between 2-4s. During no memory trials (bottom), vibrotactile stimulations and visual information remained the same. However, participants were instructed not to focus on the stimulation and also not to compare the vibrotactile frequencies. They simply had to press the button indicated by the arrow in the middle of the screen.

To disentangle WM processes from general responses to the stimuli, we also included no memory trials. During a no memory trial participants received the exact same vibratory

stimulations as during memory trials, but they were instructed not to focus on the stimuli or on their vibration frequencies. During the response period subjects were informed by a visual cue (pointing arrow) which button to press. To ensure participants did not switch cognitive strategies, the indicated response was always contrary to the response that would be expected when correctly discriminating both frequencies. Memory and no memory trials conditions were separated in mini blocks of 4 trials. Participants were informed whether they had to perform the memory or no memory task by means of a visual cue (1.5s) at the beginning of each trial. Prior to the experiment, participants were familiarized with the memory and no memory tasks by completing 12 trials.

The order of stimulus sites (stimulated finger) was counterbalanced both within and across mini blocks. Stimulation frequencies were counterbalanced across the experiment. Each stimulus frequency was presented equally often in both memory and no memory condition. Jittered timings for Inter-stimulus-interval (ISI, 6-8s) and Inter-trial-interval (ITI, 2-4s) were randomly drawn from a uniform distribution. All participants completed 4 runs consisting of 48 trials each. Each run consisted of 6 memory and 6 no memory mini blocks in a counterbalanced order.

3.3.3 Behavioral analysis

We defined the discrimination accuracy per participant as the percentage of correctly discriminated trials separately for each condition. We expected that greater frequency differences would facilitate discrimination between both tactile vibrations while the stimulus site should have no effect. We therefore investigated whether behavioral performances differed across frequency differences and across fingers using a two-way repeated-measures ANOVA.

3.3.4 MRI data acquisition

Functional as well as structural MRI images were acquired on a Philips Ingenia 3 Tesla MRI (Best, The Netherlands) using a 32-element head coil. fMRI data was collected using an echo-planar-imaging (EPI) sequence acquiring 36 transversal slices centred at the bicommissural line and with whole brain coverage, though excluding most of cerebellum (repetition time (TR): 2s, echo time (TE): 30ms, spatial resolution: $3mm^3$, FOV = $222 \times 222mm^2$, 85° flip angle, slice orientation: transversal, SENSE factor (AP): 2, 472 functional volumes per run). Anatomical images were acquired during SDT estimation using a MPRAGE T1-weighted sequence (TR = 7.7ms, TE = 3.6ms, FOV = $240 \times 240mm^2$, flip angle: 8°, resolution: $1mm^3$, number of slices: 160, slice thickness: 2.2mm, slice orientation: sagittal).

3.3.5 Preprocessing of fMRI data

Conventional pre-processing steps for fMRI data were applied to each individual run in native three-dimensional space, using FSL's Expert Analysis Tool FEAT (v6.00; fsl.fmrib.ox.ac.uk/fsl/fslwiki). The following steps were included: Motion correction using MCFLIRT (Jenkinson, 2002), brain extraction using automated brain extraction tool BET (Smith, 2002), high-pass filtering (100Hz), slice-time correction, and spatial smoothing using a 3mm FWHM (full width at half maximum) Gaussian kernel using FEAT. Functional data was aligned to structural images initially using FLIRT (Jenkinson & Smith, 2001), and optimised using boundary-based registration (Greve & Fischl, 2009a). BOLD EPI data was assessed for excessive motion using motion parameter estimates from MCFLIRT. If the functional data from a participant showed greater than 1.5 mm (half the voxel size) of absolute mean displacement, this participant was excluded from all further analysis.

To reduce physiological noise artifacts, these CSF and white matter mask were used to extract scan-wise time series which were then added to the model as nuisance regressors in addition to the standard motion parameters.

Structural images were transformed to Montreal Neurological Institute (MNI) standard space using nonlinear registration (FNIRT), and the resulting warp fields were applied to the functional statistical images.

3.3.6 Univariate analysis

First-level parameter estimates were computed for each run (4 runs in total) using a voxel-based general linear model (GLM) based on the gamma hemodynamic response function. Time series statistical analysis was carried out using FSL with local autocorrelation correction. To find finger-specific BOLD responses during vibrotactile stimulation we contrasted beta estimates from D2 stimulations to D5 stimulations and vice versa for the memory and no memory conditions together. We then used a fixed effects higher-level analysis to average activity across runs for each individual participant. To make inferences on the population level, we computed a random effects analysis. Statistical significance of the resulting group activation maps (z-statistic images) were determined at the cluster level ($Z > 3.1$, $p < .05$, family-wise-error-corrected (FWE)). These maps revealed a finger specific map (D2 cluster) in the lateral part of S1 while the reverse contrast (D5 cluster) revealed more medially located activity (**Appendix. 3.1**). The location of these S1 finger-specific activity maps were in line with previous findings on finger somatotopy (Besle et al., 2013; Martuzzi et al., 2014; Sanchez Panchuelo et al., 2018; Sanders et al., 2019). Using a similar approach,

we also obtained two group activation maps highlighting brain regions that were more activated in memory compared to no memory trials during either the first (f1) or the second (f2) vibrotactile stimulation across both fingers ($Z > 3.1$, $p < .05$, FWE; **Appendix 3.2**).

3.3.7 Psychophysiological Interaction analysis (PPI)

We conducted a standard PPI analysis to identify which brain regions change their functional connectivity with finger-specific activity in S1 depending on whether or not the vibrotactile discrimination task had to be performed (Friston et al., 1997). PPI has the ability to detect voxels that exhibit condition-dependent functional coupling with a seed region of interest (ROI). To define the seed ROIs, each participant's activation maps resulting from the D2>D5 and D5>D2 contrasts during vibrotactile stimulation were cluster-wise thresholded at $p < 0.001$, not corrected for multiple comparisons. We determined the center of the sphere ROI by the peak activation in the activation map that was lay within the group level (D2>D5 and D5>D2) clusters. We extracted the averaged time-series from the spherical ROI (sphere radius = 6mm). This approach accounted for inter-subject heterogeneity.

We utilized the standard two-level approach using separate GLMs for the D2 and the D5 ROI. At the first level, each participant's GLM included i) two 'psychological' regressors modelling the contrast (memory > no memory) of stick functions of D2 or D5 stimulation during f1 and during f2 that were convolved with the HRF, ii) one 'physiological' regressor reflecting the mean activity of the D2 or D5 seed ROI time series, (iii) two PPI regressors (i.e. the product of the mean-centered D2 or D5 ROI time series and the contrasted (memory vs. no memory) D2 or D5 stimulation onsets (f1 or f2), iv) other experimental events (e.g. D2 or D5 stimulation, button response) and nuisance regressors (cerebral spinal fluid, white matter, and standard motion parameters). The PPI regressor is used to identify brain areas that change their connectivity with finger-specific representations in S1 depending on whether vibrotactile stimuli are processed in the memory versus no-memory condition. Finally, to make inferences on the population level, we computed a mixed effects analysis (Flame 1). From this we obtained statistical group maps (Z-statistic images) for both stimulation events. We restricted the group statistical test by a gray matter mask (MNI standard brain). We computed three group activation maps: one for the D2 ROI, one for the D5 ROI and an average across both D2 and D5 ROIs. The letter group activation map was thresholded at a cluster-level by $Z > 2.3$ and FWE with an alpha of $p < 0.05$. For visualization purposes only, we also computed two group activations maps (D2 PPI and D5 PPI) that were not corrected for multiple comparisons.

Finally, for brain areas that exhibited a significant condition-dependent modulation of functional connectivity with the S1 finger-cluster, we tested whether the functional connectivity strength predicted behavior or the finger-specific information content in S1. First, we obtained for each participant PPI z-values from the PPI group-level cluster (averaged across D2 and D5), correlate these values with the participant's discrimination accuracy (percentage of correctly discriminated trials, averaged across runs). A significant relationship would suggest that the functional coupling between finger-specific clusters and the identified brain regions is relevant for task performance. Second, we investigated whether there is a relationship between the functional coupling and the level of finger-specific information content in S1 as estimated via a multivoxel pattern analysis approach. In short, during vibrotactile stimulations we trained a Support Vector Machine (SVM) to delineate between finger-specific activity patterns in S1 hand area and then let the classifier predict on unseen activity pattern, which finger was stimulated during that period. This resulted in classification accuracies reflecting the percentage of correctly decoding what finger was stimulated from activity patterns in the S1 hand area (Rabe et al., 2022). Here, any significant relationship would suggest that the functional coupling could play a role in modulating finger representations in S1 during vibrotactile stimulation.

3.3.8 Statistical data analysis

To detect outliers, we used the robustbase toolbox (Finger, 2010). $\mathbf{S_n}$ identifies an outlier (x_j) if the median distance of x_i from all other points, was greater than the outlier criterion (λ=3) times the median absolute distance of every point from every other point:

$$(4)\quad \frac{med_{j\neq i}\,|\,x_i - x_j\,|}{S_n} > \lambda \; where \; S_n = \; c_n \underset{i=1:n}{med}\left\{\underset{j\neq 1}{med}|\,x_i - x_j\right\},$$

where c_n is a bias correction factor for finite sample sizes (Rousseeuw & Croux, 1993). We detected no outliers for behavioral data that had to be excluded from any further analysis.

Before conducting any Pearson correlation, we validated the assumptions for normality using a Shapiro-Wilk test. We used Bayesian hypothesis testing, implemented by the pingouin toolbox (Vallat, 2018), to investigate the relative level of support for the null and alternative hypotheses with a Cauchy prior width set at 0.707. Following the conventional cut-offs, a BF smaller than 1/3 is considered substantial evidence in favor of the null hypothesis. A BF greater than 3 is considered substantial evidence, and a BF greater than 10 is considered

strong evidence in favor of the alternative hypothesis. A BF between 1/3 and 3 is considered weak or anecdotal evidence (Dienes, 2014; Kass & Raftery, 1995).

3.4 Results

3.4.1 Memory trials recruit a distributed network of brain regions during both vibrotactile stimulations

First, we aimed to identify brain regions that are more active during vibrotactile stimulation in memory trials compared to no memory trials. For this, we contrasted BOLD signals during vibrotactile stimulation between both conditions. Our results show that somatosensory processing in memory trials increased neural activity in a whole network of bilateral brain regions, which included bilateral posterior parietal cortex (PPC), S1, S2, pre-motor cortex and bilateral supplementary motor area (PMC, SMA), frontal lobe, bilateral (medial/inferior) frontal gyrus (MFG, IFG), dorsal striatum (DS, caudate and putamen), anterior insular cortex and thalamus (**Figure 3.2**). Individual BOLD increase for either the first or second stimulation, which show a great overlap, are displayed in **Appendix. 3.2**.

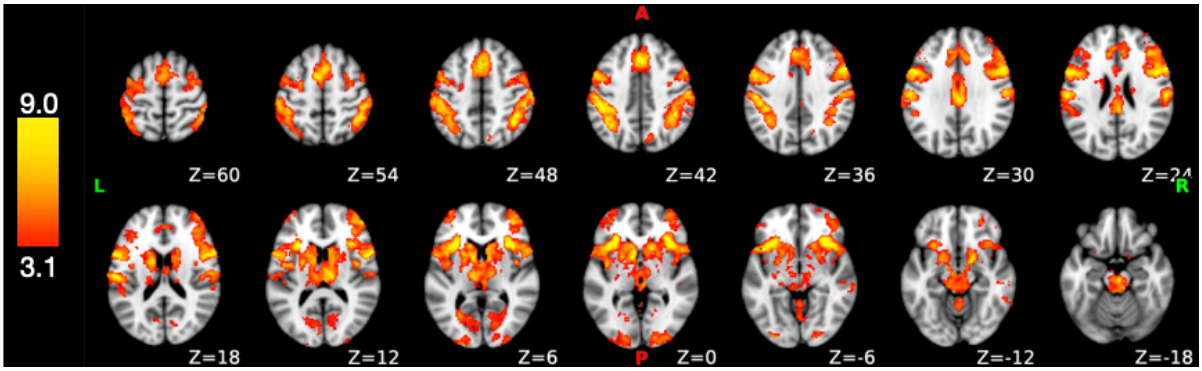

Figure 3. 2 Network of brain regions that show memory-related BOLD increases during both vibrotactile stimulations.

We identified brain regions that were more active during vibrotactile stimulation in the memory compared to the no memory condition (average across f1 and f2). The resulting statistical map was projected onto an MNI standard brain. Memory-related activity during vibrotactile stimulation resided in a network of brain regions. Specifically, there was an increase in activity in the bilateral posterior parietal cortex (PPC), bilateral primary somatosensory cortex (S1), bilateral secondary somatosensory cortex (S2), bilateral pre-motor cortex and supplementary motor area (PMC, SMA), bilateral frontal lobe, bilateral (medial/inferior) frontal gyrus (MFG, IFG), bilateral dorsal striatum (caudate and putamen), bilateral anterior insular cortex, and thalamus. Z-statistic images were determined at the cluster level ($Z > 3.1$, $p < .05$, family-wise-error-corrected (FWE).

3.4.2 Finger-specific clusters in S1 are functionally coupled to the dorsal striatum during the first vibrotactile stimulation

We then examined condition-dependent changes in functional coupling between the D2 and D5 finger ROI in S1 and the rest of the brain during vibrotactile stimulation. This was done separately for each finger cluster and for each vibrotactile stimulation event (f1 and f2). During f1 we explored what brain regions functionally interacted with individual finger clusters. For the D2 ROI, we found functional connectivity changes between S1 and left supramarginal gyrus, left inferior temporal gyrus, left lateral occipital cortex, left caudate nucleus and right putamen (see **Figure 3.3A** and **Table 3.1** for more details). These results survived FWE correction for multiple comparisons at the cluster level. For the D5 ROI, we identified left parahippocampal gyrus, right insula and right putamen. However, these results did not survive correction for multiple comparisons at the cluster level (**Figure 3.3A** and **Table 3.1)**.

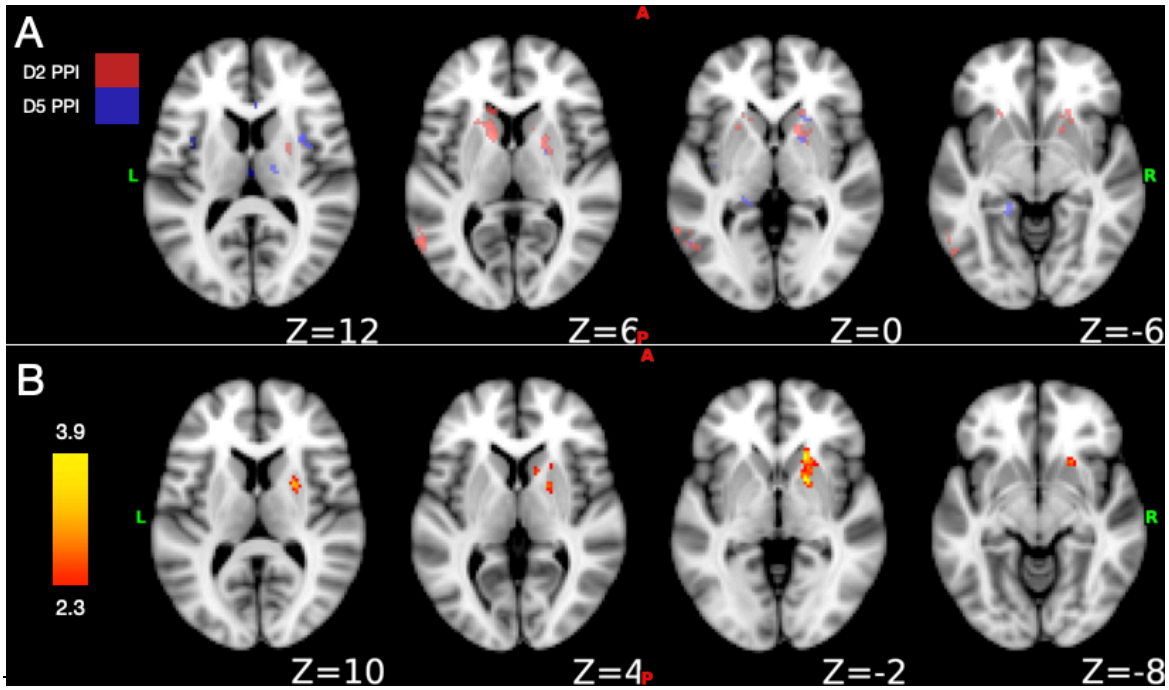

Figure 3. 3 Psychophysiological Interaction (PPI) group results.

*Based on the ROI seed time series we determined areas that showed a functional coupling with the previously defined ROIs. **A**. The D2 and D5 finger areas in S1 showed stronger functional coupling during memory compared to no memory trials to various brain regions (uncorrected PPI results, for more detail see **Table 3.1**). Z-statistic images were thresholded by Z > 2.3 uncorrected. **B**. Averaged D2 and D5 PPI results revealed increased connectivity to the right dorsal striatum. Z-statistic images were thresholded at Z > 2.3, and FWE correction was applied at the cluster level (p < .05, FWE). All group activation maps were projected onto the standard MNI 152 brain image.*

Next, we averaged the PPI results for the D2 and D5 ROI. This analysis revealed only one cluster in the right putamen (**Figure 3.3B**), the only area that changed connectivity with both S1 ROIs (**Figure 3.3A**), even though this result might have been driven by functional coupling changes with the D2 cluster. In summary, during the first stimulation (f1) of the discrimination task, WM-dependent PPI analysis (f1 memory > f1 no memory) revealed an increased functional coupling ($Z > 2.3$, $p < .05$ FWE) between both finger clusters in left S1 and right dorsal striatum (for individual participant condition-dependent correlation analysis, see **Appendix. 3.3**).

ROI	Cluster	X	Y	Z	Z stat	Cluster Size (mm3)
D2	Left Caudate	-14.0	16.0	4.0	4.19	1056
D2	Left Supramarginal Gyrus	-50.0	-40.0	56.0	3.88	312
D2	Right Putamen	16.0	12.0	0.0	3.78	776
D2	Left Lateral Occipital Cortex	-58.0	-62.0	4.0	3.75	1112
D2	Left Supramarginal Gyrus	-52.0	-28.0	43.0	3.70	1176
D2	Right Putamen	20.0	4.0	6.0	3.20	192
D2	Left Inferior Temporal Gyrus	-48.0	-56.0	-10.0	3.09	320
D5	Right Insular Cortex	34.0	6.0	10.0	3.79	264
D5	Right Putamen	18.0	4.0	0.0	3.36	264
D5	Left Parahippocampal Gyrus	-16.0	-38.0	-6.0	3.04	168

Table 3. 1 Regions that were functional coupling to either D2 or D5 clusters in S1.
Based on the D2 or D5 seed time series we determined areas that showed connectivity changes during the memory condition. The table displays brain regions that showed condition-dependent functional connectivity. Brain regions were labelled according to the Harvard-Oxford Cortical Structural Atlas. Only Clusters with a minimum distance between subpeaks of 26mm and more than 150 voxels (arbitrary extent threshold) are reported.

Clusters reported for the D2 seed ROI but not those reported for the D5 seed ROI survive FWE correction at the cluster level.

We also aimed to identify areas that are functionally coupled to the D2 and D5 finger areas in S1 during the second stimulation (f2) but, surprisingly, we could not find any significant changes in functional coupling during this time period when the memory condition was compared to the no-memory condition ($Z > 2.3$, $p < .05$ FWE).

3.4.3 Functional coupling between S1 and dorsal striatum during the first stimulation is relevant for task performance

Finally, we investigated whether the observed functional interactions were relevant for task performance (**Figure 3.4**). We hypothesized that if condition-dependent functional connectivity between the D2 and D5 areas in S1 and the right putamen is beneficial for the vibrotactile frequency discrimination task, then participant's mean connectivity scores (z-scored) between these areas should correlate with the corresponding discrimination accuracy. Interestingly, we could show that participants with a stronger increase in functional coupling during memory trials performed better on the task ($r = 0.48$, $p = 0.01$, CI 0.11 0.73, $BF = 4.35$), with the Bayes factor (BF) showing moderate evidence in favor of the alternative hypothesis (**Figure 3.4A**).

Finally, we also investigated whether there is a relationship between participant's PPI z-stat values in right putamen and previously collected classification accuracies, reflecting the percentage of correctly decoding what finger was stimulated during the first stimulation (f1) from activity patterns in the S1 hand area (Rabe et al., 2022). We could not find any relationship ($r = -0.15$, $p = 0.46$, CI -0.51 0.25, $BF = 0.32$), suggesting that the coupling between left S1 and right putamen did not modulate the finger representations in S1 (**Figure 3.4B**).

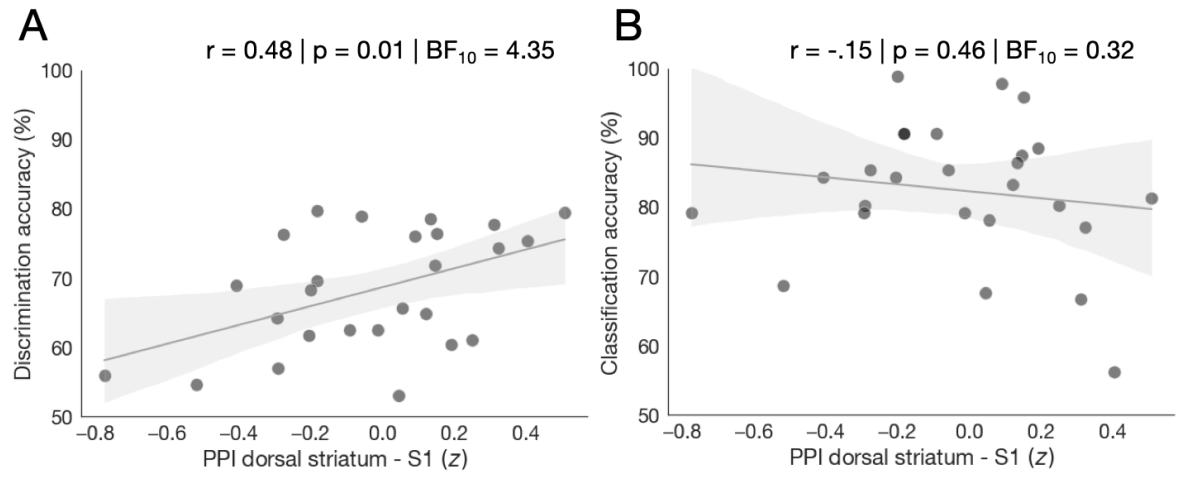

Figure 3. 4 Individual connectivity strengths in relation to discrimination and classification accuracies.

We extracted participants' mean connectivity (z-score) values from the group PPI cluster in the dorsal striatum (as visualized in ***Figure 3.3B****). A. Correlation of participant's mean connectivity values with individual discrimination accuracies (the percentage of correctly discriminated vibrotactile frequency). We found that connectivity scores in dorsal striatum were predictive of task performance. B. We also correlated connectivity scores in dorsal striatum with previously obtained classification accuracies (Rabe et al., 2022) reflecting the percentage of correctly classified finger location (D2 vs. D5) during the first stimulation across all memory trials compared to misclassifications.*

3.5 Discussion

In the current study we investigated condition-dependent whole-brain functional connectivity during somatosensory processing in a WM task. More specifically, we identified brain areas that changed their functional coupling with S1 as a function of the WM task. Using PPI analyses, we revealed that putamen and caudate, subareas of the dorsal striatum were functionally connected to both finger-specific representations in S1 when participants processed somatosensory information during memory trials. Interestingly, significant functional connectivity was only observed during the first presentation of the tactile stimulus. Furthermore, this functional coupling was behaviorally relevant as participants with stronger functional striatal-S1 coupling showed improved discrimination performance. No such relationship was found between functional coupling and classification accuracies, reflecting the information content on what finger was stimulated from activity patterns in S1 hand area. This promotes the idea that during the first vibrotactile stimulation of the WM task flexible

connectivity between subcortical areas and S1 is crucial for task performance, but not for modulating finger representations in S1.

3.5.1 The role of dorsal striatum in sensory processing

The current study suggests that dorsal striatum-S1 interactions are important for tactile discrimination. This is in agreement with previous results of both animal and human studies: Rats studies revealed that stimulus features (i.e. frequency or texture) could be decoded from the neuronal population response in the striatum and that these results correlated with the discrimination performance of the rat (Gerdjikov et al., 2010; Hawking & Gerdjikov, 2013; Hipp et al., 2006). Furthermore, studies using optogenetic stimulation in rats demonstrated that excitation of corticostriatal (S1 – striatum) terminals led to increased tactile stimulus detection performance. In contrast, inhibition of these terminal did not affect the rat's performance (Sun et al., 2021). This parallels our finding that the functional coupling between S1 and dorsal striatum is relevant for behavior.

Human neuroimaging research also suggests the involvement of the dorsal striatum in sensory processing. Peller et al (2006) used neuroimaging and demonstrated that both patients suffering from writer's cramp and healthy controls engaged anterior and posterior putamen bilaterally during tactile discrimination, with patients showing hyperactivity in the putamen (Peller, 2006). Likewise, research in patients with Parkinson's disease suggests that the striatum, beyond its well-established role as a motor structure, also processes sensory information (Sathian et al., 1997; Schneider et al., 1987; Zia et al., 2003). Our results parallel these findings by showing that functional interaction between somatotopic maps in S1 and dorsal striatum was more engaging during active compared to passive stimulus perception of vibrotactile stimuli.

3.5.2 Functional coupling does not predict finger representational changes in S1.

What neural mechanisms and brain regions are modulating somatotopic maps in S1 during such vibrotactile stimulus presentation, remains an open question. We did not observe a correlation between the functional coupling strength between the dorsal striatum and finger-specific information content in S1 and the ability (i.e., classification accuracy) to distinguish between S1 finger representations during vibrotactile stimulation. Thus, striatal projections that cross over to S1 of the other hemisphere might not be involved in shaping somatotopic maps depending on which finger has been stimulated. This does not rule out, however, that the striatum might be important for facilitating the representations of task-relevant versus

task-nonrelevant features (Peters et al., 2021) since our MVPA approach was not designed to decode characteristics of the vibrotactile stimulus (e.g. frequency information).

3.5.3 No functional interaction between S1 and dorsal striatum during the second stimulation.

Interestingly, the condition-dependent functional connectivity result was not consistent between the first and the second vibrotactile stimulation. In fact, we could not identify any brain region that functionally interacted with finger-specific activity in S1 during the second stimulation. Note, that the task demands largely differ between the first and the second stimulation, which could explain this result. During the first stimulation (f1), participants are required to encode the vibrotactile stimulus. During the second stimulation (f2) the participant has to both encode the vibrotactile stimulus, retrieve the previous stimulus, mentally compare this information, and make a decision. It is tempting to speculate that during the second tactile stimulation period different processes (encoding, retrieval, comparison and decision-making) may occur nearly simultaneously or in fast succession which requires S1 to quickly couple and decouple to various brain networks. However, given that fMRI has a low temporal resolution it is unlikely that fast, dynamic changes in functional connectivity can be reliably detected.

3.6 Conclusions

Our results contribute to a previous connectivity research on somatosensory processing. We could demonstrate that subcortical areas, specifically dorsal striatum, seems to be functionally coupled to S1 during vibrotactile stimulation in a WM-task. Crucially, connectivity changes of dorsal striatum in relation to S1 were relevant for task performance but not for shaping somatosensory maps of finger representations.

3.7 Appendices

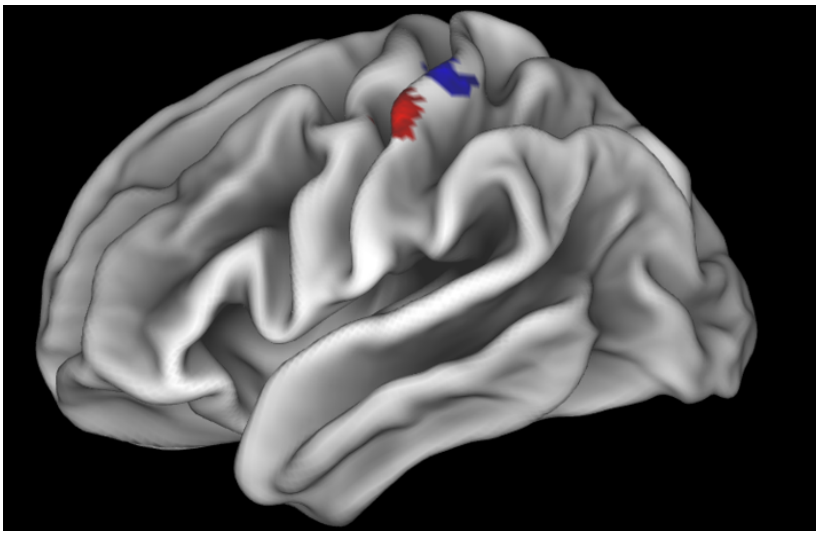

Appendix 3. 1 Finger-specific group cluster during vibrotactile stimulation

We identified finger-specific group clusters by contrasting beta estimates for each finger stimulation. Z-statistic images were thresholded using clusters determined by $Z > 3.1$, $p < .05$ family-wise-error-corrected (FWE) cluster significance. Both statistical maps (D2 in red and D5 in blue) were projected onto a cortical surface. We used these group clusters to constrain individual seed-time ROIs.

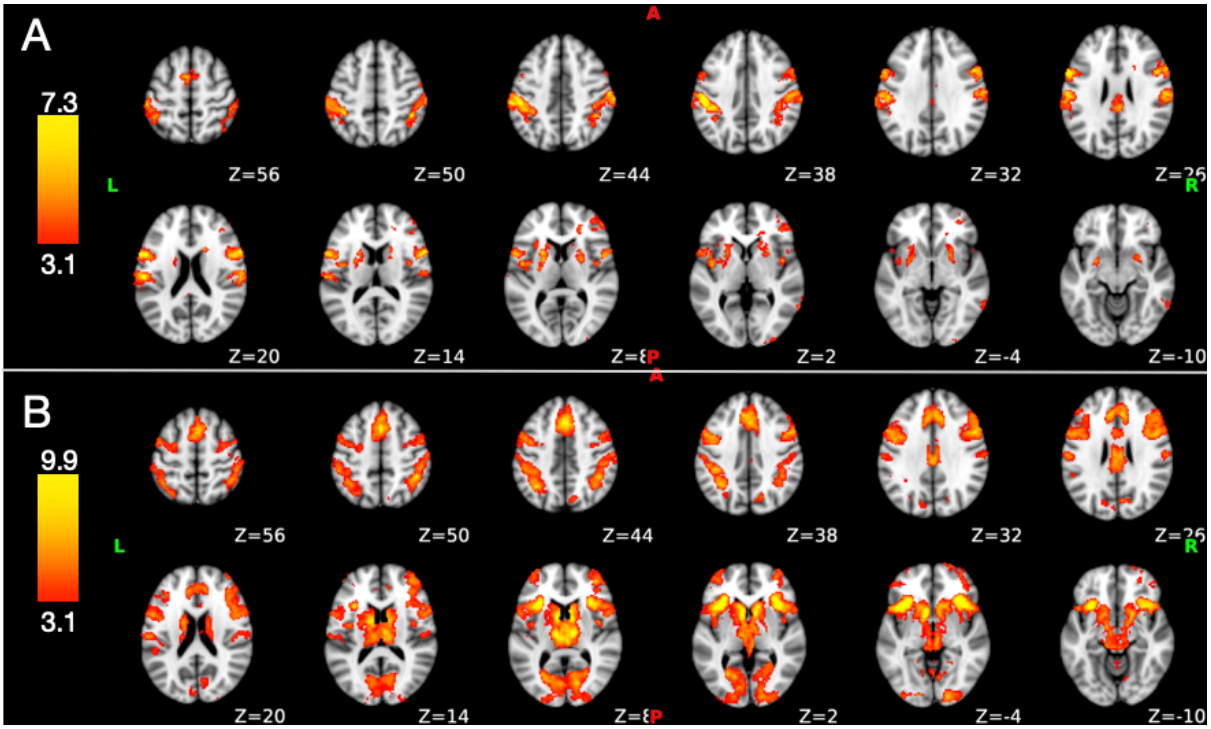

Appendix 3. 2 Network of brain region activations by stimulation timepoint

*We identified brain regions that were more active during the first (**A**) and second (**B**) vibrotactile stimulation in the memory compared to the no memory condition (average across f1 and f2). The resulting statistical map was projected onto an MNI standard brain. Memory-related activity during both vibrotactile stimulations resided in a similar network of brain regions. However, we could observe overall stronger activations during the second stimulation as well as additional SMA and thalamus involvement. Z-statistic images were determined at the cluster level (Z > 3.1, p < .05, family-wise-error-corrected (FWE).*

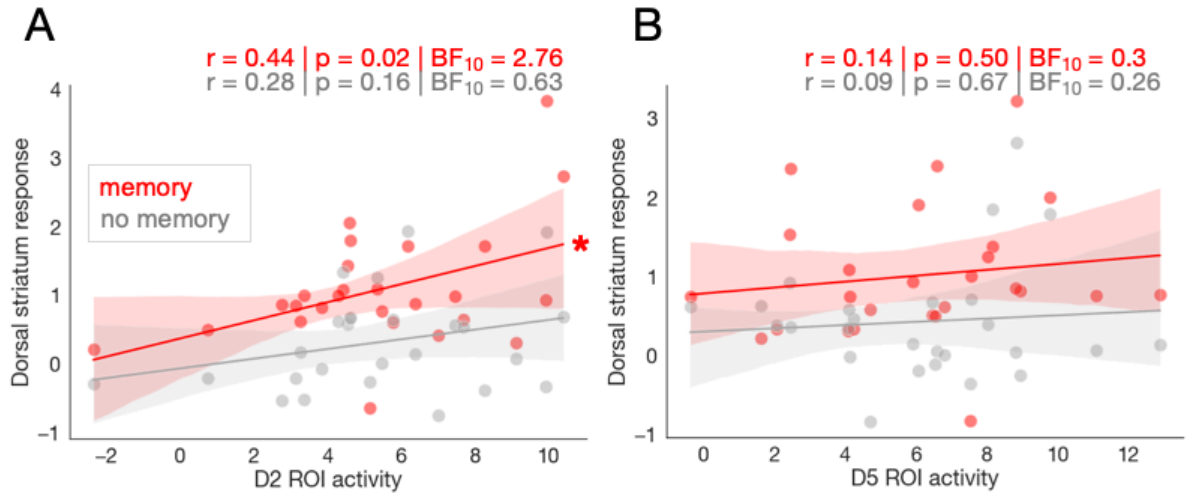

Appendix 3. 3 Correlation between finger ROIs' activity and dorsal striatum condition depending response during the first vibrotactile stimulation.

*For each participant we extracted z-scored beta estimates from three different ROIs. First, estimates from the masked PPI group cluster (dorsal striatum) for memory>rest and no memory>rest condition separately during the first stimulation. Second, for the same time period, we also extracted estimates for each individual D2 and D5 ROI during both conditions. Thus, any shift in the regression slope reflects a condition-dependent functional coupling between dorsal striatum and one of the two ROIs. **A**. We observed a significant relationship between dorsal striatum and D2 ROI activity during memory trials (r = 0.44, p = 0.02, CI 0.07 0.71, BF = 2.76) and a non-significant correlation for no memory trials (r = 0.28, p = 0.16, CI -0.12 0.61, BF = 0.63). **B**. We found no significant correlation for either memory or no memory trials between dorsal striatum and D5 ROI (memory: r = 0.14, p = 0.50, CI -0.26 0.5, BF = 0.3; no memory: r = 0.09, p = 0.67, CI -0.31 0.46, BF = 0.26).* reflects an alpha of p < .05.*

4 Ipsilateral finger representations are preserved through corticocortical connections after tetraplegia

Finn Rabe, Patrick Freund, Nicole Wenderoth, Sanne Kikkert (2022). Ipsilateral finger representations are preserved through corticocortical connection after tetraplegia.

4.1 Abstract

We, and others, recently observed that despite reduced or absent afferent inputs in tetraplegic patients, somatotopic representations can be activated in the primary somatosensory cortex during (attempted) unimanual finger movements. This finding contributed to a growing body of research suggesting that the primary somatosensory cortex may be more hard-wired, and less plastic, then initially assumed. Beyond somatotopic contralateral activity, a hallmark of an intact sensorimotor system is the presence of somatotopic ipsilateral activity in the primary sensorimotor cortices during unimanual movements. Here we used functional MRI to investigate whether tetraplegic patients with reduced or absent afferent processing activate ipsilateral finger representations within primary sensorimotor cortices while performing unimanual (attempted) individual finger movements. Our results indicate that even in the absence of peripheral inputs, somatotopic ipsilateral activation can be elicited. By using tetraplegic patients as a clinical model, we shed new light on the potential pathway generating such ipsilateral activity. Indeed, the presence of ipsilateral activity in the primary somatosensory cortices confirms that such processing is not driven by peripheral, but rather by cortical processes.

4.2 Introduction

Limb movements are primarily driven by sensorimotor cortices contralateral to the moving limb. However, unimanual movements not only elicit contralateral neural activity, but also ipsilateral activations in sensorimotor cortices (Buetefisch et al., 2014; Johansen-Berg et al., 2002; Sutherland, 2006, Seidler et al., 2004; Verstynen, 2004, Berlot et al., 2019; Diedrichsen et al., 2013). Extensive evidence from neuroimaging studies suggests that blood-oxygen-level-dependent (BOLD) activations in the ipsilateral hemisphere are significantly lower compared to the contralateral side during unimanual movements (Allison et al., 1989; Amann et al., 2009; Grefkes et al., 2008; Hamzei et al., 2002). It is assumed that by switching from bilateral to unimanual movements ipsilateral activity is reduced in order to avoid overt mirror movements (Daffertshofer et al., 1999; Hübers et al., 2008). Interestingly, unimanual movement not only elicit a detailed somatotopic map of ipsilateral body parts in the primary motor (M1), but also primary somatosensory cortex (S1), including individual finger representations (Berlot et al., 2019; Diedrichsen, Wiestler, & Krakauer, 2013). Previous findings attributed these ipsilateral representations a movement planning role (Berlot et al., 2019).

The precise pathways mediating these ipsilateral representations are not fully resolved, especially for S1 (for review, see Chettouf et al., 2020). The coupling between both hemispheres occurs very likely through the corpus callosum (Diedrichsen, Wiestler, & Krakauer, 2013). These transcallosal pathways can be both excitatory and inhibitory (Swinnen, 2002; van der Knaap & van der Ham, 2011; Ziemann et al., 1999). Thus, during unimanual movements inhibitory transcallosal input could explain the suppressed BOLD in the ipsilateral hemisphere. Previous findings on effective connectivity suggest that instead of direct inhibition between homologous areas, inter-hemispheric-inhibition (IHI) occurs through intra-hemispheric connections to premotor cortices (PMC) and supplementary motor area (SMA; Grefkes et al., 2008; Ruddy et al., 2017; Volz et al., 2015). This would suggest that the contralateral hemisphere activates PMC and SMA and these areas then inhibit homologous ipsilateral areas through cortico-cortical connections. This has been underpinned by a TMS-fMRI study showing that the strength of IHI for longer interstimulus intervals (40ms), associated with polysynaptic connections to neighboring regions, e.g. PMC and SMA, predicted the suppressed ipsilateral BOLD responses ((Talelli et al., 2008, but also see Devor et al., 2008).

Even though these inter-hemispheric connections mainly focused on M1, it is very likely that also ipsilateral S1 activity might not only be driven by direct transcallosal

projections between left and right S1, but it might also be mediated by transcallosal connections between neighboring brain regions. Meanwhile, ipsilateral S1 also receives uncrossed ascending sensory feedback during movements, which would question the pure cortico-cortical account (Kanno et al., 2003).

If ipsilateral activity is solely cortically driven, then we should be able to observe this even after a spinal cord injury (SCI) that can lead to reduced or absent sensorimotor functions of the upper limb(s), depending on the level of injury. Upper limbs and torso are affected following a cervical SCI, also called tetraplegia (Curt et al., 1998; Kalsi-Ryan et al., 2014; Petersen et al., 2012). Consequently, S1 receives dampened or no afferent input and could result in changes of motor behavior (Ozdemir & Perez, 2018). Seminal non-human primate studies showed that this results in extensive reorganization in sensorimotor cortex where deprived body part representations (e.g., of the hand) become responsive to cortically adjacent and intact body parts (e.g., of the lips; Halder et al., 2018; Jain et al., 2008; Kambi et al., 2014). Furthermore, studies on SCI patients found that finger representations became less distinct in S1 and additionally, S1 decreased its response to tactile stimulations (Cramer et al., 2005; Freund, Weiskopf, et al., 2011; Hotz-Boendermaker et al., 2008). However, we (Kikkert et al., 2021) and others (Flesher et al., 2016; Guan et al., 2021) recently revealed that even tetraplegic patients who suffer from a complete SCI and therefore have no retained connections between the periphery and brain, have a preserved contralateral representation of individual fingers of the paralyzed hand that can be activated through attempted hand movements. By contrast, it is unknown whether homotopic areas in the other hemisphere are simultaneously activated via cortico-cortical connections instead of uncrossed afferent projections.

In the current study we used an (attempted) unimanual finger movement paradigm combined with functional magnetic resonance imaging (fMRI) in 14 tetraplegic patients to investigate whether corticospinal connections are necessary to maintain ipsilateral somatotopic representations in S1. We further examined whether retained sensorimotor function and time since SCI may, similar to our previous findings on contralateral representations, affect ipsilateral S1 representations.

4.3 Materials and Methods

The data used in this manuscript have been previously published in eLife (Kikkert et al., 2021). While we previously used this dataset to examine preserved contralateral representations in S1, here we focus on ipsilateral counterpart and its role during unimanual movements. The experimental task, fMRI data acquisition, and fMRI data preprocessing were therefore identical to what was described in (Kikkert et al., 2021). We briefly restate them here for the reader's convenience.

4.3.1 Participants

We recruited 15 chronic tetraplegic patients, of which 14 completed the measurements (mean age ± s.e.m. = 55 ± 3.6 years; one female; six dominant left-handers; see **Table 1** or demographic and clinical details). The following inclusion criteria applied to our recruitment: aged 18–75 years, no MRI contraindications, chronic tetraplegia (i.e. > 6 months post injury), no neurological impairment or body function impairments not induced by SCI, and able to provide informed consent.

We further recruited 18 age-, sex-, and handedness-matched able-bodied control participants (age = 56 ± 3.6 years; one female; five dominant left-handers). Inclusion criteria for the control participants included: aged 18–75 years, no MRI contraindications, no impairment of body function induced by SCI, no neurological illness, no hand impairments, and able to provide informed consent.

We obtained participants' informed consent according to the Declaration of Helsinki prior to study onset. Ethical approval was granted by the Kantonale Ethikkommission Zürich (KEK-2018-00937) and this study is registered on clinicaltrials.gov under NCT03772548. Two patients and one control participant were scanned twice due to excessive head motion during fMRI acquisition or suboptimal slice placement. We had to exclude one patient due to withdrawal from the study and one control participant due to distorted data.

4.3.2 Clinical characterization

We collected clinical data in a separate session. We scored patients' completeness of injury and impairment level based on the International Standards for Neurological Classification of Spinal Cord Injury (ISNCSCI). To assess the level of remaining sensorimotor upper limb function we gathered GRASSP scores (Kalsi-Ryan et al. 2012). The maximum GRASSP score per upper limb is 116 which equates to a healthy condition. Note that we only used GRASSP

scores reflecting motor function of the hands for our correlation analyses which included motor function of Opponens Pollicis, Finger Flexion of digit 3, Finger abductor of digit 5, Finger abductor of digit 2 (**Table 4.1**).

ID	*Sex*	*Age*	*Years since injury*	*AIS grade*	*Cause of injury*	*Neurological level of injury*	*Dominant hand*	*GRASSP score*	*Hand tested*	*GRASSP tested Hand. motor/sensory*	*GRASSP other Hand. motor/sensory*
S01	M	57	33	C	trauma	C6	L	145	R	3/19	3/22
S02	M	52	32	A	trauma	C5	R	78	L	0/5	0/16
S03	M	35	4	A	trauma	C5	R	90	L	0/17	0/13
S04	M	67	26	A	trauma	C7	R	119	L	5/2	4/4
S05	M	59	12	D	trauma	C4	R	187	R	8/9	9/15
S06	M	67	4	D	trauma	C5	L	173	L	6/9	5/15
S07	F	71	16	D	trauma	C6	R	196	R	4/24	20/24
S08	M	41	19	A	trauma	C5	L	105	L	0/11	0/22
S09	M	52	10	A	trauma	C3	L	118	R	9/0	7/0
S10	M	32	4	A	trauma	C4	L	21	L	0/0	0/4
S11	M	74	6	D	surgery	C3	L	220	R	16/24	17/24
S12	M	42	2	D	trauma	C3	R	187	R	16/13	19/15
S13	M	65	1	D	trauma	C2	R	218	R	15/24	16/24
S14	M	58	0	D	ischemic	C4	R	194	R	11/17	13/23

Table 4. 1 Demographics and clinical scores of tetraplegic patients

Remaining sensorimotor function of tetraplegic patients was assessed by Graded Redefined Assessment of Strength, Sensibility and Prehension test GRASSP). Table was ordered by years since injury. Sex: F, female; M, male; Age, age in years; AIS grade, American Spinal Injury Association (ASIA) Impairment Scale grade defined based on the International Standards for Neurological Classification of Spinal Cord Injury (ISNCSCI); A, complete; B, sensory incomplete; C, motor incomplete; D, motor incomplete; E, normal; Neurological level of injury, defined based on the ISNCSCI; dominant hand, defined using the Edinburgh handedness inventory: L, left; R, right; GRASSP, Graded Redefined Assessment of Strength, Sensibility and Prehension (maximum score: 232 points); tested side, side with the lowest score on the GRASSP measurement; GRASSP motor/sensory scores of the tested hands (maximum scores: 20/24). Adapted from (Kikkert et al., 2021).

4.3.3 Experimental Procedure and Tasks

To explore fine-grained somatotopic representations ipsilateral to the moved fingers, we used neuroimaging. Participants were instructed to make unimanual individual fingers

movements while their palm was facing upwards. We only tested patients' most impaired upper limp (as assessed by GRASSP). This laterization was matched to the patients. For some patients the loss of sensorimotor function after SCI did not allow them to make overt movements. If this was the case, then they were carefully instructed to make attempted (i.e., not imagined) movements. Our fMRI paradigm was carried out in a blocked design fashion with six conditions: movement conditions for each of the five fingers and a rest condition. Participants viewed a screen with five white circles corresponding to the five fingers. For participants moving their left hand the leftmost and rightmost circles corresponded to the thumb and little finger, respectively. For participants moving the right hand the leftmost circle corresponded to the little finger and the rightmost circle to the thumb. To instruct participants to make self-paced flexion/extension with one of the fingers, the corresponding circle on the screen turned red. The word 'Rest' on the screen indicated a rest condition during which participants were instructed to not move. A movement or rest block lasted 8 s, and each condition was repeated five times per run in a counterbalanced order. Each run comprised a different block order and had a duration of 4 min and 14 s. We acquired four runs, with a total duration of 16 min and 56 s. Instructions were delivered using Psychtoolbox (v3) implemented in MATLAB (v2014). We minimized head motion using over-ear MRI-safe headphones or padded cushions.

4.3.4 MRI data acquisition

We acquired MRI data using a Philips 3 Tesla Ingenia system (Best, The Netherlands) with a 17-channel HeadNeckSpine or, in case of participant discomfort due to the coil's narrowness, a 15-channel HeadSpine coil. Anatomical T1-weighted images covering the brain and cervical spinal cord were acquired using the following acquisition parameters: 0.8 mm^3 resolution, repetition time (TR) = 9.3 ms, echo time (TE) = 4.4 ms, and flip angle 8°. Task-fMRI data were acquired using an echo-planar-imaging (EPI) sequence with partial brain coverage: 22 sagittal slices were centred on the anatomical location of the hand knob with coverage over the thalamus and brainstem. We used the following acquisition parameters: 2 mm^3 resolution, TR = 2000 ms, TE = 30 ms, flip angle = 82°, and SENSE factor = 2.2. We acquired 127 volumes for each blocked design run.

4.3.5 Analysis of fMRI data

fMRI analysis was implemented using FSL v6.0 (https://fsl.fmrib.ox.ac.uk/fsl/fslwiki), Advanced Normalization Tools (ANTs) v2.3.1 (http://stnava.github.io/ANTs), the RSA toolbox (Nili et al., 2014; Wesselink DB & Maimon-Mor R, 2017), and MATLAB (R2018a).

4.3.6 Preprocessing of fMRI data

Common preprocessing steps were applied using FSL's Expert Analysis Tool (FEAT). The following preprocessing steps were included: motion correction using MCFLIRT (Jenkinson, 2002), brain extraction using automated brain extraction tool BET (Smith, 2002), spatial smoothing using a 2 mm full-width-at-half-maximum (FWHM) Gaussian kernel, and high-pass temporal filtering with a 100 s (blocked design runs) or 90 s (travelling wave runs) cut-off. Image co-registration was done in separate, visually inspected, steps. For each participant, a midspace was calculated between the four blocked design runs, that is, an average space in which images are minimally reoriented. We then transformed all fMRI data to this midspace using purely rigid probability mapping in ANTs. Next, we registered each participant's midspace to the T1-weighted image, initially using 6 degrees of freedom and the mutual information cost function, and then optimized using boundary-based registration (BBR; (Greve & Fischl, 2009b)) Each co-registration step was visually inspected and, if needed, manually optimized using blink comparison in Freeview.

4.3.7 Univariate analysis

To assess univariate task-related activity of the blocked design data, time-series statistical analysis was carried out per run using FMRIB's Improved Linear Model (FILM) with local autocorrelation correction, as implemented in FEAT. We obtained activity estimates using a general linear modelling (GLM) based on the double-gamma HRF and its temporal derivative. Each finger movement condition was contrasted with rest. A further contrast was defined for overall task-related activity by contrasting all movement conditions with rest. A fixed effects higher-level analysis was run for each participant to average across runs.

We defined an S1 hand ROI by converting the S1 ROI used to calculate split-half consistency to volumetric space. Any holes were filled and non-zero voxels were mean dilated. Next, the axial slices spanning 2 cm medial/lateral to the hand knob (T. Yousry, 1997) were identified on the 2 mm MNI standard brain (min-max MNI z-coordinates = 40–62). This mask was non-linearly transformed to each participant's native structural space. Finally, we used this mask to restrict the S1 ROI and extracted an S1 hand area ROI. The z-scored BOLD response for overall task-related activity was then extracted for voxels underlying the contra- and ipsilateral S1 hand ROIs per participant. A similar analysis was used to investigate overall task-related activity in contra- and ipsilateral M1 hand ROIs (see **Appendix 4.1**).

4.3.8 Representational similarity analysis (RSA)

The somatotopic hand representation is characterized by a representational distance between fingers that has been shown to be consistent across healthy individuals in both the contra- (Akselrod et al., 2017; G. Ariani et al., 2022; Ejaz et al., 2015; Gooijers et al., 2022; Kieliba et al., 2021; Kolasinski et al., 2016b; Liu et al., 2021) and ipsilateral sensorimotor cortex (Berlot et al., 2019; Diedrichsen, Wiestler, & Krakauer, 2013). Such intricate inter-finger relationship patterns can be estimated using representational similarity analysis (RSA; Kriegeskorte, 2008). In this study we therefore used RSA to estimate the intricate representational relationship between finger representations in the ipsilateral S1 hand area of both control participants and tetraplegic patients. We computed the distance between the activity patterns measured for each finger pair within the ipsilateral S1 hand ROI using the cross-validated squared Mahalanobis distance (or crossnobis distance; Walther et al., 2016). We extracted the blocked design voxel-wise parameter estimates (betas) for each finger movement condition versus rest and the model fit residuals under the S1 hand ROI. We prewhitened the extracted betas using the model fit residuals. We then calculated the cross-validated squared Mahalanobis distances between each possible finger pair, using our four runs as independent cross-validation folds, and averaged the resulting distances across the folds. If it is impossible to statistically differentiate between conditions (i.e., when this parameter is not represented in the ROI), then the expected value of the distance estimate would be 0. If it is possible to distinguish between activity patterns, then this value will be larger than 0. We assembled all finger pair distances in a representational dissimilarity matrix (RDM), with a width and height corresponding to the five finger movement conditions. Since the RDM is mirrored across the diagonal with meaningless zeros on the diagonal, all statistical analyses were conducted on the 10 unique off-diagonal values of the RDM. We first estimated the strength of the finger representation or 'finger separability' by averaging the 10 unique off-diagonal values of the RDM. If there is no information in the ROI that can statistically distinguish between the finger conditions, then due to cross-validation the expected separability would be 0. If there is differentiation between the finger conditions, the separability would be larger than 0 (Walther et al., 2016). To further ensure that our S1 hand ROIs was activated distinctly for different fingers, we created a CSF ROI that would not contain finger-specific information. We repeated our RSA analysis in this ROI and statistically compared the separability of the CSF and ipsilateral S1 hand area ROIs. Second, we tested whether the inter-finger distances were different between controls and patients using a robust mixed ANOVA with a within-participants factor for finger pair (10 levels) and a

between-participants factor for group (two levels: controls and SCI patients). Third, we estimated the somatotopic typicality (or normality) of each participant's RDM (Dempsey-Jones et al., 2019; Ejaz et al., 2015; Kieliba et al., 2021; Kikkert et al., 2021; Wesselink et al., 2019) by correlating it with a canonical RDM using a mantel permutation test. The canonical RDM was computed as the group average of controls. To validate our results we also computed the same correlation with typicality scores, obtained in another study (only contralateral typicality data; publicly available on https://osf.io/gmvua/; Wesselink et al., 2019). The spearman correlations were Fisher r-to-z transformed prior to statistical analysis (the spearman correlations (r_s) are used solely for visualization). Controls' and SCI patients' correlations coefficients were compared to each other and to those of a group of individuals with congenital hand loss (n = 13), hereafter one-handers, obtained in another study (data publicly available on https://osf.io/gmvua/; Wesselink et al., 2019). Congenital one-handers are born without a hand and do not have an S1 hand representation contralateral to the missing hand. Finally, we performed multidimensional scaling (MDS) to visualize the distance structure of the RDM in both contra- and ipsilateral S1 in an intuitive manner. MDS projects the higher-dimensional RDM into a lower-dimensional space, while preserving the inter-finger distance values as well as possible (Borg & Groenen, 2005). MDS was performed for each individual participant and then averaged per group after Procrustes alignment to remove arbitrary rotation induced by MDS.

4.3.9 Statistical data analysis

Statistical analysis was carried out using statsmodels (v0.13.1). Standard approaches were used for statistical analysis, as mentioned in the Results section. To detect outliers, we used the robustbase toolbox (Finger, 2010). $\mathbf{S_n}$ identifies an outlier (x_i) if the median distance of x_i from all other points, was greater than the outlier criterion (λ=2) times the median absolute distance of every point from every other point:

$$(1)\quad \frac{med_{j\neq i}\,|\,x_i - x_j\,|}{S_n} > \lambda \; where \; S_n = \; c_n \underset{i=1:n}{med} \left\{ \underset{j\neq 1}{med} |\, x_i - x_j \right\},$$

where c_n is a bias correction factor for finite sample sizes (Rousseeuw & Croux, 1993).

We detected no outliers for clinical data and z-scored BOLD responses and one outlier for the separability and typicality scores that was excluded from any further analysis.

If normality was violated (assessed using the Shapiro–Wilk test), non-parametric statistical testing or robust ANOVAs were used trough the bioinfo-kit and pingouin toolbox

(Huang et al., 2014; Vallat, 2018). Mauchly's test of sphericity was used to determine whether p-values needed to be Greenhouse-Geisser corrected. We used a Crawford–Howell t-test to compare single patients to the congenital and control groups (Corballis, 2009). All testing was two-tailed, and corrected p-values were calculated using the Benjamini–Hochberg procedure to control the FDR with $q < 0.05$. The correlational analysis was considered exploratory and we did not correct for multiple comparisons in this analysis.

Bayesian analysis was carried out using pingouin toolbox for the main comparisons to investigate support for the null hypothesis, no differences between groups, with a Cauchy prior width set at 0.707. Following the conventional cut-offs, a BF smaller than 1/3 is considered substantial evidence in favor of the null hypothesis. A BF greater than 3 is considered substantial evidence, and a BF greater than 10 is considered strong evidence in favor of the alternative hypothesis. A BF between 1/3 and 3 is considered weak or anecdotal evidence (Dienes, 2014; Kass & Raftery, 1995).

4.4 Results

4.4.1 Global suppression of ipsilateral sensorimotor activity during unimanual movements

We first investigated neural activity in ipsilateral S1 during unimanual finger movements. Movement-related beta estimates were extracted from the S1 hand area ipsilateral to the moved fingers. To compare BOLD activations between both hemispheres we also added here the equivalent beta estimates in contralateral S1 hand area from our previously published results (Kikkert et al., 2021; see **Figure 4.1**). Both groups were able to engage their ipsi- and contralateral S1 hand area by unimanual individual finger movements (controls ipsilateral: $t_{(17)} = 1.96$, $p_{corr} = 0.07$, $BF_{10} = 1.16$; controls contralateral: $t_{(17)} = 9.89$, $p < 0.001$, $BF_{10} > 100$ and patients ipsilateral: $t_{(13)} = 4.36$, $p < 0.01$, $BF_{10} = 49.05$; patients contralateral: $t_{(13)} = 9.16$, $p < 0.001$, $BF_{10} > 100$, respectively). A robust mixed ANOVA revealed no significant difference in task-related activity between controls and tetraplegic patients ($F_{(1,21.66)} = 1.07$, $p = 0.31$, $\eta^2 = 0.02$). As expected, beta estimates were lower in the ipsi- than in the contralateral S1 hand area ($F_{(9,15.38)} = 201.06$, $p < 0.001$, $\eta^2 = 0.45$). This difference in beta estimates did not reach significance when compared between groups and hemispheres (i.e., no interaction effect; $F_{(9,15.38)} = 2.72$, $p = 0.11$, $\eta^2 = 0.01$), even though ipsilateral activity tended to be higher in patients than controls, which might reach significance with greater sample sizes. Similar

results were found when exploring univariate task-related activity in the contralateral M1 hand ROI (see **Appendix 4.1**).

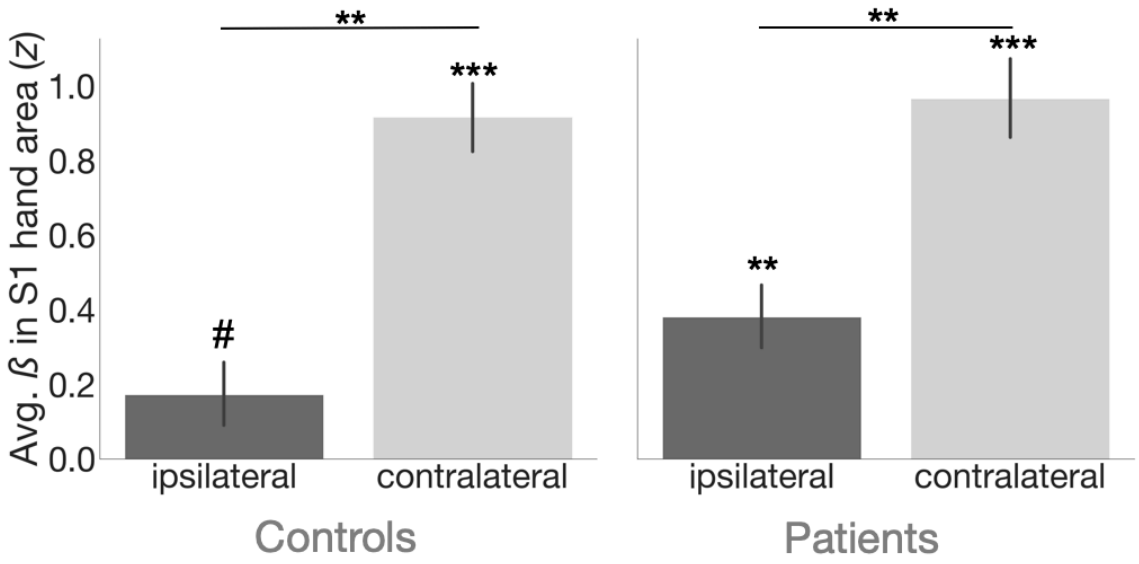

Figure 4. 1 Z-scored BOLD response in the contra- and ipsilateral S1 hand area during unimanual movements.

*Beta estimates (ß) in the ipsilateral S1 hand area were significantly lower than within the contralateral S1 hand area, as confirmed by a post hoc test (Tuckey's HSD) on pairwise comparisons within each group (Controls: $p < .01$, $BF_{10} > 100$; Patients: $p < .01$, $BF_{10} = 48.83$). However, beta estimates were not significantly different between tetraplegic patients and healthy controls. The black error bars indicate the standard error. Single t-statistics are correct for multiple comparisons. ** = p < .01; *** = p < .001; # = tends to significance.*

4.4.2 Preserved sensory function in hands is inversely correlated to cortical activity in ipsilateral S1

Given that our sample of tetraplegic patients was heterogenous, group comparisons may overlook individual differences. To detect any potential effects of the SCI we explored potential clinical determinants for neural activity in ipsilateral S1 during individual finger movements. We investigated how retained sensory function in both hands, motor function in both hands and years since injury related to ipsilateral S1 hand area activity. First, we computed correlations between each determinant and the z-scored beta estimates extracted from the ipsilateral S1 hand area. We found that patients with less sensory function in both hands had higher activity in the ipsilateral S1 hand area ($r = -0.55$, $p < 0.05$; **Figure 4.2A**). No significant correlation was found for retained motor function in hands ($r = -0.12$, $p = 0.69$;

Figure 4.2B) or time since injury (r = -0.14, p = 0.63; **Figure 4.2C**) and ipsilateral S1 hand area activity.

Second, we conducted an explorative robust stepwise linear regression to investigate whether these potential clinical determinants predicted activity levels in the ipsilateral S1 hand area during movement. Sensory functions in both hands significantly predicted beta estimates extracted from the ipsilateral S1 hand area (R^2 = 0.31, $F_{(1,12)}$ = 5.26, p < 0.05). This effect was mainly driven by the more impaired hand (**Appendix 4.2** for individual hand correlations). We found no relationship for the other regressors (motor function: t = -1.458, p = 0.18, years since injury: t = -1.79, p = 0.11, t = 1.9, p = 0.09).

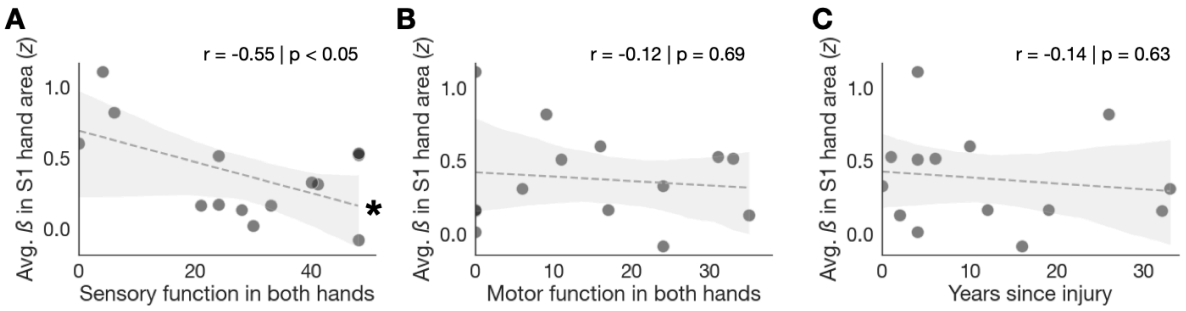

Figure 4. 2 Clinical determinants in relation to ipsilateral S1 hand area activity.
*Activity in the ipsilateral S1 hand area significantly correlated with sensory function of both hands (A), but not retained motor function in both hands (moved) hand (B) and years since injury (C). Single grey dots reflect individual patients. Dashed dark grey line reflects regression line. Shaded area corresponds to the confidence interval (ci=95). * = p < 0.05.*

4.4.3 Preserved ipsilateral finger representations in tetraplegic patients

Next, we investigated the fine-grained inter-finger representational patterns in the ipsi- and contralateral S1 hand area of tetraplegic patients and healthy controls using RSA (**Figure 4.3**). We computed RDMs for each participant and averaged them within each group (**Figure 4.3A**). To visualize the distance structure of the RDM in both controls and patients, we employed MDS (**Figure 4.3B**). For both patients and controls the inter-finger pattern was similar to what has previously been reported (Kikkert et al., 2021). In addition, the inter-finger distances were drastically reduced in the ipsilateral hemisphere, however, still following the typical inter-finger distance pattern, as we previously observed (Kikkert et al., 2021). We then calculated the averaged inter-finger distance per participant, also termed separability. We found that inter-finger separability (**Figure. 4.4A**) was greater than 0 in the S1 hand area

ipsilateral to the moved fingers both for healthy controls and tetraplegic patients (Controls: $t_{(17)} = 13.96$, $p<0.001$; Patients: $t_{(12)} = 8.64$, $p < 0.001$). This shows that ipsilateral S1 contains representational information of individuals fingers during their (attempted) movements even after tetraplegia. More importantly, a Welch two-samples t-test showed no differences in separability between groups ($t_{(30)} = -0.82$, $p = 0.42$, $BF_{10} = 0.44$), indicating our patient group maintained the same degree of representational finger information. In addition, a Games-Howell post-hoc test revealed that separability (representational strength) in the ipsilateral S1 hand area was significantly greater than in a control cerebral spinal fluid (CSF) control ROI (i.e., where one would not representation information about finger representations) in both controls ($p < 0.01$) and patients ($p < 0.01$).

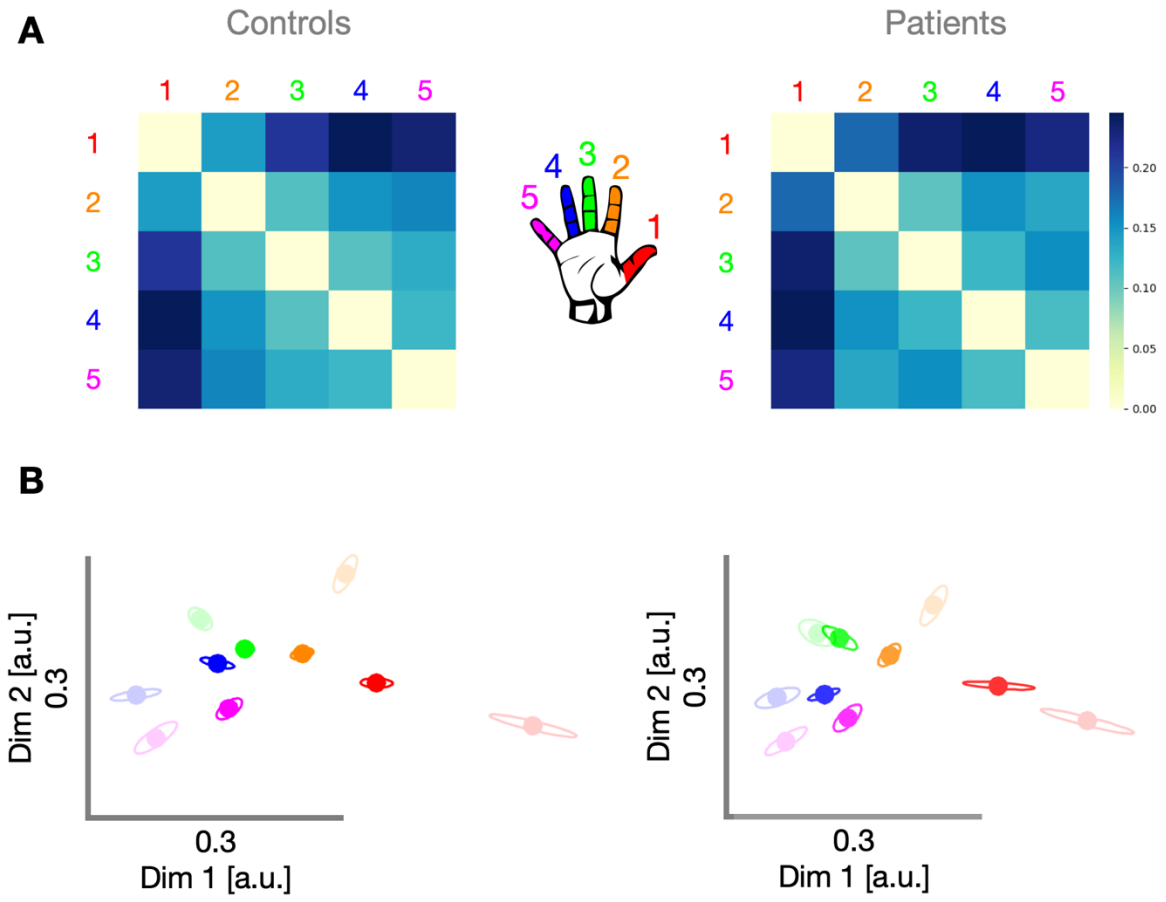

Figure 4. 3 Preserved finger representations in ipsilateral S1

A. *Dissimilarity matrices reflecting the inter-finger Mahalanobis distances in the ipsilateral S1 hand area for controls (left) and tetraplegic patients (right). Individual fingers are represented by different numbers and colours: thumb, 1 (red); index finger, 2 (yellow); middle finger, 3 (green); ring finger, 4 (blue); little finger, 5 (pink).* ***B.*** *Two-dimensional projections of the RDMs. The relative distances between the dots reflect the inter-finger distances. Ellipses represent the between-participants' standard error after Procrustes alignment. Clear dots and ellipses*

reflect the fingers within the ipsilateral S1 hand area, while the more transparent dots reflect the fingers in the contralateral S1 hand area. Dim = dimension; a.u. = arbitrary dimension.

Note that even though separability might be similar both in tetraplegic patients and healthy controls, the organization of the finger representations could be atypical when suffering from tetraplegia. To address this, we first examined the inter-finger distances across pairs of fingers and between groups. Our robust mixed ANOVA revealed no significant difference in inter-finger distances between tetraplegic patients and healthy controls ($F_{(1,30)} = 0.67$, $p = 0.42$, $\eta^2 = 0.01$). The inter-finger distances were significantly different across finger pairs, as would be expected based on somatotopic mapping ($F_{(9,270)} = 27.92$, $p < 0.001$, $\eta^2 = 0.23$). This pattern of inter-finger distances was not significantly different between groups (i.e., no significant finger pair by group interaction; $F_{(9,270)} = 0.91$, $p = 0.51$, $\eta^2 = 0.01$). Second, we calculated, per participant, a measure of representational typicality. To do so, we calculated a spearman correlation between each participant's inter-finger distance pattern in the ipsilateral S1 hand area and a canonical inter-finger distance pattern (taken from the group RDM of controls). We then compared the resulting ipsilateral S1 typicality scores between controls, patients, and an additional control group (contralateral scores) of congenital one-handers (Wesselink et al., 2019 ; **Figure 4.4B**). The latter group consisted of people who were born without a hand and consequently do not have a representation of their missing hand. Our ANOVA results suggested a significant difference in typicality between the three groups ($F_{(2,39)} = 11.67$, $p < 0.001$, $\eta^2 = 0.36$). Pairwise comparisons revealed higher ipsilateral S1 hand representation typicality in controls compared to contralateral S1 hand representations of congenital one-handers ($t = -4.12$, $p < 0.01$, $BF_{10} = 85.63$), as expected. More interestingly, ipsilateral hand representation typicality scores of tetraplegic patients were significantly higher than the contralateral S1 hand representation typicality scores of the congenital one-handers ($t = -4.34$, $p < 0.01$, BF10 = 105.05). In contrast, ipsilateral S1 hand representation typicality scores of tetraplegic patients did not significantly differ from the ipsilateral hand representation typicality scores of controls ($t = -0.56$, $p = 0.83$, $BF_{10} = 0.39$), with Bayes Factor showing anecdotal evidence in favor of the null hypothesis. This shows that tetraplegic patients generally preserve ipsilateral somatotopic finger representations in S1. Furthermore, we investigated in both controls and patients to which extend the finger representational structure in the ipsilateral S1 hand area is explained by contralateral finger representations (**Figure 4.4C**). Correlations coefficients between finger-specific S1 hand area representations of both hemispheres did not significantly differ between both groups ($t = 0.49$, $p = 0.63$, $BF_{10} = 0.37$), with BF reflecting anecdotal evidence in favor of no differences

between groups. Indeed, overall, the representational geometry of fingers in tetraplegic patients during unimanual movements seems to remain similar between both hemispheres.

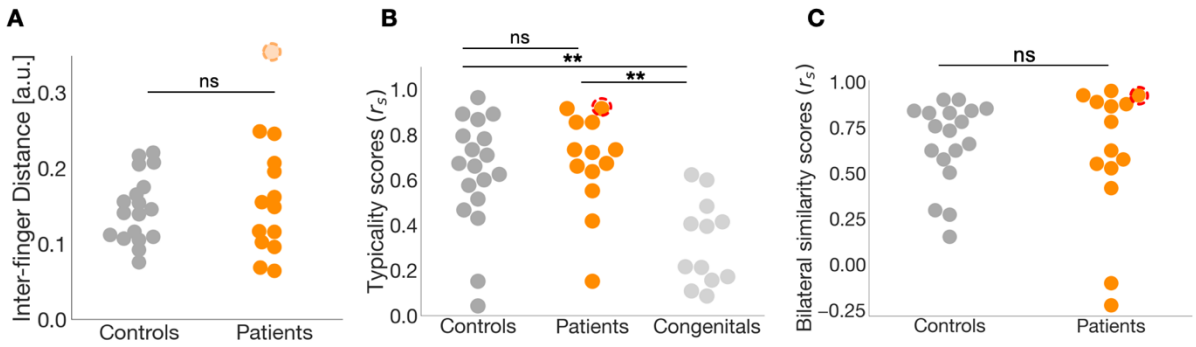

Figure 4. 4 Evaluation of geometric structure of finger representations

(A) *Strength of representations measured as the mean inter-finger distance of the representational structure in ipsilateral S1 hand area for both controls and tetraplegic patients. Both groups exhibited a similar representational geometry of finger representation.* ***(B).*** *Typicality of the representational structure in controls and patients, calculated as the spearman correlation coefficient (r_s) between each participant's ipsilateral representational geometry of fingers and a canonical RDM (defined as the control group average RDM). Congenital one-handers data from a previous study (Wesselink et al., 2019) was added as an additional control group.* ***(C).*** *Similarity analysis between representational structure in S1 hand area of controls and tetraplegic patients, contralateral and ipsilateral to the moved fingers. The patient with the most severe sensorimotor function impairment (i.e., a complete paralysis and complete loss of sensory function of the tested hand) is highlighted in red, appears with greater opacity in (A) due to being an outlier. Error bars reflect the standard error. ** = $p < 0.01$, *** = $p < 0.001$, ns = non-significant.*

However, due to the heterogeneity of our group, any deterioration of ipsilateral finger somatotopy after SCI may not be found at a group level. To investigate in more detail whether retained connections between the periphery and brain are necessary to preserve ipsilateral finger somatotopy we explored patient S10 in further detail. This tetraplegic patient experienced complete hand paralysis as well as no remaining sensory function in the more impaired hand and near complete loss of sensory function in the other hand (see **Table 4.1**). However, this patient showed a highly typical hand representation pattern in ipsilateral S1 hand area. Crawford Howell t-tests revealed that patient S10's typicality of ipsilateral hand representation was significantly different from congenital one-handers ($t_{(11)} = 3.03$, $p < 0.05$, $BF_{10} = 5.3$) but not from controls ($t_{(16)} = 1.15$, $p = 0.27$, $BF_{10} = 0.44$). Thus, we suggest that preserved pathways between periphery and the brain are not essential to maintaining typical representational structures in S1 ipsilateral to the moved fingers.

4.4.4 Ipsilateral finger representations do not predict clinical determinants

We then related clinical and behavioral determinants with finger representation typicality in ipsilateral S1. Retained sensory function in both hands (r_s = 0.19, p = 0.53; **Figure 4.5A**), retained motor function in hands (r_s = 0.29, p = 0.33; **Figure 4.5B**), and time since injury (r_s = -0.45, p = 0.13; **Figure 4.5C**) did not correlate with the obtained typicality scores from ipsilateral S1 hand area. We conducted an explorative stepwise linear regression to investigate whether these potential clinical determinants predicted typical representational patterns in ipsilateral hand area during movement. We found that none of the regressors significantly predicted typicality scores extracted from the ipsilateral S1 hand area (sensory function: t = 0.12, p = 0.91, motor function: t = 0.8, p = 0.45, years since injury: t = -0.69, p = 0.51, age: t = -0.91, p = 0.39).

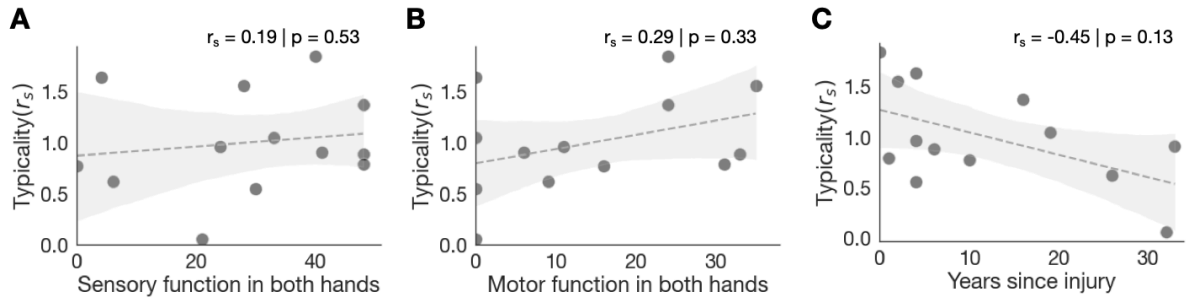

Figure 4. 5 Clinical determinants in relation to ipsilateral S1 hand area finger representation typicality.

*Finger representation typicality in the S1 hand area, ipsilateral to individual moved fingers, did not significantly correlated with (**A**) retained sensory function in both hands (assessed by GRASSP scores), (**B**) retained motor function in both hands, and (**C**) years since injury. Single grey dots reflect each patients' score. Dashed dark grey line reflects regression line. Shaded area corresponds to the confidence interval (ci=95). * = p < 0.05*

4.5 Discussion

In the current study, we revealed that following cervical SCI, peripheral inputs are not essential to preserve finger representations in the ipsilateral S1 hand area during attempted finger movements. Our results show that also in ipsilateral S1, individual finger representations are preserved during attempted movements, even when sensorimotor functions in upper limbs are reduced or fully absent. Interestingly, lower or absent sensory

function of tetraplegic patients' hands led to higher BOLD responses in S1 ipsilateral to the attempted moved finger.

4.5.1 Geometry of finger representations in ipsilateral S1

The typicality of ipsilateral representations differed from congenital one-handers but not from controls. This was also the case for a patient with an almost complete absence of sensorimotor function in both hands. Since also ipsilateral finger representations are a hallmark of hand representations, this discovery extends our previous findings in tetraplegic patients (Kikkert et al., 2021) and others (Fifer et al., 2021; Flesher et al., 2016) as well as findings from studies in amputees (Bruurmijn et al., 2021; Kikkert et al., 2016; Wesselink et al., 2019) highlighting preserved sensorimotor processing years after SCI or hand amputation.

In contrast to contralateral representations, we did not find a deterioration of ipsilateral representations across the years after SCI. However, the small trend we observed could be larger with increasing sample size.

4.5.2 Modulation of ipsilateral finger representations through interhemispheric connections

What mechanism could drive this preservation of finger representations in tetraplegic patients and how do they differ between contralateral and ipsilateral S1 during unimanual movements? Since peripheral information flow was reduced or absent in our patients, we suggest that these somatotopic representations are cortically driven. Previously we argued that it is likely that contralateral finger representations could be activated through different simultaneous mechanisms including i) a cortical copy of efferent output signals when producing individual finger movements, so called efference copies (Adams et al., 2013; London & Miller, 2013), ii) shifting attention through top-down processes (Kuehn et al., 2018; Puckett et al., 2017) or hardwired maps that are resilient against neural plastic changes (Bruurmijn et al., 2021; Ejaz et al., 2015; Kikkert et al., 2016; Wesselink et al., 2019). The underlying neurophysiological processes generating ipsilateral representations during unimanual movements are still not fully understood. It has been proposed that ipsilateral representations could be provoked via i) transcallosal connection to the contralateral hemisphere (Allison et al., 1989; Diedrichsen, Wiestler, & Ejaz, 2013; Grefkes et al., 2008; Volz et al., 2015)or ii) direct uncrossed afferent inputs to ipsilateral hemisphere (Kanno et al., 2003).

Our results presented here favor the former. We found BOLD responses in ipsilateral S1 despite dampened or complete loss of sensory function in tetraplegic patients. More strikingly, these patients were able to generate ipsilateral finger representation during (attempted) unimanual individuated finger movements.

Thus, we suggest that cortico-cortical connections mediate this effect, presumably through transcallosal pathways. It is very likely that ipsilateral finger representations in tetraplegic patients are preserved through inter-hemispheric excitation and inhibition and intrahemispheric inhibition while performing unimanual movements. It is important to note that even though one of our tetraplegic patients appeared to have near to complete absence of sensorimotor function, the majority of patients preserved some sensorimotor function in their hands. This potentially might still enable ipsilateral representations to be generated via reafferent sensory input.

4.5.3 Ipsilateral activity in S1 is inversely correlated to preserved sensory function in the hands

Furthermore, we observed that activity in ipsilateral S1 but not typicality depends on the remaining sensory function of patients. Previously, it was shown that acute unilateral deafferentation of the hand induced by anesthesia resulted in greater motor-evoked potentials (MEP) in the other hand (Werhahn et al., 2002), accompanied by a decreased concentrations of GABA and GABA/creatine (inhibitory neurotransmitters) ratios in the ipsilateral sensorimotor cortex (Levy et al., 2002; Werhahn et al., 2002). These changes are likely of cortical origin since they only appeared when applying Transcranial Magnetic Stimulation (TMS) pulses over the ipsilateral sensorimotor cortex but were absent during brainstem electrical stimulation (Ugawa et al. 1991). This means that our observed enhancement of ipsilateral BOLD response in ipsilateral S1 could be also due to a reduction of IHI. Note, the previous measured MEP returned to baseline after anesthesia. Therefore, it still needs to be determined whether permanent (partial) deafferentation following tetraplegia lead to similar reductions in GABA and GABA/creatine concentrations. Nonetheless, this transfer of cortical excitability between hemispheres might mediate compensatory processes (Kinsbourne, 1987; Rauschecker, 1995), e.g. following a SCI, whereby a lack of sensorimotor functions of the ‘more’ impaired hand (as assessed by our GRASSP measurements) is compensated for by ipsilateral sensorimotor cortex.

4.5.4 Final considerations

Finally, we also observed a partial overlap in typicality of ipsilateral and contralateral finger representations during unimanual movements. However, our analysis did not allow to make any further interpretations. This overlap could reflect both similar activity patterns of S1 neurons in both hemispheres that are responsible for contralateral movements and similar activity patterns between a subgroup of S1 neurons coding contralateral movements in one hemisphere and another subgroup of S1 neurons coding ipsilateral movements in the other hemisphere (Diedrichsen, Wiestler, & Ejaz, 2013).

Note, we instructed the patients to perform attempted (i.e. not imagined) individuated finger movements. We did so, because previous studies demonstrated that imagined movements result in lower sensorimotor cortex activity compared to attempted movements (Cramer et al., 2005) and that complete paraplegic patients are able to differentiate between both movements with the impaired body part (Cramer et al., 2005; Hotz-Boendermaker et al., 2008; Sabbah et al., 2002). Moreover, paraplegic patients appeared to engage a similar motor network during attempted compared to overt foot movements (Cramer et al., 2005; Hotz-Boendermaker et al., 2008; Sabbah et al., 2002). However, whether attempted and overt movements have the same underlying neural mechanisms is still to be determined.

Together our results suggest that following SCI, individual finger representations in ipsilateral S1 are preserved even after years of complete absence of sensorimotor function of the upper limbs. Interestingly, reduced sensory function in both hands appears to be linked to greater neural activity in S1 ipsilateral to the moved fingers. A better understanding or bilateral integration and adaptation during unimanual movement control may improve rehabilitation approaches following SCI.

4.6 Appendices

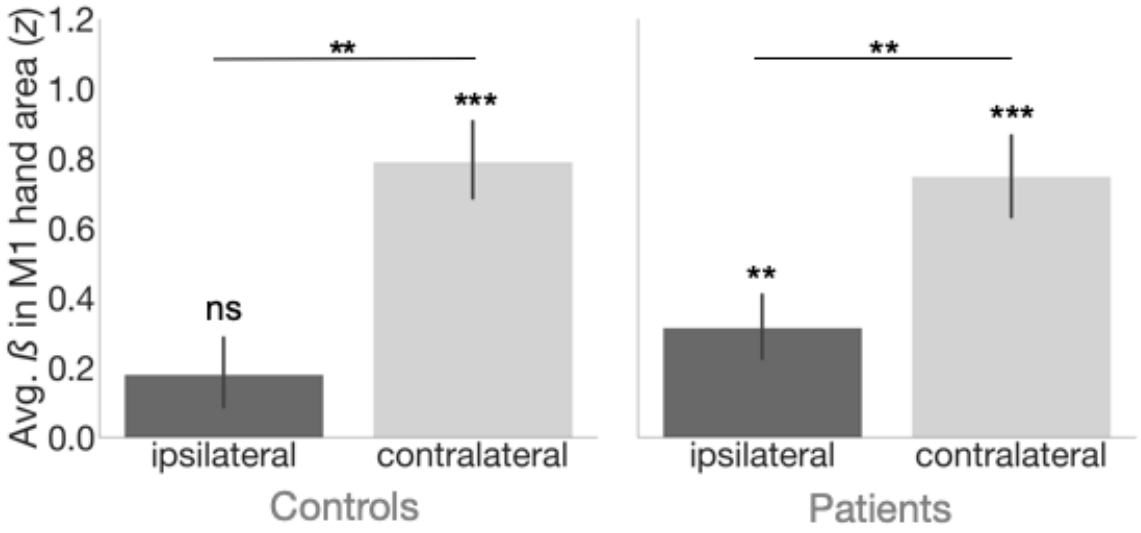

Appendix 4. 1 Z-scored BOLD response in bilateral M1 during unimanual movements.

*Extracted z-scored beta estimates (ß) from M1 hand area in ipsilateral and contralateral M1. Again both groups were able to engage their ipsi- and contralateral M1 hand area by unimanual individual finger movements, apart from ipsilateral M1 in healthy controls (controls ipsilateral: $t_{(17)} = 1.76$, $p_{corr} = 0.09$, $BF_{10} = 0.87$; controls contralateral: $t_{(17)} = 6.83$, $p < 0.001$, $BF_{10} > 100$ and patients ipsilateral: $t_{(13)} = 3.23$, $p < 0.01$, $BF_{10} = 8.02$; patients contralateral: $t_{(13)} = 6.16$, $p < 0.001$, $BF_{10} > 100$, respectively). A robust mixed ANOVA revealed no significant difference in task-related activity between controls and tetraplegic patients ($F_{(1,21.66)} = 0.09$, $p = 0.76$, $\eta^2 < 0.05$). As expected, beta estimates were lower in the ipsi- than in the contralateral S1 hand area ($F_{(9,15.38)} = 148.99$, $p < 0.001$, $\eta^2 = 0.28$). This difference in beta estimates tended to be significant between groups and hemispheres (i.e., tendency to interaction effect; $F_{(9,15.38)} = 4.$, $p = 0.05$, $\eta^2 = 0.01$). The black error bars indicate the standard error of beta estimates. *** = p < .001; # = tendency to significance.*

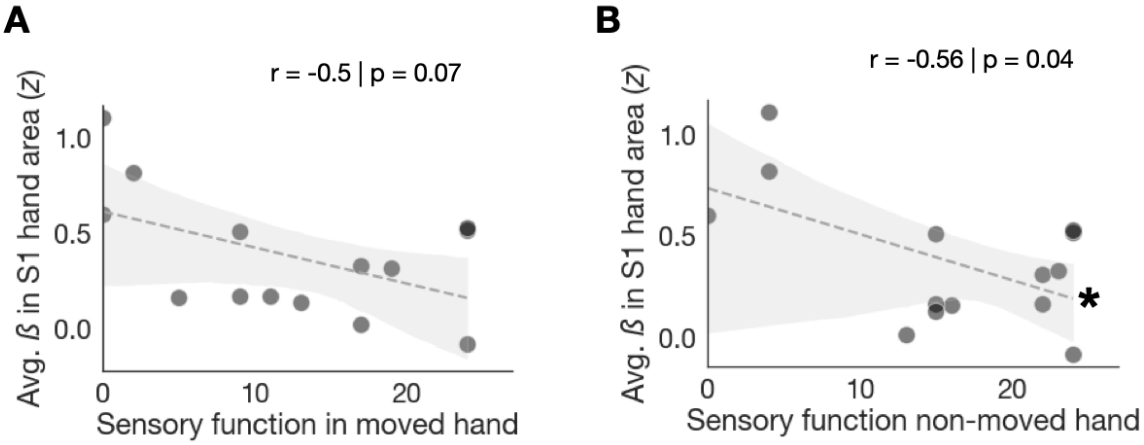

Appendix 4. 2 Sensory function of each hand in relation to ipsilateral S1 hand area activity.

*Activity in the ipsilateral S1 hand area showed a tendency to reach a significant correlation with sensory function of (**A**) the (attempted) moved hand and was significantly correlated to (**B**) the hand that was not instructed to move. Single grey dots reflect individual patient's scores. Dark grey line reflects regression line. Shaded area corresponds to the confidence interval (ci=95). * = $p < 0.05$.*

5 General Discussion

The aim of this PhD thesis was to shed light on the question of whether finger representations within somatotopic maps of S1 could still be activated in the absence of sensory input and what cognitive processes might influence these activations. To test this, we collected neuroimaging data and used state-of-the-art analysis approaches.

In chapter 2, we demonstrated that task demands can modulate the finger-specific information content in the S1 hand area during different time points of a vibrotactile discrimination task, presumably even in the absence of tactile inputs. The latter should be interpreted with caution. We will describe the difficulties with this interpretation in sections **5.1** and **5.4**.

Chapter 3 builds on the previous chapter. Here, we identified subcortical regions, i.e. dorsal striatum, that showed functional coupling with finger-related neural activity in S1 hand area. This connectivity changes in the network appeared to be related to task performance.

In chapter 4, we extended previous findings on neural plasticity following tetraplegia by providing evidence for bi-hemispheric interactions in order to preserve finger representations in S1. Even with a complete loss of sensory functions in the hands, patients were able to activate ipsilateral finger representations via attempted but not overt unimanual movements.

In the following sections we will outline the significance of each individual finding, embed it in the current literature, look at the limitations of our studies, and outline future considerations.

5.1 WM-task demands modulate finger representations in S1

In chapter 2, we investigated both somatosensory and tactile WM-processing within the somatotopic map in S1 during a vibrotactile frequency discrimination task. Even though the task goal was to discriminate between two frequencies presented consecutively and separated by a delay period, we hypothesized that the processing of task-relevant features would reside within somatotopic maps of S1. Since the low spatial resolution of our neuroimaging data did not allow us to capture small groups of frequency-tuned neurons, we used finger representation activations in S1 hand area as an indicator for somatosensory information processing and information retention. Our findings suggest that task demands

influence the finger representations not only during stimulus perception but to a lesser extend also during stimulus storage, presumably by feature-selective tuning of top-down mechanisms. This provides new evidence for the debate of S1 involvement during vibrotactile frequency discrimination, specifically during the delay period. According to sensory recruitment models, primary sensory areas are not only involved in stimulus processing but also retention and manipulation of stimulus information during the delay period (Pasternak & Greenlee, 2005). Previous studies were not able to decode any frequency information from S1 activity patterns during the delay period, but instead from higher-level brain areas (i.e. SPL, IFG and PMC Schmidt et al., 2017; Wu et al., 2018). We in turn did not attempt to decode frequency information but instead tried to decode the information about the stimulus location (i.e. what finger was stimulated). Thus, we did not aim to decode a specific feature of the stimulus but rather the somatotopic component which provides a framework for tactile information processing and its potential storage. Our results suggest that somatosensory information does not only reside in somatotopic maps during vibrotactile stimulation but also during the delay period. This latter result parallels recent findings where spatial stimulus properties, applied by vibrotactile stimulation, could be decoded from S1 in the absence of any tactile stimulation (Schmidt & Blankenburg, 2018). Their whole-brain decoding approach allowed them to identify voxels that showed the highest classification accuracies for the spatial stimulus properties. Interestingly, these voxels were also located in the area that usually reflects the stimulated finger (i.e index). Thus, somatotopic processing of WM contents is likely, however, the delay period in our paradigm did not allow for a clear distinction between stimulus perception and WM and thus, the result can only provide a new hypothesis to be tested in the future.

In addition, our parametric modulation results suggest that during the delay period activity in S1 temporally unfolded in a U-shaped manner. This corroborates findings revealing that information retention in the absence of sensory information is not always reflected in constant delay activity, especially when temporal structure of the delay period can be anticipated (Rose et al., 2016). Even though we randomly varied the duration of the delay period, its temporal structure could be somewhat predicted by our participants and might drive this effect. However, even though a similar U-shape has been observed in monkey studies in higher-level processing areas, none was yet observed during the delay period in S1 (for review, see Romo & Rossi-Pool, 2020). Note, we only modelled the activity for three consecutive time-bins. Techniques with better temporal resolution could be able to shed more light on this temporal unfolding.

5.2 Dorsal striatum and S1 increase functional connectivity during vibrotactile stimulation to meet task demands

In chapter 3, our study hypotheses were driven by previous findings in chapter 2. We aimed to identify potential regions that interact with somatotopic activations in S1 in a condition-dependent manner during vibrotactile stimulations in a vibrotactile frequency discrimination task. We computed a PPI analysis on the previously collected neuroimaging data. Our results indicate that dorsal striatum (putamen and caudate) are functionally coupled to finger-specific ROIs during the first vibrotactile stimulation of the task. This interaction appears plausible given previous neurophysiological findings. These show that basal ganglia and thalamus receive a great amount of somatotopically organized projections from the somatosensory cortices (Kunzle, 1977; Selemon & Goldman-Rakic, 1985). Further examination of the corticostriatal projections led to the distinction between 'association neostriatum', consisting of the caudate nucleus and anterior putamen, and the 'motor neostriatum, which includes more posterior regions of the putamen (Selemon & Goldman-Rakic, 1985). Our results closely overlap with the former, suggesting higher-level processing of somatosensory information. Further evidence on the importance of dorsal striatum in somatosensory processing is mostly provided by studies on neurodegenerative diseases, i.e. Parkinson's Disease (Sathian et al., 1997; Schneider et al., 1987; Zia et al., 2003). However, in WM studies, the role of the striatum mostly is mostly confined to a terminal for PFC top-down control. Here, fronto-striatal loops have been attributed a gatekeeping function, via top-down control, in WM tasks whereby this function filters out task-relevant features from the to-be encoded stimulus (Edin et al., 2009; McNab & Klingberg, 2008). Since we did not observe functional coupling between S1 and PFC, presumably due to differences in HRFs, the question whether such loops could also explain our results remains unanswered.

Finally and interestingly, we could also observe a positive relationship between connectivity changes in dorsal striatum and task performance, which highlights the involvement of dorsal striatum in mediating task-relevant neural activity. Such a relationship to behavior has previously only been shown to influence discrimination performance in rats (Gerdjikov et al., 2010; Hawking & Gerdjikov, 2013; Hipp et al., 2006) and needs further investigations in humans.

5.3 Following tetraplegia, patients can still activate ipsilateral finger representations during unimanual (attempted) movements through transcallosal pathways.

In chapter 4, we investigated the effects of abrupt (partial) loss of sensorimotor function following a cervical SCI on finger representations in bilateral S1. More specifically, we examined whether tetraplegic patients could still activate ipsilateral finger representations in S1 during unimanual movements. In addition to neuroimaging data, we also collected clinical determinants, e.g. remaining sensorimotor function in both hands and years since injury. Our findings highlight that even with a complete loss of sensory input from the periphery, patients are still able to activate finger representation in ipsilateral S1 and that the representational geometry appears to be coherent with healthy controls. This extends previous findings on preserved finger representations after SCI (Fifer et al., 2021; Flesher et al., 2016; Kikkert et al., 2021).

Our results also have the potential to resolve to the debate on whether mirror movements are inhibited via interhemispheric connection (Diedrichsen, Wiestler, & Krakauer, 2013; Wiestler & Diedrichsen, 2013) or reafferent sensory pathways (Kanno et al., 2003). Strikingly, even the patient with a complete loss of sensory function was still able to activate finger representation in ipsilateral S1 during unimanual movements, suggesting that interhemispheric connections were highly likely to drive this effect. We propose that higher-level areas, i.e SMA, have the potential to activate these representations via transcallosal pathways.

Finally, we also found that activity in ipsilateral S1 but not the typicality of finger representations depends on the remaining sensory function of patients. Previous studies on acute deafferentation suggest that our observed enhancement of ipsilateral BOLD response in ipsilateral S1 with decreasing sensory function in the hands could be due to a disinhibition (Levy et al., 2002; Werhahn et al., 2002). This needs further investigations whether such changes in fact reflect a compensatory effect between hemispheres.

5.4 Limitations

In chapter 2, we used a delay period between two vibrotactile stimulations to investigate somatotopic changes in the absence of any tactile input. However, the duration of the period (6-8s) is short compared to conventional vibrotactile WM-tasks. A comparable example of a

no-memory condition for visual WM has been previously reported where using a longer delay allowed comparing the results to a similarly long ITI, which in turn enabled the authors to demonstrate that the activity persist late into the delay (Ester et al., 2009). Notably, other work has simply used very long delays to separate perceptual processing (12 s; Rademaker et al., 2018). The purpose of this was to disentangle neural processes that underly stimulus perception from WM, which might be 'blurred' during shorter delay periods due to the sluggishness of BOLD response. Even though our low variance inflation indicated that our model could discriminate between both timepoints, this bleeding-in effect could still occur.

Furthermore, we estimated a specific HRF for S1 during our vibrotactile frequency discrimination task. This might be appropriate during short events, such as stimulus presentations (Pleger et al., 2008; Preuschhof et al., 2006), but could be flawed for the longer delay period. Temporal unfolding of WM related signals might follow other temporal profiles. To counteract this, Finite Impulse Response (FIR) modelling could be a useful tool that approximates the temporal profiles, with the consequence that the analysis is less powerful. Therefore, a balance between the appropriate delay duration and a function that best models the temporal unfolding might be ideal to separate stimulus perception from WM.

In chapter 3, the PPI analysis allowed us to identify brain regions that showed a condition-dependent interaction with finger-specific clusters in S1 during vibrotactile stimulation. From this analysis, we could only infer that dorsal striatum's BOLD signal changes appeared to interact with BOLD signals changes in S1, meaning that both showed BOLD signal increases during memory trials. However, PPI generally entails interpretational issues (Friston et al., 1997), meaning, the results could be driven by two phenomena. First, the WM task could have in general modulated responses in both S1 and dorsal striatum during the memory condition (context-specific interpretation). Alternatively, memory-related modulation of responses in dorsal striatum occurs through S1 inputs (stimulus specific).

This could be overcome with more elaborate analysis approaches, e.g. dynamic causal modelling. With this, one could test whether fronto-striatal loops are in fact entail top-down control mechanisms that alter the activity in somatotopic maps in S1.

In chapter 4, our relatively small and heterogenous group of patients hampers generalizations. First, with a greater range of years since SCI the deteriorating effect of ipsilateral finger representations might be larger than what we observed. This would mean that loss of sensory function might lead to deformations of the ipsilateral finger

representations (as shown for the contralateral hemisphere, (Kikkert et al., 2021). Second, our patients had different levels of preserved sensory function. Even though the patient with a complete loss of sensory function following tetraplegia could activate ipsilateral finger representations during attempted movements, most of our patients preserved some sort of sensory function. To underscore our assumption that loss of sensory input does not influence the preservation of finger representations, it would be interesting to study more patients with a complete loss of sensory function.

5.5 Future considerations

5.5.1 A complete multicomponent model of WM

The realm of WM has been extensively shaped by the multicomponent model. Within this realm multiple components have been suggested to interact with each other (for review, see Chai et al., 2018). Currently, the multicomponent model of WM (Baddeley, 2012) consists of three components: a phonological loop, a visuospatial sketchpad and a central executive involving the attentional control system (Baddeley, 2003, 2012). The central executive component was introduced as an "episodic buffer", accounting for the integration of cross-modality information (Baddeley, 2000). Our results give rise to a new component to be studied in the future with a more elaborate study design. If it can be verified, then this would emphasize the necessity to extend the current multicomponent model of WM with a modality-specific storage component for sensory information. Other models of sensory recruitment have proposed that somatosensory cortex not only engages in stimulus perception, but also WM storage with engagement depending on selective attention (D'Esposito & Postle, 2015; Pasternak & Greenlee, 2005; Postle, 2016). According to this model, memory traces could reside in somatotopically organized areas that act as a storage system that can be modulated depending on task demands. Top-down control mechanisms might be responsible for updating these memory traces in the somatosensory cortex. The rehearsal of tactile stimulus information could be driven by spatial attention (Katus et al., 2014).

5.5.2 Dynamic causal modelling of brain network guiding unimanual movements after tetraplegia

In the study of tetraplegic patients our field of view (FOV) did not include PMC and SMA. Nonetheless, these brain regions have been implicated to play a somewhat top-down role in

activating ipsilateral sensorimotor cortex during unimanual movements (Grefkes et al., 2008; Volz et al., 2015). An outstanding question is whether in tetraplegic patients these pathways are reflected in their effective connectivity during unimanual movements. Using DCM would enable to identify the bihemispheric information flow during these movements.

5.6 Conclusions

Over the last century, extensive research on somatosensory processing in the brain provided us with insights on how the brain makes sense of the world around us through bodily experiences. Of particular interest is the discovery of somatotopic maps which build the anatomical foundation through which we can localize somatosensory inputs and create awareness of one's own body. The work presented in this thesis underscores the well-documented role of somatotopic maps in somatosensory processing and reveals previously unknown roles of these maps in the (partial) absence of sensory inputs. For the first time, we could show that patients with a complete loss of sensory function in their hands were still able to activate ipsilateral finger representations within the somatotopic map of S1 during (attempted) unimanual movements. Our other findings also provide new intriguing questions in WM research. Even though, our paradigm did not allow to distinguish stimulus perception and WM-related processes beyond doubt, our findings create new hypotheses to test in future, e.g somatotopic processing of WM contents is necessary for accurate vibrotactile discrimination.

References

Abraham, A., Pedregosa, F., Eickenberg, M., Gervais, P., Mueller, A., Kossaifi, J., Gramfort, A., Thirion, B., & Varoquaux, G. (2014). Machine learning for neuroimaging with scikit-learn. *Frontiers in Neuroinformatics*, *8*. https://doi.org/10.3389/fninf.2014.00014

Adams, R. A., Shipp, S., & Friston, K. J. (2013). Predictions not commands: active inference in the motor system. *Brain Structure and Function*, *218*(3). https://doi.org/10.1007/s00429-012-0475-5

Akselrod, M., Martuzzi, R., Serino, A., van der Zwaag, W., Gassert, R., & Blanke, O. (2017). Anatomical and functional properties of the foot and leg representation in areas 3b, 1 and 2 of primary somatosensory cortex in humans: A 7T fMRI study. *NeuroImage*, *159*. https://doi.org/10.1016/j.neuroimage.2017.06.021

Alexander, G. E., DeLong, M. R., & Strick, P. L. (1986). Parallel Organization of Functionally Segregated Circuits Linking Basal Ganglia and Cortex. *Annual Review of Neuroscience*, *9*(1). https://doi.org/10.1146/annurev.ne.09.030186.002041

Allison, T., McCarthy, G., Wood, C. C., Darcey, T. M., Spencer, D. D., & Williamson, P. D. (1989). Human cortical potentials evoked by stimulation of the median nerve. II. Cytoarchitectonic areas generating short-latency activity. *Journal of Neurophysiology*, *62*(3). https://doi.org/10.1152/jn.1989.62.3.694

Amann, M., Hirsch, J. G., & Gass, A. (2009). A serial functional connectivity MRI study in healthy individuals assessing the variability of connectivity measures: reduced interhemispheric connectivity in the motor network during continuous performance. *Magnetic Resonance Imaging*, *27*(10). https://doi.org/10.1016/j.mri.2009.05.016

Ariani, G., Pruszynski, J. A., & Diedrichsen, J. (2022). Motor planning brings human primary somatosensory cortex into action-specific preparatory states. *ELife*, *11*. https://doi.org/10.7554/eLife.69517

Ariani, P., Pruszynski, J. A., & Diedrichsen, J. (2021). Motor planning brings human primary somatosensory cortex into action-specific preparatory states. *BioRxiv*.

Awh, E., Anllo-Vento, L., & Hillyard, S. A. (2000). The Role of Spatial Selective Attention in Working Memory for Locations: Evidence from Event-Related Potentials. *Journal of Cognitive Neuroscience*, *12*(5). https://doi.org/10.1162/089892900562444

Awh, E., & Jonides, J. (2001). Overlapping mechanisms of attention and spatial working memory. *Trends in Cognitive Sciences*, *5*(3). https://doi.org/10.1016/S1364-6613(00)01593-X

Awh, E., Vogel, E. K., & Oh, S.-H. (2006). Interactions between attention and working memory. *Neuroscience*, *139*(1). https://doi.org/10.1016/j.neuroscience.2005.08.023

Baddeley, A. (2000). The episodic buffer: a new component of working memory? *Trends in Cognitive Sciences*, *4*(11). https://doi.org/10.1016/S1364-6613(00)01538-2

Baddeley, A. (2003). Working memory: looking back and looking forward. *Nature Reviews Neuroscience*, *4*(10). https://doi.org/10.1038/nrn1201

Baddeley, A. (2012). Working Memory: Theories, Models, and Controversies. *Annual Review of Psychology*, *63*(1). https://doi.org/10.1146/annurev-psych-120710-100422

Baumgartner, C., Doppelbauer, A., Sutherling, W. W., Zeitlhofer, J., Lindinger, G., Lind, C., & Deecke, L. (1991). Human somatosensory cortical finger representation as studied by combined neuromagnetic and neuroelectric measurements. *Neuroscience Letters*, *134*(1). https://doi.org/10.1016/0304-3940(91)90518-X

Ben-Yishai, R., Bar-Or, R. L., & Sompolinsky, H. (1995). Theory of orientation tuning in visual cortex. *Proceedings of the National Academy of Sciences*, *92*(9). https://doi.org/10.1073/pnas.92.9.3844

Berlot, E., Prichard, G., O'Reilly, J., Ejaz, N., & Diedrichsen, J. (2019). Ipsilateral finger representations in the sensorimotor cortex are driven by active movement processes, not passive sensory input. *Journal of Neurophysiology*, *121*(2). https://doi.org/10.1152/jn.00439.2018

Besle, J., Sánchez-Panchuelo, R.-M., Bowtell, R., Francis, S., & Schluppeck, D. (2013). Single-subject fMRI mapping at 7 T of the representation of fingertips in S1: a comparison of event-related and phase-encoding designs. *Journal of Neurophysiology*, *109*(9). https://doi.org/10.1152/jn.00499.2012

Bican, O., Minagar, A., & Pruitt, A. A. (2013). The Spinal Cord. *Neurologic Clinics*, *31*(1). https://doi.org/10.1016/j.ncl.2012.09.009

Bisley, J. W. (2011). The neural basis of visual attention. *The Journal of Physiology*, *589*(1). https://doi.org/10.1113/jphysiol.2010.192666

Bolton, D. A. E., & Staines, W. R. (2011). Transient inhibition of the dorsolateral prefrontal cortex disrupts attention-based modulation of tactile stimuli at early stages of somatosensory processing. *Neuropsychologia*, *49*(7). https://doi.org/10.1016/j.neuropsychologia.2011.03.020

Borg, I., & Groenen, P. (2005). Modern Multidimensional Scaling. *Springer*.

Bruurmijn, M. L. C. M., Raemaekers, M., Branco, M. P., Ramsey, N. F., & Vansteensel, M. J. (2021). Distinct representation of ipsilateral hand movements in sensorimotor areas. *European Journal of Neuroscience*, *54*(10). https://doi.org/10.1111/ejn.15501

Buetefisch, C. M., Revill, K. P., Shuster, L., Hines, B., & Parsons, M. (2014). Motor demand-dependent activation of ipsilateral motor cortex. *Journal of Neurophysiology*, *112*(4). https://doi.org/10.1152/jn.00110.2014

Burton, H., & Sinclair, R. J. (2000). Attending to and Remembering Tactile Stimuli. *Journal of Clinical Neurophysiology*, *17*(6). https://doi.org/10.1097/00004691-200011000-00004

Cacioppo, J. T., & Decety, J. (2011). Social neuroscience: challenges and opportunities in the study of complex behavior. *Annals of the New York Academy of Sciences*, *1224*(1). https://doi.org/10.1111/j.1749-6632.2010.05858.x

Campbell, F. W., Cleland, B. G., Cooper, G. F., & Enroth-Cugell, C. (1968). The angular selectivity of visual cortical cells to moving gratings. *The Journal of Physiology*, *198*(1). https://doi.org/10.1113/jphysiol.1968.sp008604

Chai, W. J., Abd Hamid, A. I., & Abdullah, J. M. (2018). Working Memory From the Psychological and Neurosciences Perspectives: A Review. *Frontiers in Psychology*, *9*. https://doi.org/10.3389/fpsyg.2018.00401

Chettouf, S., Rueda-Delgado, L. M., de Vries, R., Ritter, P., & Daffertshofer, A. (2020). Are unimanual movements bilateral? *Neuroscience & Biobehavioral Reviews*, *113*. https://doi.org/10.1016/j.neubiorev.2020.03.002

Christophel, T. B., Klink, P. C., Spitzer, B., Roelfsema, P. R., & Haynes, J.-D. (2017). The Distributed Nature of Working Memory. *Trends in Cognitive Sciences*, *21*(2). https://doi.org/10.1016/j.tics.2016.12.007

Corballis, M. C. (2009). Comparing a single case with a control sample: Refinements and extensions. *Neuropsychologia*, *47*(13). https://doi.org/10.1016/j.neuropsychologia.2009.04.007

Corbetta, M., & Shulman, G. L. (2002). Control of goal-directed and stimulus-driven attention in the brain. *Nature Reviews Neuroscience*, *3*(3). https://doi.org/10.1038/nrn755

Cowan, N., Blume, C. L., & Saults, J. S. (2013). Attention to attributes and objects in working memory. *Journal of Experimental Psychology: Learning, Memory, and Cognition*, *39*(3). https://doi.org/10.1037/a0029687

Cramer, S. C., Lastra, L., Lacourse, M. G., & Cohen, M. J. (2005). Brain motor system function after chronic, complete spinal cord injury. *Brain*, *128*(12). https://doi.org/10.1093/brain/awh648

Cunningham, D. A., Machado, A., Yue, G. H., Carey, J. R., & Plow, E. B. (2013). Functional somatotopy revealed across multiple cortical regions using a model of complex motor task. *Brain Research*, *1531*. https://doi.org/10.1016/j.brainres.2013.07.050

Curt, A., Keck, M. E., & Dietz, V. (1998). Functional outcome following spinal cord injury: Significance of motor-evoked potentials and ASIA scores. *Archives of Physical Medicine and Rehabilitation*, *79*(1). https://doi.org/10.1016/S0003-9993(98)90213-1

Daffertshofer, A., van den Berg, C., & Beek, P. J. (1999). A dynamical model for mirror movements. *Physica D: Nonlinear Phenomena*, *132*(1–2). https://doi.org/10.1016/S0167-2789(99)00044-5

del Cul, A., Baillet, S., & Dehaene, S. (2007). Brain Dynamics Underlying the Nonlinear Threshold for Access to Consciousness. *PLoS Biology*, *5*(10). https://doi.org/10.1371/journal.pbio.0050260

Dempsey-Jones, H., Wesselink, D. B., Friedman, J., & Makin, T. R. (2019). Organized Toe Maps in Extreme Foot Users. *Cell Reports*, *28*(11). https://doi.org/10.1016/j.celrep.2019.08.027

Desimone, R., & Duncan, J. (1995). Neural Mechanisms of Selective Visual Attention. *Annual Review of Neuroscience*, *18*(1). https://doi.org/10.1146/annurev.ne.18.030195.001205

D'Esposito, M., & Postle, B. R. (2015). The Cognitive Neuroscience of Working Memory. *Annual Review of Psychology*, *66*(1). https://doi.org/10.1146/annurev-psych-010814-015031

Devor, A., Hillman, E. M. C., Tian, P., Waeber, C., Teng, I. C., Ruvinskaya, L., Shalinsky, M. H., Zhu, H., Haslinger, R. H., Narayanan, S. N., Ulbert, I., Dunn, A. K., Lo, E. H., Rosen, B. R., Dale, A. M., Kleinfeld, D., & Boas, D. A. (2008). Stimulus-Induced Changes in Blood Flow and 2-Deoxyglucose Uptake Dissociate in Ipsilateral Somatosensory Cortex. *Journal of Neuroscience*, *28*(53). https://doi.org/10.1523/JNEUROSCI.4307-08.2008

Diedrichsen, J., & Kriegeskorte, N. (2017). Representational models: A common framework for understanding encoding, pattern-component, and representational-similarity analysis. *PLOS Computational Biology*, *13*(4). https://doi.org/10.1371/journal.pcbi.1005508

Diedrichsen, J., Wiestler, T., & Ejaz, N. (2013). A multivariate method to determine the dimensionality of neural representation from population activity. *NeuroImage*, *76*. https://doi.org/10.1016/j.neuroimage.2013.02.062

Diedrichsen, J., Wiestler, T., & Krakauer, J. W. (2013). Two Distinct Ipsilateral Cortical Representations for Individuated Finger Movements. *Cerebral Cortex*, *23*(6). https://doi.org/10.1093/cercor/bhs120

Dienes, Z. (2014). Using Bayes to get the most out of non-significant results. *Frontiers in Psychology*, *5*. https://doi.org/10.3389/fpsyg.2014.00781

Drevets, W. C., Burton, H., Videen, T. O., Snyder, A. Z., Simpson, J. R., & Raichle, M. E. (1995). Blood flow changes in human somatosensory cortex during anticipated stimulation. *Nature*, *373*(6511). https://doi.org/10.1038/373249a0

Edin, F., Klingberg, T., Johansson, P., McNab, F., Tegnér, J., & Compte, A. (2009). Mechanism for top-down control of working memory capacity. *Proceedings of the National Academy of Sciences*, *106*(16). https://doi.org/10.1073/pnas.0901894106

Eickhoff, S. B., Stephan, K. E., Mohlberg, H., Grefkes, C., Fink, G. R., Amunts, K., & Zilles, K. (2005). A new SPM toolbox for combining probabilistic cytoarchitectonic maps and functional imaging data. *NeuroImage*, *25*(4). https://doi.org/10.1016/j.neuroimage.2004.12.034

Ejaz, N., Hamada, M., & Diedrichsen, J. (2015). Hand use predicts the structure of representations in sensorimotor cortex. *Nature Neuroscience*, *18*(7). https://doi.org/10.1038/nn.4038

Ester, E. F., Serences, J. T., & Awh, E. (2009). Spatially Global Representations in Human Primary Visual Cortex during Working Memory Maintenance. *Journal of Neuroscience*, *29*(48). https://doi.org/10.1523/JNEUROSCI.4388-09.2009

Fifer, M. S., McMullen, D. P., Osborn, L. E., Thomas, T. M., Christie, B. P., Nickl, R. W., Candrea, D. N., Pohlmeyer, E. A., Thompson, M. C., Anaya, M. A., Schellekens, W., Ramsey, N. F., Bensmaia, S. J., Anderson, W. S., Wester, B. A., Crone, N. E., Celnik, P. A., Cantarero, G. L., & Tenore, F. v. (2021). Intracortical Somatosensory Stimulation to Elicit Fingertip Sensations in an Individual With Spinal Cord Injury. *Neurology*. https://doi.org/10.1212/WNL.0000000000013173

Finger, R. (2010). Review of 'Robustbase' software for R. *Journal of Applied Econometrics*, *25*(7). https://doi.org/10.1002/jae.1194

Fischl, B. (2012). FreeSurfer. *NeuroImage*, *62*(2). https://doi.org/10.1016/j.neuroimage.2012.01.021

Fischl, B., Sereno, M. I., & Dale, A. M. (1999). Cortical Surface-Based Analysis. *NeuroImage*, *9*(2). https://doi.org/10.1006/nimg.1998.0396

Flesher, S. N., Collinger, J. L., Foldes, S. T., Weiss, J. M., Downey, J. E., Tyler-Kabara, E. C., Bensmaia, S. J., Schwartz, A. B., Boninger, M. L., & Gaunt, R. A. (2016). Intracortical microstimulation of human somatosensory cortex. *Science Translational Medicine*, *8*(361). https://doi.org/10.1126/scitranslmed.aaf8083

Fox, P. T., Burton, H., & Raichle, M. E. (1987). Mapping human somatosensory cortex with positron emission tomography. *Journal of Neurosurgery*, *67*(1). https://doi.org/10.3171/jns.1987.67.1.0034

Francis, S. T., Kelly, E. F., Bowtell, R., Dunseath, W. J. R., Folger, S. E., & McGlone, F. (2000a). fMRI of the Responses to Vibratory Stimulation of Digit Tips. *NeuroImage*, *11*(3). https://doi.org/10.1006/nimg.2000.0541

Francis, S. T., Kelly, E. F., Bowtell, R., Dunseath, W. J. R., Folger, S. E., & McGlone, F. (2000b). fMRI of the Responses to Vibratory Stimulation of Digit Tips. *NeuroImage*, *11*(3). https://doi.org/10.1006/nimg.2000.0541

Freund, P., Rothwell, J., Craggs, M., Thompson, A. J., & Bestmann, S. (2011). Corticomotor representation to a human forearm muscle changes following cervical spinal cord injury. *European Journal of Neuroscience*, *34*(11). https://doi.org/10.1111/j.1460-9568.2011.07895.x

Freund, P., Weiskopf, N., Ward, N. S., Hutton, C., Gall, A., Ciccarelli, O., Craggs, M., Friston, K., & Thompson, A. J. (2011). Disability, atrophy and cortical reorganization following spinal cord injury. *Brain*, *134*(6). https://doi.org/10.1093/brain/awr093

Friston, K. J. (2011). Functional and Effective Connectivity: A Review. *Brain Connectivity*, *1*(1). https://doi.org/10.1089/brain.2011.0008

Friston, K. J., Buechel, C., Fink, G. R., Morris, J., Rolls, E., & Dolan, R. J. (1997). Psychophysiological and Modulatory Interactions in Neuroimaging. *NeuroImage*, *6*(3). https://doi.org/10.1006/nimg.1997.0291

Friston, K. J., Holmes, A. P., Worsley, K. J., Poline, J.-P., Frith, C. D., & Frackowiak, R. S. J. (1994). Statistical parametric maps in functional imaging: A general linear approach. *Human Brain Mapping*, *2*(4). https://doi.org/10.1002/hbm.460020402

Fujiwara, N., Imai, M., Nagamine, T., Mima, T., Oga, T., Takeshita, K., Toma, K., & Shibasaki, H. (2002). Second somatosensory area (SII) plays a significant role in selective somatosensory attention. *Cognitive Brain Research*, *14*(3). https://doi.org/10.1016/S0926-6410(02)00141-6

Gazzaley, A., & Nobre, A. C. (2012). Top-down modulation: bridging selective attention and working memory. *Trends in Cognitive Sciences*, *16*(2). https://doi.org/10.1016/j.tics.2011.11.014

Gelnar, P. A., Krauss, B. R., Szeverenyi, N. M., & Apkarian, A. V. (1998). Fingertip Representation in the Human Somatosensory Cortex: An fMRI Study. *NeuroImage*, *7*(4). https://doi.org/10.1006/nimg.1998.0341

Georgopoulos, A. P., Schwartz, A. B., & Kettner, R. E. (1986). Neuronal Population Coding of Movement Direction. *Science*, *233*(4771). https://doi.org/10.1126/science.3749885

Gerdjikov, T. v., Bergner, C. G., Stüttgen, M. C., Waiblinger, C., & Schwarz, C. (2010). Discrimination of Vibrotactile Stimuli in the Rat Whisker System: Behavior and Neurometrics. *Neuron*, *65*(4). https://doi.org/10.1016/j.neuron.2010.02.007

Gogulski, J., Boldt, R., Savolainen, P., Guzmán-López, J., Carlson, S., & Pertovaara, A. (2015). A Segregated Neural Pathway for Prefrontal Top-Down Control of Tactile Discrimination. *Cerebral Cortex*, *25*(1). https://doi.org/10.1093/cercor/bht211

Goltz, D., Pleger, B., Thiel, S., Villringer, A., & Müller, M. M. (2013). Sustained Spatial Attention to Vibrotactile Stimulation in the Flutter Range: Relevant Brain Regions and Their Interaction. *PLoS ONE*, *8*(12). https://doi.org/10.1371/journal.pone.0084196

Gomez-Ramirez, M., Kelly, S. P., Molholm, S., Sehatpour, P., Schwartz, T. H., & Foxe, J. J. (2011). Oscillatory Sensory Selection Mechanisms during Intersensory Attention to Rhythmic Auditory and Visual Inputs: A Human Electrocorticographic Investigation. *Journal of Neuroscience*, *31*(50). https://doi.org/10.1523/JNEUROSCI.2164-11.2011

Gooijers, J., Chalavi, S., Koster, L. K., Roebroeck, A., Kaas, A., & Swinnen, S. P. (2022). Representational Similarity Scores of Digits in the Sensorimotor Cortex Are Associated with Behavioral Performance. *Cerebral Cortex*. https://doi.org/10.1093/cercor/bhab452

Grefkes, C., Eickhoff, S. B., Nowak, D. A., Dafotakis, M., & Fink, G. R. (2008). Dynamic intra- and interhemispheric interactions during unilateral and bilateral hand movements assessed with fMRI and DCM. *NeuroImage*, *41*(4). https://doi.org/10.1016/j.neuroimage.2008.03.048

Greve, D. N., & Fischl, B. (2009a). Accurate and robust brain image alignment using boundary-based registration. *NeuroImage*, *48*(1), 63–72. https://doi.org/10.1016/j.neuroimage.2009.06.060

Greve, D. N., & Fischl, B. (2009b). Accurate and robust brain image alignment using boundary-based registration. *NeuroImage*, *48*(1). https://doi.org/10.1016/j.neuroimage.2009.06.060

Guan, C., Aflalo, T., Zhang, C. Y., Rosario, E. R., Pouratian, N., & Andersen, R. A. (2021). Preserved motor representations after paralysis. *BioRxiv*.

Halder, P., Kambi, N., Chand, P., & Jain, N. (2018). Altered Expression of Reorganized Inputs as They Ascend From the Cuneate Nucleus to Cortical Area 3b in Monkeys With Long-Term Spinal Cord Injuries. *Cerebral Cortex*, *28*(11). https://doi.org/10.1093/cercor/bhx256

Hamzei, F., Dettmers, C., Rzanny, R., Liepert, J., Büchel, C., & Weiller, C. (2002). Reduction of Excitability ("Inhibition") in the Ipsilateral Primary Motor Cortex Is Mirrored by fMRI Signal Decreases. *NeuroImage*, *17*(1). https://doi.org/10.1006/nimg.2002.1077

Harris, J. A., Arabzadeh, E., Fairhall, A. L., Benito, C., & Diamond, M. E. (2006). Factors Affecting Frequency Discrimination of Vibrotactile Stimuli: Implications for Cortical Encoding. *PLoS ONE*, *1*(1). https://doi.org/10.1371/journal.pone.0000100

Harris, J. A., Harris, I. M., & Diamond, M. E. (2001). The Topography of Tactile Working Memory. *The Journal of Neuroscience*, *21*(20). https://doi.org/10.1523/JNEUROSCI.21-20-08262.2001

Harris, J. A., Miniussi, C., Harris, I. M., & Diamond, M. E. (2002). Transient Storage of a Tactile Memory Trace in Primary Somatosensory Cortex. *The Journal of Neuroscience*, *22*(19). https://doi.org/10.1523/JNEUROSCI.22-19-08720.2002

Harrison, S. A., & Tong, F. (2009). Decoding reveals the contents of visual working memory in early visual areas. *Nature*, *458*(7238). https://doi.org/10.1038/nature07832

Hawking, T. G., & Gerdjikov, T. v. (2013). Populations of striatal medium spiny neurons encode vibrotactile frequency in rats: modulation by slow wave oscillations. *Journal of Neurophysiology*, *109*(2). https://doi.org/10.1152/jn.00489.2012

Haynes, J.-D., & Rees, G. (2006). Decoding mental states from brain activity in humans. *Nature Reviews Neuroscience*, *7*(7). https://doi.org/10.1038/nrn1931

Hebart, M. N., & Baker, C. I. (2018). Deconstructing multivariate decoding for the study of brain function. *NeuroImage*, *180*. https://doi.org/10.1016/j.neuroimage.2017.08.005

Henry, G. H., Dreher, B., & Bishop, P. O. (1974). Orientation specificity of cells in cat striate cortex. *Journal of Neurophysiology*, *37*(6). https://doi.org/10.1152/jn.1974.37.6.1394

Hipp, J., Arabzadeh, E., Zorzin, E., Conradt, J., Kayser, C., Diamond, M. E., & König, P. (2006). Texture Signals in Whisker Vibrations. *Journal of Neurophysiology*, *95*(3). https://doi.org/10.1152/jn.01104.2005

Hotz-Boendermaker, S., Funk, M., Summers, P., Brugger, P., Hepp-Reymond, M.-C., Curt, A., & Kollias, S. S. (2008). Preservation of motor programs in paraplegics as demonstrated by attempted and imagined foot movements. *NeuroImage*, *39*(1). https://doi.org/10.1016/j.neuroimage.2007.07.065

Huang, Y., Wang, J. Y., Wei, X. M., & Hu, B. (2014). Bioinfo-Kit: A Sharing Software Tool for Bioinformatics. *Applied Mechanics and Materials*, *472*. https://doi.org/10.4028/www.scientific.net/AMM.472.466

Hubel, D. H., & Wiesel, T. N. (1968). Receptive fields and functional architecture of monkey striate cortex. *The Journal of Physiology*, *195*(1). https://doi.org/10.1113/jphysiol.1968.sp008455

Hübers, A., Orekhov, Y., & Ziemann, U. (2008). Interhemispheric motor inhibition: its role in controlling electromyographic mirror activity. *European Journal of Neuroscience*, *28*(2). https://doi.org/10.1111/j.1460-9568.2008.06335.x

Jain, N., Qi, H.-X., Collins, C. E., & Kaas, J. H. (2008). Large-Scale Reorganization in the Somatosensory Cortex and Thalamus after Sensory Loss in Macaque Monkeys. *Journal of Neuroscience*, *28*(43). https://doi.org/10.1523/JNEUROSCI.2334-08.2008

Jenkinson, M. (2002). Improved Optimization for the Robust and Accurate Linear Registration and Motion Correction of Brain Images. *NeuroImage*, *17*(2). https://doi.org/10.1016/S1053-8119(02)91132-8

Jenkinson, M., & Smith, S. M. (2001). A global optimization method for robust affine registration of brain images. *Medical Imaging Analysis*, *5*, 143–156.

Jensen, M. P., Kuehn, C. M., Amtmann, D., & Cardenas, D. D. (2007). Symptom Burden in Persons With Spinal Cord Injury. *Archives of Physical Medicine and Rehabilitation*, *88*(5). https://doi.org/10.1016/j.apmr.2007.02.002

Jha, A. P. (2002). Tracking the time-course of attentional involvement in spatial working memory: an event-related potential investigation. *Cognitive Brain Research*, *15*(1). https://doi.org/10.1016/S0926-6410(02)00216-1

Johansen-Berg, H., Rushworth, M. F. S., Bogdanovic, M. D., Kischka, U., Wimalaratna, S., & Matthews, P. M. (2002). The role of ipsilateral premotor cortex in hand movement after stroke. *Proceedings of the National Academy of Sciences*, *99*(22). https://doi.org/10.1073/pnas.222536799

Johnston, R., Jones, K., & Manley, D. (2018). Confounding and collinearity in regression analysis: a cautionary tale and an alternative procedure, illustrated by studies of British voting behaviour. *Quality & Quantity*, *52*(4). https://doi.org/10.1007/s11135-017-0584-6

Kaas, A. L., van Mier, H., Visser, M., & Goebel, R. (2013). The neural substrate for working memory of tactile surface texture. *Human Brain Mapping*, *34*(5). https://doi.org/10.1002/hbm.21500

Kaas, J. (1997). Topographic Maps are Fundamental to Sensory Processing. *Brain Research Bulletin*, *44*(2). https://doi.org/10.1016/S0361-9230(97)00094-4

Kaas, J. H. (1993). The functional organization of somatosensory cortex in primates. *Annals of Anatomy - Anatomischer Anzeiger*, *175*(6). https://doi.org/10.1016/S0940-9602(11)80212-8

Kalsi-Ryan, S., Beaton, D., Curt, A., Popovic, M. R., Verrier, M. C., & Fehlings, M. G. (2014). Outcome of the upper limb in cervical spinal cord injury: Profiles of recovery and insights for clinical studies. *The Journal of Spinal Cord Medicine*, *37*(5). https://doi.org/10.1179/2045772314Y.0000000252

Kambi, N., Halder, P., Rajan, R., Arora, V., Chand, P., Arora, M., & Jain, N. (2014). Large-scale reorganization of the somatosensory cortex following spinal cord injuries is due to brainstem plasticity. *Nature Communications*, *5*(1). https://doi.org/10.1038/ncomms4602

Kanno, A., Nakasato, N., Hatanaka, K., & Yoshimoto, T. (2003). Ipsilateral Area 3b Responses to Median Nerve Somatosensory Stimulation. *NeuroImage*, *18*(1). https://doi.org/10.1006/nimg.2002.1283

Kass, R. E., & Raftery, A. E. (1995). Bayes Factors. *Journal of the American Statistical Association*, *90*(430). https://doi.org/10.2307/2291091

Katus, T., Andersen, S. K., & Muller, M. M. (2014). Common Mechanisms of Spatial Attention in Memory and Perception: A Tactile Dual-Task Study. *Cerebral Cortex*, *24*(3). https://doi.org/10.1093/cercor/bhs350

Katus, T., Grubert, A., & Eimer, M. (2015). Electrophysiological Evidence for a Sensory Recruitment Model of Somatosensory Working Memory. *Cerebral Cortex*, *25*(12). https://doi.org/10.1093/cercor/bhu153

Kieliba, P., Clode, D., Maimon-Mor, R. O., & Makin, T. R. (2021). Robotic hand augmentation drives changes in neural body representation. *Science Robotics*, *6*(54). https://doi.org/10.1126/scirobotics.abd7935

Kikkert, S., Kolasinski, J., Jbabdi, S., Tracey, I., Beckmann, C. F., Johansen-Berg, H., & Makin, T. R. (2016). Revealing the neural fingerprints of a missing hand. *ELife*, *5*. https://doi.org/10.7554/eLife.15292

Kikkert, S., Pfyffer, D., Verling, M., Freund, P., & Wenderoth, N. (2021). Finger somatotopy is preserved after tetraplegia but deteriorates over time. *ELife*, *10*. https://doi.org/10.7554/eLife.67713

Kinsbourne, M. (1987). *Mechanisms of Unilateral Neglect*. https://doi.org/10.1016/S0166-4115(08)61709-4

Kolasinski, J., Makin, T. R., Jbabdi, S., Clare, S., Stagg, C. J., & Johansen-Berg, H. (2016a). Investigating the Stability of Fine-Grain Digit Somatotopy in Individual Human Participants. *Journal of Neuroscience*, *36*(4). https://doi.org/10.1523/JNEUROSCI.1742-15.2016

Kolasinski, J., Makin, T. R., Jbabdi, S., Clare, S., Stagg, C. J., & Johansen-Berg, H. (2016b). Investigating the Stability of Fine-Grain Digit Somatotopy in Individual Human Participants. *Journal of Neuroscience*, *36*(4). https://doi.org/10.1523/JNEUROSCI.1742-15.2016

Kriegeskorte, N. (2008). Representational similarity analysis – connecting the branches of systems neuroscience. *Frontiers in Systems Neuroscience*. https://doi.org/10.3389/neuro.06.004.2008

Kriegeskorte, N., & Bandettini, P. (2007). Analyzing for information, not activation, to exploit high-resolution fMRI. *NeuroImage*, *38*(4). https://doi.org/10.1016/j.neuroimage.2007.02.022

Kriegeskorte, N., & Diedrichsen, J. (2019). Peeling the Onion of Brain Representations. *Annual Review of Neuroscience*, *42*(1). https://doi.org/10.1146/annurev-neuro-080317-061906

Kriegeskorte, N., & Wei, X.-X. (2021). Neural tuning and representational geometry. *Nature Reviews Neuroscience*, *22*(11). https://doi.org/10.1038/s41583-021-00502-3

Kuehn, E., Haggard, P., Villringer, A., Pleger, B., & Sereno, M. I. (2018). Visually-Driven Maps in Area 3b. *The Journal of Neuroscience*, *38*(5). https://doi.org/10.1523/JNEUROSCI.0491-17.2017

Kunzle, H. (1977). Projections from the primary somatosensory cortex to basal ganglia and thalamus in the monkey. *Experimental Brain Research*, *30*(4). https://doi.org/10.1007/BF00237639

LaBar, K. S., Gitelman, D. R., Parrish, T. B., & Mesulam, M.-M. (1999). Neuroanatomic Overlap of Working Memory and Spatial Attention Networks: A Functional MRI Comparison within Subjects. *NeuroImage*, *10*(6). https://doi.org/10.1006/nimg.1999.0503

Ledberg, A., O'Sullivan, B. T., Kinomura, S., & Roland, P. E. (1995). Somatosensory Activations of the Parietal Operculum of Man. A PET Study. *European Journal of Neuroscience*, *7*(9). https://doi.org/10.1111/j.1460-9568.1995.tb00716.x

Levy, L. M., Ziemann, U., Chen, R., & Cohen, L. G. (2002). Rapid modulation of GABA in sensorimotor cortex induced by acute deafferentation. *Annals of Neurology*, *52*(6). https://doi.org/10.1002/ana.10372

Liu, P., Chrysidou, A., Doehler, J., Hebart, M. N., Wolbers, T., & Kuehn, E. (2021). The organizational principles of de-differentiated topographic maps in somatosensory cortex. *ELife*, *10*. https://doi.org/10.7554/eLife.60090

Logie, R. H., & Cowan, N. (2015). Perspectives on working memory: introduction to the special issue. *Memory & Cognition*, *43*(3). https://doi.org/10.3758/s13421-015-0510-x

Logothetis, N. K. (2002). The neural basis of the blood–oxygen–level–dependent functional magnetic resonance imaging signal. *Philosophical Transactions of the Royal Society of London. Series B: Biological Sciences*, *357*(1424). https://doi.org/10.1098/rstb.2002.1114

London, B. M., & Miller, L. E. (2013). Responses of somatosensory area 2 neurons to actively and passively generated limb movements. *Journal of Neurophysiology*, *109*(6). https://doi.org/10.1152/jn.00372.2012

Maffei, L., & Fiorentini, A. (1976). The unresponsive regions of visual cortical receptive fields. *Vision Research*, *16*(10). https://doi.org/10.1016/0042-6989(76)90253-4

Manita, S., Suzuki, T., Homma, C., Matsumoto, T., Odagawa, M., Yamada, K., Ota, K., Matsubara, C., Inutsuka, A., Sato, M., Ohkura, M., Yamanaka, A., Yanagawa, Y., Nakai, J., Hayashi, Y., Larkum, M. E., & Murayama, M. (2015). A Top-Down Cortical Circuit for Accurate Sensory Perception. *Neuron*, *86*(5). https://doi.org/10.1016/j.neuron.2015.05.006

Marcus, D. S., Harwell, J., Olsen, T., Hodge, M., Glasser, M. F., Prior, F., Jenkinson, M., Laumann, T., Curtiss, S. W., & van Essen, D. C. (2011). Informatics and Data Mining Tools and Strategies for the Human Connectome Project. *Frontiers in Neuroinformatics*, *5*. https://doi.org/10.3389/fninf.2011.00004

Martuzzi, R., van der Zwaag, W., Farthouat, J., Gruetter, R., & Blanke, O. (2014). Human finger somatotopy in areas 3b, 1, and 2: A 7T fMRI study using a natural stimulus. *Human Brain Mapping*, *35*(1). https://doi.org/10.1002/hbm.22172

McAdams, C. J., & Maunsell, J. H. R. (1999). Effects of Attention on Orientation-Tuning Functions of Single Neurons in Macaque Cortical Area V4. *The Journal of Neuroscience*, *19*(1). https://doi.org/10.1523/JNEUROSCI.19-01-00431.1999

McNab, F., & Klingberg, T. (2008). Prefrontal cortex and basal ganglia control access to working memory. *Nature Neuroscience*, *11*(1). https://doi.org/10.1038/nn2024

Mesulam, M. (1998). From sensation to cognition. *Brain*, *121*(6). https://doi.org/10.1093/brain/121.6.1013

Meyer, E., Ferguson, S. S. G., Zatorre, R. J., Alivisatos, B., Marrett, S., Evans, A. C., & Hakim, A. M. (1991). Attention modulates somatosensory cerebral blood flow response to vibrotactile stimulation as measured by positron emission tomography. *Annals of Neurology*, *29*(4). https://doi.org/10.1002/ana.410290418

Miller, E. K., & Cohen, J. D. (2001). An Integrative Theory of Prefrontal Cortex Function. *Annual Review of Neuroscience*, *24*(1). https://doi.org/10.1146/annurev.neuro.24.1.167

Mima, T., Nagamine, T., Nakamura, K., & Shibasaki, H. (1998). Attention Modulates Both Primary and Second Somatosensory Cortical Activities in Humans: A Magnetoencephalographic Study. *Journal of Neurophysiology*, *80*(4). https://doi.org/10.1152/jn.1998.80.4.2215

Mountcastle, V. B., Talbot, W. H., Darian-Smith, I., & Kornhuber, H. H. (1967). Neural Basis of the Sense of Flutter-Vibration. *Science*, *155*(3762). https://doi.org/10.1126/science.155.3762.597

Mountcastle, V. B., Talbot, W. H., Sakata, H., & Hyvärinen, J. (1969). Cortical neuronal mechanisms in flutter-vibration studied in unanesthetized monkeys. Neuronal periodicity and frequency discrimination. *Journal of Neurophysiology*, *32*(3). https://doi.org/10.1152/jn.1969.32.3.452

Movshon, J., & Lennie, P. (1979). Pattern-selective adaptation in visual cortical neurones. *Nature*, *278*(5707). https://doi.org/10.1038/278850a0

Naghavi, H. R., & Nyberg, L. (2005). Common fronto-parietal activity in attention, memory, and consciousness: Shared demands on integration? *Consciousness and Cognition*, *14*(2). https://doi.org/10.1016/j.concog.2004.10.003

Nelson, A. J., Staines, W. R., Graham, S. J., & McIlroy, W. E. (2004a). Activation in SI and SII; the influence of vibrotactile amplitude during passive and task-relevant stimulation. *Cognitive Brain Research*, *19*(2). https://doi.org/10.1016/j.cogbrainres.2003.11.013

Nelson, A. J., Staines, W. R., Graham, S. J., & McIlroy, W. E. (2004b). Activation in SI and SII; the influence of vibrotactile amplitude during passive and task-relevant stimulation. *Cognitive Brain Research*, *19*(2). https://doi.org/10.1016/j.cogbrainres.2003.11.013

Nili, H., Wingfield, C., Walther, A., Su, L., Marslen-Wilson, W., & Kriegeskorte, N. (2014). A Toolbox for Representational Similarity Analysis. *PLoS Computational Biology*, *10*(4). https://doi.org/10.1371/journal.pcbi.1003553

Norman, K. A., Polyn, S. M., Detre, G. J., & Haxby, J. v. (2006). Beyond mind-reading: multi-voxel pattern analysis of fMRI data. *Trends in Cognitive Sciences*, *10*(9). https://doi.org/10.1016/j.tics.2006.07.005

Oberauer, K. (2019). Working Memory and Attention – A Conceptual Analysis and Review. *Journal of Cognition*, *2*(1). https://doi.org/10.5334/joc.58

Ogawa, S., Lee, T. M., Kay, A. R., & Tank, D. W. (1990). Brain magnetic resonance imaging with contrast dependent on blood oxygenation. *Proceedings of the National Academy of Sciences*, *87*(24). https://doi.org/10.1073/pnas.87.24.9868

O'Reilly, J. X., Woolrich, M. W., Behrens, T. E. J., Smith, S. M., & Johansen-Berg, H. (2012). Tools of the trade: psychophysiological interactions and functional connectivity. *Social Cognitive and Affective Neuroscience*, *7*(5). https://doi.org/10.1093/scan/nss055

Ozdemir, R. A., & Perez, M. A. (2018). Afferent input and sensory function after human spinal cord injury. *Journal of Neurophysiology*, *119*(1). https://doi.org/10.1152/jn.00354.2017

Pasternak, T., & Greenlee, M. W. (2005). Working memory in primate sensory systems. *Nature Reviews Neuroscience*, *6*(2). https://doi.org/10.1038/nrn1603

Peirce, J., Gray, J. R., Simpson, S., MacAskill, M., Höchenberger, R., Sogo, H., Kastman, E., & Lindeløv, J. K. (2019). PsychoPy2: Experiments in behavior made easy. *Behavior Research Methods*, *51*(1). https://doi.org/10.3758/s13428-018-01193-y

Peller, M. (2006). The basal ganglia are hyperactive during the discrimination of tactile stimuli in writer's cramp. *Brain*, *129*(10). https://doi.org/10.1093/brain/awl181

Penfield, W. (1947). Ferrier Lecture - Some observations on the cerebral cortex of man. *Proceedings of the Royal Society of London. Series B - Biological Sciences*, *134*(876). https://doi.org/10.1098/rspb.1947.0017

Penfield, W., & Boldrey, E. (1937). Somatic motor and sensory representation in the cerebral cortex of man as studied by electrical stimulation. *Brain*, *60*(4). https://doi.org/10.1093/brain/60.4.389

Pereira, F., Mitchell, T., & Botvinick, M. (2009). Machine learning classifiers and fMRI: A tutorial overview. *NeuroImage*, *45*(1). https://doi.org/10.1016/j.neuroimage.2008.11.007

Peters, A. J., Fabre, J. M. J., Steinmetz, N. A., Harris, K. D., & Carandini, M. (2021). Striatal activity topographically reflects cortical activity. *Nature*, *591*(7850). https://doi.org/10.1038/s41586-020-03166-8

Petersen, J. A., Wilm, B. J., von Meyenburg, J., Schubert, M., Seifert, B., Najafi, Y., Dietz, V., & Kollias, S. (2012). Chronic Cervical Spinal Cord Injury: DTI Correlates with Clinical and Electrophysiological Measures. *Journal of Neurotrauma*, *29*(8). https://doi.org/10.1089/neu.2011.2027

Pleger, B., Blankenburg, F., Ruff, C. C., Driver, J., & Dolan, R. J. (2008). Reward Facilitates Tactile Judgments and Modulates Hemodynamic Responses in Human Primary Somatosensory Cortex. *Journal of Neuroscience*, *28*(33). https://doi.org/10.1523/JNEUROSCI.1093-08.2008

Pleger, B., Ruff, C. C., Blankenburg, F., Bestmann, S., Wiech, K., Stephan, K. E., Capilla, A., Friston, K. J., & Dolan, R. J. (2006). Neural Coding of Tactile Decisions in the Human Prefrontal Cortex. *Journal of Neuroscience*, *26*(48). https://doi.org/10.1523/JNEUROSCI.4275-06.2006

Pleger, B., Ruff, C. C., Blankenburg, F., Klöppel, S., Driver, J., & Dolan, R. J. (2009). Influence of Dopaminergically Mediated Reward on Somatosensory Decision-Making. *PLoS Biology*, *7*(7). https://doi.org/10.1371/journal.pbio.1000164

Postle, B. R. (2016). How Does the Brain Keep Information "in Mind"? *Current Directions in Psychological Science*, *25*(3). https://doi.org/10.1177/0963721416643063

Preuschhof, C., Heekeren, H. R., Taskin, B., Schubert, T., & Villringer, A. (2006). Neural Correlates of Vibrotactile Working Memory in the Human Brain. *Journal of Neuroscience*, *26*(51). https://doi.org/10.1523/JNEUROSCI.2767-06.2006

Puckett, A. M., Bollmann, S., Barth, M., & Cunnington, R. (2017). Measuring the effects of attention to individual fingertips in somatosensory cortex using ultra-high field (7T) fMRI. *NeuroImage*, *161*. https://doi.org/10.1016/j.neuroimage.2017.08.014

Rabe, F., Kikkert, S., & Wenderoth, N. (2022). Finger representations in primary somatosensory cortex are modulated by a vibrotactile working memory task. *BioRxiv*.

Rademaker, R. L., Park, Y. E., Sack, A. T., & Tong, F. (2018). Evidence of gradual loss of precision for simple features and complex objects in visual working memory. *Journal of Experimental Psychology: Human Perception and Performance*, *44*(6). https://doi.org/10.1037/xhp0000491

Rauschecker, J. P. (1995). Compensatory plasticity and sensory substitution in the cerebral cortex. *Trends in Neurosciences*, *18*(1). https://doi.org/10.1016/0166-2236(95)93948-W

Reynolds, J. H., Pasternak, T., & Desimone, R. (2000). Attention Increases Sensitivity of V4 Neurons. *Neuron*, *26*(3). https://doi.org/10.1016/S0896-6273(00)81206-4

Roland, P. E. (1981). Somatotopical tuning of postcentral gyrus during focal attention in man. A regional cerebral blood flow study. *Journal of Neurophysiology*, *46*(4). https://doi.org/10.1152/jn.1981.46.4.744

Roland, P. E. (1982). Cortical regulation of selective attention in man. A regional cerebral blood flow study. *Journal of Neurophysiology*, *48*(5). https://doi.org/10.1152/jn.1982.48.5.1059

Romo, R., Brody, C. D., Hernández, A., & Lemus, L. (1999). Neuronal correlates of parametric working memory in the prefrontal cortex. *Nature*, *399*(6735). https://doi.org/10.1038/20939

Romo, R., Hernández, A., Zainos, A., & Salinas, E. (1998). Somatosensory discrimination based on cortical microstimulation. *Nature*, *392*(6674). https://doi.org/10.1038/32891

Romo, R., & Rossi-Pool, R. (2020). Turning Touch into Perception. *Neuron*, *105*(1). https://doi.org/10.1016/j.neuron.2019.11.033

Romo, R., & Salinas, E. (2003). Flutter Discrimination: neural codes, perception, memory and decision making. *Nature Reviews Neuroscience*, *4*(3). https://doi.org/10.1038/nrn1058

Rose, N. S., LaRocque, J. J., Riggall, A. C., Gosseries, O., Starrett, M. J., Meyering, E. E., & Postle, B. R. (2016). Reactivation of latent working memories with transcranial magnetic stimulation. *Science*, *354*(6316). https://doi.org/10.1126/science.aah7011

Rousseeuw, P. J., & Croux, C. (1993). Alternatives to the Median Absolute Deviation. *Journal of the American Statistical Association*, *88*(424). https://doi.org/10.1080/01621459.1993.10476408

Ruddy, K. L., Leemans, A., Woolley, D. G., Wenderoth, N., & Carson, R. G. (2017). Structural and Functional Cortical Connectivity Mediating Cross Education of Motor Function. *The Journal of Neuroscience*, *37*(10). https://doi.org/10.1523/JNEUROSCI.2536-16.2017

Sabbah, P., de Schonen, S., Leveque, C., Gay, S., Pfefer, F., Nioche, C., Sarrazin, J.-L., Barouti, H., Tadie, M., & Cordoliani, Y.-S. (2002). Sensorimotor Cortical Activity in Patients with Complete Spinal Cord Injury: A Functional Magnetic Resonance Imaging Study. *Journal of Neurotrauma*, *19*(1). https://doi.org/10.1089/089771502753460231

Sanchez Panchuelo, R. M., Besle, J., Schluppeck, D., Humberstone, M., & Francis, S. (2018). Somatotopy in the Human Somatosensory System. *Frontiers in Human Neuroscience*, *12*. https://doi.org/10.3389/fnhum.2018.00235

Sanchez-Panchuelo, R. M., Besle, J., Mougin, O., Gowland, P., Bowtell, R., Schluppeck, D., & Francis, S. (2014). Regional structural differences across functionally parcellated Brodmann areas of human primary somatosensory cortex. *NeuroImage*, *93*. https://doi.org/10.1016/j.neuroimage.2013.03.044

Sanchez-Panchuelo, R. M., Francis, S., Bowtell, R., & Schluppeck, D. (2010). Mapping Human Somatosensory Cortex in Individual Subjects With 7T Functional MRI. *Journal of Neurophysiology*, *103*(5). https://doi.org/10.1152/jn.01017.2009

Sanders, Z.-B., Wesselink, D. B., Dempsey-Jones, H., & Makin, T. R. (2019). Similar somatotopy for active and passive digit representation in primary somatosensory cortex. *BioRxiv*.

Sathian, K., Zangaladze, A., Green, J., Vitek, J. L., & DeLong, M. R. (1997). Tactile spatial acuity and roughness discrimination: Impairments due to aging and Parkinson's disease. *Neurology*, *49*(1). https://doi.org/10.1212/WNL.49.1.168

Schmidt, T. T., & Blankenburg, F. (2018). Brain regions that retain the spatial layout of tactile stimuli during working memory – A 'tactospatial sketchpad'? *NeuroImage*, *178*. https://doi.org/10.1016/j.neuroimage.2018.05.076

Schmidt, T. T., & Blankenburg, F. (2019). The Somatotopy of Mental Tactile Imagery. *Frontiers in Human Neuroscience*, *13*. https://doi.org/10.3389/fnhum.2019.00010

Schmidt, T. T., Ostwald, D., & Blankenburg, F. (2014). Imaging tactile imagery: Changes in brain connectivity support perceptual grounding of mental images in primary sensory cortices. *NeuroImage*, *98*. https://doi.org/10.1016/j.neuroimage.2014.05.014

Schmidt, T. T., Schröder, P., Reinhardt, P., & Blankenburg, F. (2021). Rehearsal of tactile working memory: Premotor cortex recruits two dissociable neuronal content representations. *Human Brain Mapping*, *42*(1). https://doi.org/10.1002/hbm.25220

Schmidt, T. T., Wu, Y., & Blankenburg, F. (2017). Content-Specific Codes of Parametric Vibrotactile Working Memory in Humans. *The Journal of Neuroscience*, *37*(40). https://doi.org/10.1523/JNEUROSCI.1167-17.2017

Schneider, J. S., Diamond, S. G., & Markham, C. H. (1987). Parkinson's disease: Sensory and motor problems in arms and hands. *Neurology*, *37*(6). https://doi.org/10.1212/WNL.37.6.951

Schoups, A., Vogels, R., Qian, N., & Orban, G. (2001). Practising orientation identification improves orientation coding in V1 neurons. *Nature*, *412*(6846). https://doi.org/10.1038/35087601

Schweizer, R., Voit, D., & Frahm, J. (2008). Finger representations in human primary somatosensory cortex as revealed by high-resolution functional MRI of tactile stimulation. *NeuroImage*, *42*(1). https://doi.org/10.1016/j.neuroimage.2008.04.184

Scobey, R. P., & Gabor, A. J. (1989). Orientation discrimination sensitivity of single units in cat primary visual cortex. *Experimental Brain Research*, *77*(2). https://doi.org/10.1007/BF00274997

Selemon, L., & Goldman-Rakic, P. (1985). Longitudinal topography and interdigitation of corticostriatal projections in the rhesus monkey. *The Journal of Neuroscience*, *5*(3). https://doi.org/10.1523/JNEUROSCI.05-03-00776.1985

Shea, N. (2018). *Representation in Cognitive Science* (Vol. 1). Oxford University Press. https://doi.org/10.1093/oso/9780198812883.001.0001

Shoham, D., & Grinvald, A. (2001). The Cortical Representation of the Hand in Macaque and Human Area S-I: High Resolution Optical Imaging. *The Journal of Neuroscience*, *21*(17). https://doi.org/10.1523/JNEUROSCI.21-17-06820.2001

Silver, M. A., & Kastner, S. (2009). Topographic maps in human frontal and parietal cortex. *Trends in Cognitive Sciences*, *13*(11). https://doi.org/10.1016/j.tics.2009.08.005

Sinclair, R., Kuo, J., & Burton, H. (2000). Effects on discrimination performance of selective attention to tactile features. *Somatosensory & Motor Research*, *17*(2). https://doi.org/10.1080/08990220050020562

Smith, S. M. (2002). Fast robust automated brain extraction. *Human Brain Mapping*, *17*(3). https://doi.org/10.1002/hbm.10062

Smith, S. M., Miller, K. L., Moeller, S., Xu, J., Auerbach, E. J., Woolrich, M. W., Beckmann, C. F., Jenkinson, M., Andersson, J., Glasser, M. F., van Essen, D. C., Feinberg, D. A., Yacoub, E. S., & Ugurbil, K. (2012). Temporally-independent functional modes of spontaneous brain activity. *Proceedings of the National Academy of Sciences*, *109*(8). https://doi.org/10.1073/pnas.1121329109

Sörös, P., Marmurek, J., Tam, F., Baker, N., Staines, W. R., & Graham, S. J. (2007). Functional MRI of working memory and selective attention in vibrotactile frequency discrimination. *BMC Neuroscience*, *8*(1). https://doi.org/10.1186/1471-2202-8-48

Staines, W. R., Graham, S. J., Black, S. E., & McIlroy, W. E. (2002). Task-Relevant Modulation of Contralateral and Ipsilateral Primary Somatosensory Cortex and the Role of a Prefrontal-Cortical Sensory Gating System. *NeuroImage*, *15*(1). https://doi.org/10.1006/nimg.2001.0953

Stephan, K. E. (2004). On the role of general system theory for functional neuroimaging. *Journal of Anatomy*, *205*(6). https://doi.org/10.1111/j.0021-8782.2004.00359.x

Sterr, A., Shen, S., Zaman, A., Roberts, N., & Szameitat, A. (2007). Activation of SI is modulated by attention: a random effects fMRI study using mechanical stimuli. *NeuroReport*, *18*(6). https://doi.org/10.1097/WNR.0b013e3280b07c34

Stippich, C., Hofmann, R., Kapfer, D., Hempel, E., Heiland, S., Jansen, O., & Sartor, K. (1999). Somatotopic mapping of the human primary somatosensory cortex by fully automated tactile stimulation using functional magnetic resonance imaging. *Neuroscience Letters*, *277*(1). https://doi.org/10.1016/S0304-3940(99)00835-6

Sun, Z., Schneider, A., Alyahyay, M., Karvat, G., & Diester, I. (2021). Effects of Optogenetic Stimulation of Primary Somatosensory Cortex and Its Projections to Striatum on Vibrotactile Perception in Freely Moving Rats. *Eneuro*, *8*(2). https://doi.org/10.1523/ENEURO.0453-20.2021

Sutherland, M. T. (2006). The Hand and the Ipsilateral Primary Somatosensory Cortex. *Journal of Neuroscience*, *26*(32). https://doi.org/10.1523/JNEUROSCI.2698-06.2006

Swinnen, S. P. (2002). Intermanual coordination: From behavioural principles to neural-network interactions. *Nature Reviews Neuroscience*, *3*(5). https://doi.org/10.1038/nrn807

Talbot, W. H., Darian-Smith, I., Kornhuber, H. H., & Mountcastle, V. B. (1968). The sense of flutter-vibration: comparison of the human capacity with response patterns of mechanoreceptive afferents from the monkey hand. *Journal of Neurophysiology*, *31*(2). https://doi.org/10.1152/jn.1968.31.2.301

Talelli, P., Waddingham, W., Ewas, A., Rothwell, J. C., & Ward, N. S. (2008). The effect of age on task-related modulation of interhemispheric balance. *Experimental Brain Research*, *186*(1). https://doi.org/10.1007/s00221-007-1205-8

Theeuwes, J., Belopolsky, A., & Olivers, C. N. L. (2009). Interactions between working memory, attention and eye movements. *Acta Psychologica*, *132*(2). https://doi.org/10.1016/j.actpsy.2009.01.005

Tomita, H., Ohbayashi, M., Nakahara, K., Hasegawa, I., & Miyashita, Y. (1999). Top-down signal from prefrontal cortex in executive control of memory retrieval. *Nature*, *401*(6754). https://doi.org/10.1038/44372

Tommerdahl, M., Favorov, O., Whitsel, B. L., Nakhle, B., & Gonchar, Y. A. (1993). Minicolumnar Activation Patterns in Cat and Monkey SI Cortex. *Cerebral Cortex*, *3*(5). https://doi.org/10.1093/cercor/3.5.399

Treue, S., & Trujillo, J. C. M. (1999). Feature-based attention influences motion processing gain in macaque visual cortex. *Nature*, *399*(6736). https://doi.org/10.1038/21176

Vallat, R. (2018). Pingouin: statistics in Python. *Journal of Open Source Software*, *3*(31). https://doi.org/10.21105/joss.01026

van der Knaap, L. J., & van der Ham, I. J. M. (2011). How does the corpus callosum mediate interhemispheric transfer? A review. *Behavioural Brain Research*, *223*(1). https://doi.org/10.1016/j.bbr.2011.04.018

Volz, L. J., Eickhoff, S. B., Pool, E.-M., Fink, G. R., & Grefkes, C. (2015). Differential modulation of motor network connectivity during movements of the upper and lower limbs. *NeuroImage*, *119*. https://doi.org/10.1016/j.neuroimage.2015.05.101

Walther, A., Nili, H., Ejaz, N., Alink, A., Kriegeskorte, N., & Diedrichsen, J. (2016). Reliability of dissimilarity measures for multi-voxel pattern analysis. *NeuroImage*, *137*. https://doi.org/10.1016/j.neuroimage.2015.12.012

Wang, L., Bodner, M., & Zhou, Y.-D. (2013). Distributed neural networks of tactile working memory. *Journal of Physiology-Paris*, *107*(6). https://doi.org/10.1016/j.jphysparis.2013.06.001

Watson, A. B., & Pelli, D. G. (1983). Quest: A Bayesian adaptive psychometric method. *Perception & Psychophysics*, *33*(2). https://doi.org/10.3758/BF03202828

Weaverdyck, M. E., Lieberman, M. D., & Parkinson, C. (2020). Tools of the Trade Multivoxel pattern analysis in fMRI: a practical introduction for social and affective neuroscientists. *Social Cognitive and Affective Neuroscience*, *15*(4). https://doi.org/10.1093/scan/nsaa057

Werhahn, K. J., Mortensen, J., Kaelin-Lang, A., Boroojerdi, B., & Cohen, L. G. (2002). Cortical excitability changes induced by deafferentation of the contralateral hemisphere. *Brain*, *125*(6). https://doi.org/10.1093/brain/awf140

Wesselink, D. B., van den Heiligenberg, F. M., Ejaz, N., Dempsey-Jones, H., Cardinali, L., Tarall-Jozwiak, A., Diedrichsen, J., & Makin, T. R. (2019). Obtaining and maintaining cortical hand representation as evidenced from acquired and congenital handlessness. *ELife*, *8*. https://doi.org/10.7554/eLife.37227

Wesselink DB, & Maimon-Mor R. (2017). rsatoolbox Github. *Https://Github.Com/Ronimaimon/Rsatoolbox*.

Wiestler, T., & Diedrichsen, J. (2013). Skill learning strengthens cortical representations of motor sequences. *ELife*, *2*. https://doi.org/10.7554/eLife.00801

Willoughby, W. R., Thoenes, K., & Bolding, M. (2021). Somatotopic Arrangement of the Human Primary Somatosensory Cortex Derived From Functional Magnetic Resonance Imaging. *Frontiers in Neuroscience*, *14*. https://doi.org/10.3389/fnins.2020.598482

Wu, Y., Uluç, I., Schmidt, T. T., Tertel, K., Kirilina, E., & Blankenburg, F. (2018). Overlapping frontoparietal networks for tactile and visual parametric working memory representations. *NeuroImage*, *166*. https://doi.org/10.1016/j.neuroimage.2017.10.059

Yousry, T. (1997). Localization of the motor hand area to a knob on the precentral gyrus. A new landmark. *Brain*, *120*(1). https://doi.org/10.1093/brain/120.1.141

Yousry, T. A., Schmid, U. D., Alkadhi, H., Schmidt, D., Peraud, A., Buettner, A., & Winkler, P. (1997). Localization of the motor hand area to a knob on the precentral gyrus. A new landmark. *Brain*, *120*(1), 141–157. https://doi.org/10.1093/brain/120.1.141

Zanto, T. P., Rubens, M. T., Thangavel, A., & Gazzaley, A. (2011). Causal role of the prefrontal cortex in top-down modulation of visual processing and working memory. *Nature Neuroscience*, *14*(5). https://doi.org/10.1038/nn.2773

Zhou, Y. D., & Fuster, J. M. (1996). Mnemonic neuronal activity in somatosensory cortex. *Proceedings of the National Academy of Sciences*, *93*(19). https://doi.org/10.1073/pnas.93.19.10533

Zhou, Y. D., & Fuster, J. M. (2000). Visuo-tactile cross-modal associations in cortical somatosensory cells. *Proceedings of the National Academy of Sciences*, *97*(17). https://doi.org/10.1073/pnas.97.17.9777

Zia, S., Cody, F. W. J., & O'Boyle, D. J. (2003). Discrimination of bilateral differences in the loci of tactile stimulation is impaired in subjects with Parkinson's disease. *Clinical Anatomy*, *16*(3). https://doi.org/10.1002/ca.10100

Ziemann, U., Ishii, K., Borgheresi, A., Yaseen, Z., Battaglia, F., Hallett, M., Cincotta, M., & Wassermann, E. M. (1999). Dissociation of the pathways mediating ipsilateral and contralateral motor-evoked potentials in human hand and arm muscles. *The Journal of Physiology*, *518*(3). https://doi.org/10.1111/j.1469-7793.1999.0895p.x

Zuur, A. F., Ieno, E. N., & Elphick, C. S. (2010). A protocol for data exploration to avoid common statistical problems. *Methods in Ecology and Evolution*, *1*(1). https://doi.org/10.1111/j.2041-210X.2009.00001.x